Age-associated changes in lineage composition of the enteric nervous system regulate gut health and disease

Subhash Kulkarni[1#], Monalee Saha[1], Jared Slosberg[2], Alpana Singh[1], Sushma Nagaraj[1], Laren Becker[3], Chengxiu Zhang[1], Alicia Bukowski[1], Zhuolun Wang[1], Guosheng Liu[1], Jenna Leser[1,] Mithra Kumar[1], Shriya Bakhshi[1], Matthew Anderson[4], Mark Lewandoski[4], Elizabeth Vincent[2], Loyal A. Goff[2, 5, 6], Pankaj Jay Pasricha[1, 7]

[1]Center for Neurogastroenterology, Department of Medicine, Johns Hopkins University – School of Medicine, Baltimore, MD 21205

[2]Department of Genetic Medicine, Johns Hopkins University – School of Medicine, Baltimore, MD 21205

[3]Division of Gastroenterology, Stanford University – School of Medicine, Stanford CA 94301

[4]Center for Cancer Research, National Cancer Institute, Frederick, MD 21702

[5]Department of Neuroscience, Johns Hopkins University – School of Medicine, Baltimore, MD 21205

[6]Kavli Neurodiscovery Institute, Johns Hopkins University – School of Medicine, Baltimore, MD 21205

[7]Department of Medicine, Mayo Clinic, Scottsdale, AZ 85259

[#]Address all correspondence to:

Subhash Kulkarni, Ph.D.

Assistant Professor

Department of Medicine

skulkar9@jh.edu

Abstract

The enteric nervous system (ENS), a collection of neural cells contained in the wall of the gut, is of fundamental importance to gastrointestinal and systemic health. According to the prevailing paradigm, the ENS arises from progenitor cells migrating from the neural crest and remains largely unchanged thereafter. Here, we show that the lineage composition of maturing ENS changes with time, with a decline in the canonical lineage of neural-crest derived neurons and their replacement by a newly identified lineage of mesoderm-derived neurons. Single cell transcriptomics and immunochemical approaches establish a distinct expression profile of mesoderm-derived neurons. The dynamic balance between the proportions of neurons from these two different lineages in the post-natal gut is dependent on the availability of their respective trophic signals, GDNF-RET and HGF-MET. With increasing age, the mesoderm-derived neurons become the dominant form of neurons in the ENS, a change associated with significant functional effects on intestinal motility which can be reversed by GDNF supplementation. Transcriptomic analyses of human gut tissues show reduced GDNF-RET signaling in patients with intestinal dysmotility which is associated with reduction in neural crest-derived neuronal markers and concomitant increase in transcriptional patterns specific to mesoderm-derived neurons. Normal intestinal function in the adult gastrointestinal tract therefore appears to require an optimal balance between these two distinct lineages within the ENS.

Introduction

The enteric nervous system (ENS) is a large collection of neurons, glial, and precursor cells that resides within the gastrointestinal wall and regulates gut motility and secretion along with modulating epithelial and immune cell function[1,2]. During fetal development, the mammalian ENS is populated by neurons and glia derived from neural crest (NC)-derived precursors[3-9]. These precursors follow diverse migratory routes to colonize and innervate various parts of the gut before birth[10-12]. It is not clear, however, that this lineage persists in its entirety in the adult gut, as indicated by the observed lack of expression of fluorescent reporter protein in a subpopulation of adult enteric neurons in NC-lineage-traced mice[13,14]. Alternative sources of enteric neurons that have been proposed in the literature include the ventral neural tube (VENT)[15], or the Pdx1-expressing pancreatic endoderm[14], but the interpretation of these studies has been limited by the lack of robust lineage markers for non-NC derived neurons[16]. In addition, while prior studies have documented cellular changes to the ageing ENS[17], the developmental mechanisms behind these changes are unknown. Thus, confirmation of a second, distinct lineage of enteric neurons in adults is important for our understanding of the healthy post-natal development and aging of the ENS, as well as for the pathogenesis of acquired disorders of the ENS.

In this study, we found that while the early post-natal ENS is derived from the canonical NC-lineage, this pattern changes rapidly as the ENS matures, due to the arrival and continual expansion of a novel population of Mesoderm-derived Enteric Neurons (MENs) which represent an equal proportion of the ENS in young adulthood and with increasing age, eventually outnumber the NC-derived Enteric Neurons (NENs). We also found that, while the NEN population is regulated by glial derived neurotrophic factor (GDNF) signaling through its receptor RET, the MEN population is regulated by hepatocyte growth factor (HGF) signaling. Increasing HGF levels during maturation or by pharmacological dosing increase proportions of MENs. Similarly, decrease in

66 GDNF with age decrease NENs; and increasing GDNF levels by pharmacological dosing increase
67 NENs proportions in the adult ENS to impact intestinal motility.

68 These results indicate for the first time that the mesoderm is an important source of neurons in
69 the second largest nervous system of the body. The increasing proportion of neurons of meso-
70 dermal lineage is a natural consequence of maturation and aging; further, this lineage can be
71 expected to have vulnerabilities to disease that are distinct from those affecting the NEN popula-
72 tion. These findings therefore provide a new paradigm for understanding the structure and func-
73 tion of the adult and aging ENS in health, age-related gut dysfunction and other acquired disorders
74 of gastrointestinal motility.

75 **Results**

76 **Only half of all mid-age adult enteric neurons are derived from the neural crest.** We ana-
77 lyzed small intestinal longitudinal muscle-myenteric plexus (LM-MP) from adult (post-natal day
78 60; P60) Wnt1-cre:*Rosa26*-tdTomato mice, in which tdTomato is expressed by all derivatives of
79 Wnt1^{+} NC-cells[18]. In these tissues, while GFAP, a glial marker, was always co-expressed with
80 tdTomato (Fig 1a), tdTomato-expression was absent in many myenteric neurons (Fig 1b, c). By
81 careful enumeration, almost half of all myenteric neurons expressing the pan-neuronal marker Hu
82 were found to not express the reporter (percent tdTomato^{-} neurons: 44.27 ± 2.404 SEM; enumer-
83 ated from 2216 neurons from 6 mice, Fig 1d). In these lineage-traced mice, myenteric ganglia
84 were found to contain tdTomato^{high} and tdTomato^{low} neurons and due care was taken to image
85 subsets (Suppl. Fig 1a). Both tdTomato^{high} and tdTomato^{low} neurons were classified as tdTomato^{+}
86 and only neurons that did not show any tdTomato-expression were classified as tdTomato^{-} neu-
87 rons. Immunofluorescence staining of small intestinal LM-MP tissue from adult Wnt1-cre:*Rosa26*-
88 tdTomato mice using antibodies against tdTomato protein showed a consistent lack of reporter
89 expression in a population of myenteric neurons (Suppl. Fig 1b). This lack of reporter expression

90 is not a function of tissue peeling or fixation, as the tdTomato^{-} cells within the myenteric ganglia
91 were also observed in freshly harvested unpeeled gut tissue, when imaged using a live tissue
92 fluorescence microscope (Suppl. Fig 1c). In addition, we noticed that myenteric ganglia of the
93 Wnt1-cre:*Rosa26*-tdTomato transgenic mouse show similar tdTomato aggregation in cells of the
94 myenteric plexus from both freshly harvested and immediately fixed tissue (Suppl. Fig 1d, e).
95 Since we previously showed ongoing neuronal loss in healthy ENS[19], we reasoned that cells that
96 show hyper-aggregation of tdTomato are in advanced stages of cell death. Cells with hyper-ag-
97 gregation of tdTomato showed a lack of staining for the nuclear marker DAPI (Suppl. Fig 1e),
98 suggesting that these are indeed cells in the advanced stages of death, and given that they are
99 not labeled with antibodies against Hu, their presence does not alter our estimation of tdTomato-
100 expressing neurons (Suppl. Fig 1f). Thus, the absence of reporter expression in myenteric ganglia
101 of freshly harvested tissue and the presence of tdTomato aggregation in both freshly harvested
102 and fixed tissues shows that our observations are not caused due to any technical issues in tissue
103 isolation and preservation.

104 Additional confirmation was provided by an analogous Wnt1-cre:*Hprt*-tdTomato lineage-traced
105 mouse line, in which tdTomato was expressed from the *Hprt* locus in a Wnt1-cre-dependent man-
106 ner (*Hprt* locus is X-inactivated in females, hence only adult male mice were used)[20]; and by the
107 Pax3-cre:*Rosa26*-tdTomato lineage-traced mouse line, where *Rosa26*-tdTomato driven by the
108 Pax3-cre transgene labels the derivatives of the neural tube and pre-migratory NC (Suppl. Fig 1g,
109 h)[21]. Similar lack of reporter expression was previously observed in adult myenteric neurons from
110 Sox10-cre NC-lineage-traced mice, and more recently in significant numbers of myenteric neu-
111 rons from Wnt1-cre:*Rosa26*-H2B-mCherry mice, which expresses nuclear localized reporter
112 mCherry in NC-lineage cells, further confirming our observations of the presence of non-NC-de-
113 rived neurons in the adult ENS[13,22]. In addition to the ANNA-1 antisera, which is known to detect
114 all neuronally significant Hu proteins (HuB, HuC, and HuD)[23], we found that another often used

115 antibody thought to be specific to HuC and HuD also detects HuB protein (Suppl. Fig 1l) – showing
116 that these antibodies do not detect the expression of a specific neuronal Hu antigen.

117 **Lineage-tracing confirms a mesodermal derivation for half of all adult myenteric neurons.**
118 Alternative sources of enteric neurons proposed previously include the ventral neural tube[15], and
119 the pancreatic endoderm[14], but the interpretation of these studies was limited by the lack of robust
120 lineage markers[16]. Brokhman et al.[14] found evidence of labeled neurons in inducible Pdx1-cre,
121 Foxa2-cre, and Sox17-cre lineage-traced mouse lines and inferred their derivation from pancre-
122 atic endoderm. However, in a Pdx1-cre lineage-traced mouse line, many neuroectoderm-derived
123 neurons of the central nervous system have also been previously shown to be derived from Pdx1-
124 expressing cells[24], suggesting that Pdx1 is not an exclusive endodermal marker. Foxa2 is ex-
125 pressed by mesoderm-derived cells in the heart[25] and Sox17 also labels mesoderm-derived cells,
126 especially cells of the intestinal vasculature[26-29]. We therefore hypothesized that the embryonic
127 mesoderm may be the true developmental source of the non-NC enteric neurons.

128 Mesoderm-derived cells during embryogenesis express Tek[25] and analysis of LM-MP tissues from
129 adult male Tek-cre:*Hprt*-tdTomato lineage-traced mice revealed the presence of a population of
130 tdTomato$^+$ neurons (Fig 2a). Since Tek is not expressed in the adult ENS (Suppl. Fig 2a), the
131 presence of Tek-derived adult myenteric neurons suggested their mesodermal origin. We then
132 used *mesoderm posterior 1* or Mesp1 as a definitive developmental marker for the embryonic
133 mesoderm[30-34] to confirm the mesodermal derivation of the non-NC derived adult enteric neurons.
134 Reporter expression in this mouse line has been previously studied in cardiac development, which
135 we confirmed by observing its expression in the adult heart tissue (Fig 2b). Expression of
136 tdTomato in vascular cells of both Tek-cre and Mesp1-cre mice was more pronounced than in
137 myenteric neurons (Fig 2a, c, d) and in cardiac myocytes of Mesp1-cre mice (Fig 2b, Suppl. Fig
138 2b), which reflects the variable expression of the reporter gene in both the neural crest-lineage
139 and mesoderm-lineage specific transgenic mouse lines (Fig 2b, c; Suppl. Figs 1a, 2c). Using an

140 analogous Mesp1-cre:*Rosa26*-EGFP lineage-traced mouse line, in which EGFP was expressed
141 from the *Rosa26* locus in a Mesp1-cre-dependent manner, we next confirmed the derivation of a
142 population of myenteric neurons from Mesp1-expressing mesoderm (Fig 2e, Suppl. Fig 2d, e).
143 Similar to our observations with the tdTomato reporter (Fig 2a-d), we observed lower expression
144 of the reporter EGFP in myenteric neurons as compared to vascular cells (Fig 2e; Suppl. Fig 2d,
145 e). Variable expression of CAG and other pan-cellular promoters in various cell-types and during
146 processes of maturation have previously been reported[35-38]. In addition, an earlier study by Agah
147 et al. showed differing degrees of CAG-driven LacZ reporter activation in a cardiac-specific trans-
148 genic cre mouse line, which were unrelated to copy number, suggesting insertional and positional
149 effects or, potentially, differential methylation[39]. These reports are consistent with our observation
150 and could potentially help explain the observed variable expression of CAG and CMV promoter-
151 driven reporter genes in our study.

152 Analysis of small intestinal LM-MP from P60 Mesp1-cre:*Rosa26*-tdTomato lineage-traced mice
153 showed that tdTomato-expression was observed in about half of all myenteric neurons (Fig 2f;
154 percent tdTomato$^+$ neurons: 50.28 ± 2.89 SEM; enumerated from 484 neurons from 3 mice). Be-
155 cause of the variable expression of the reporter gene in the transgenic mice described above, we
156 also labeled Mesp1-cre:*Rosa26*-tdTomato$^+$ neurons with the S46 antibody, which was raised
157 against the slow tonic myosin heavy chain protein MHCst derived from avian embryonic upper
158 leg muscle, and is expressed exclusively by mesoderm-derived cell populations (Fig 2g)[40-43].
159 MHCst immunostaining was exclusively observed in all Tek-cre:*Rosa26*-tdTomato$^+$ MENs (Suppl.
160 Fig 2f). None of the 107 MHCst$^+$ intra-ganglionic cells observed (35.67 ± 6.17 SEM MHCst$^+$ cells
161 per mouse) across 3 Wnt1-cre:*Rosa26*-tdTomato mice expressed tdTomato, suggesting that
162 MHCst immunostaining was exclusive to non-NC lineage neurons (Fig 2h, Suppl. Fig 3a shows
163 the same image where the MHCst immunostained ganglia can be observed with and without the
164 tdTomato channel for better visualization). MHCst antibody was also found to label extra-

165 ganglionic smooth muscle cells in the LM-MP tissue (Suppl. Fig 3a). Thus, both lineage tracing
166 and protein biomarker expression provides strong support for their mesodermal origin (Fig 2g,
167 Suppl. Fig 3a). Along with our observations on Wnt1-cre:*Rosa26*-tdTomato mice (Fig 1c), our
168 results indicate that these two distinct lineages together account for all the adult small intestinal
169 myenteric neurons.

170 The proteins RET, a receptor tyrosine kinase that transduces GDNF signaling in NC-derived en-
171 teric neuronal precursors, and MET, a receptor for hepatocyte growth factor (HGF), are expressed
172 by different subsets of adult myenteric neurons[44]. MET is classically expressed by mesoderm-
173 derived cells[45], and by using immunostaining of small intestinal LM-MP tissues from Wnt1-
174 cre:*Rosa26*-tdTomato and Mesp1-cre:*Rosa26*-tdTomato mice, we found that the expression of
175 MET was restricted to a sub-population of adult MENs (Fig 3a, b). By contrast, RET expression
176 was confined to NENs (Fig 3c).

177 We then studied whether MENs and NENs differed phenotypically. In the current paradigm re-
178 garding the neurochemical basis for the functional classification of adult enteric neurons, inhibitory
179 enteric motor neurons express the nitric oxide-producing enzyme nitric oxide synthase 1 (NOS1),
180 excitatory motor neurons express the acetylcholine-producing enzyme choline acetyl transferase
181 (ChAT), and enteric sensory neurons, called intrinsic primary afferent neurons (IPANs) express
182 the neuropeptide calcitonin gene related peptide (CGRP)[9,44,46]. Immunostaining using antibodies
183 against NOS1, ChAT, and CGRP in the LM-MP from P60 Wnt1-cre:*Rosa26*-tdTomato mice
184 showed that both tdTomato$^+$ NENs and tdTomato$^-$ MENs express these neuronal markers (Fig
185 3d, f, h). Quantification of proportions in these neuronal lineages shows that the majority of NOS1$^+$
186 inhibitory neurons and ChAT$^+$ excitatory neurons are NENs (Fig 3e; of the 616 NOS1$^+$ neurons
187 observed across 3 mice, NOS1$^+$ tdTomato$^-$: 27.06% ± 4.46 SEM; $p < 0.0001$; Fisher's exact test);
188 (Fig 3g; of the 912 ChAT+ neurons observed across 3 mice, ChAT$^+$ tdTomato$^-$: 26.34% ± 2.54

189 SEM; $p < 0.0001$; Fisher's exact test). By contrast, the majority (~75%) of $CGRP^+$ neurons were
190 found to be MENs (Fig 3i; of the 146 $CGRP^+$ neurons observed across 3 mice, $CGRP^+$ $tdTomato^-$
191 : 75.76% ± 0.63 SEM; $p < 0.0001$; Fisher's exact test). These results are in keeping with a previ-
192 ous report by Avetisyan et al. that shows low expression of NOS1 (0% of MET^+ neurons were
193 NOS^+) and ChAT (<8% of MET^+ neurons were $ChAT^+$) and abundant expression of CGRP by
194 MET^+ neurons in the adult ENS[44], previously not known to be derived from a different lineage. In
195 addition, MENs also express Cadherin-3 (CDH3, Suppl. Fig 3b), which is known to also mark a
196 sub-population of mechanosensory spinal neurons[47]. Apart from their derivation from a distinct
197 developmental lineage, the mean cell size of MENs was significantly larger than that of NENs
198 (Suppl. Fig 4a; n = 143 neurons/group observed across 3 mice; Feret diameter (μm) MENs: 17.47
199 ± 0.50 SEM, NENs: 13.03 ± 0.36 SEM, $p = 0.002$; Student's t-test).

200 **An expanded molecular characterization of MENs using unbiased single cell RNA se-**
201 **quencing (scRNAseq)-based analyses.** Recent studies have used single cell or single nuclei-
202 based transcriptomic analyses to query molecular diversity of enteric neurons. These studies
203 have used either used enrichment methods based on FACS sorting neural crest-derived cells
204 (using reporter-expression from neural crest-specific lineage fate mapping mice)[22,48,49], Phox2b-
205 expressing cells[50], Baf53-derived cells[51] or used classical NENs markers such as Snap25 to drive
206 identification and/or enrichment of enteric neurons[49]. Instead of using these strategies, we relied
207 upon another accepted use of scRNAseq, which allows for sequencing of diverse un-enriched
208 cell populations from a tissue, to discover any novel cell types in that tissue[52]. We performed truly
209 unbiased and agnostic clustering of the scRNAseq data from tissues of two 6-month-old adult
210 male C57BL/6 wildtype mice (Fig 4a; Suppl. Fig 4b, c). We identified clusters of NC-derived cells
211 by exclusive expression of canonical NC markers Ret and Sox10 (which include the clusters of
212 Ret-expressing NENs and Sox10-expressing Neuroglia); and the MENs cluster by its co-

213 expression of the genes Calcb (CGRP), Met, and Cdh3 (Fig 4a, b). With cells from both samples
214 pooled together, we compared 1,737 NC-derived cells across the NENs (77 cells) and Neuroglia
215 (1660 cells) clusters with 2,223 cells in the MENs cluster. A list of top marker genes for every
216 cluster are provided in Table S2.

217 The neuronal nature of MENs was first established by testing our scRNAseq dataset for expres-
218 sion of genes known to be expressed by enteric or other neurons. We found detectable expres-
219 sion of genes Elavl2 (HuB), Hand2, Pde10a, Vsnl1, Tubb2b, Stmn2, Stx3, and Gpr88 in the MENs
220 as well as in the NC-derived cell clusters (Fig 4b). While expression of Elavl2, Stmn2 and Hand2
221 has been previously observed in enteric neurons[53,54], the expression of neuronal marker genes
222 Pde10a (expressed by medium spiny neurons in the striatum[55]), Vsnl1 (expressed by hippocam-
223 pal neurons[56]), Gpr88 (expressed by striatal neurons[57]), Stx3 (expressed by hippocampal neu-
224 rons[58]), and Tubb2b (expressed by adult retinal neurons[59]) has not been studied. Using antibodies
225 against these markers along with co-staining with anti-Hu ANNA1 antisera to label neurons, we
226 visualized the expression of these neuronal markers in both tdTomato^{+} NENs and tdTomato^{-}
227 MENs of the small intestinal myenteric plexus tissue from adult Wnt1-cre:*Rosa26*-tdTomato mice
228 (Fig 4c, Suppl. Fig 3l-q). In addition, the MENs cluster was also enriched in previously character-
229 ized ENS markers, such as Ntf3 and Il18[2,60] (Fig 4b). We validated the MEN-specificity of these
230 markers using immunochemical analyses (Fig 4c; Suppl. Fig 3b - k). In addition, we also detected
231 >40 neuronally significant genes whose expression was unique to or enriched in MENs scRNAseq
232 cluster, when compared with other larger cell clusters of macrophages, smooth muscle cells, neu-
233 roglia, and vascular endothelium (Suppl. Fig 5). These genes include neurotransmitter receptor
234 genes (such as Gabra1, Gabra3, Gria3, Grik5, Grind2d, Npy1r); ion channels genes (such as
235 Cacna1a, Cacna1g, Cacnb3, Clcn3); gap junction genes (Gjc1, Gjb5); transient receptor potential
236 channel genes (Trpv4, Trpc1, Trpc6); potassium channel genes (such as Kcnn1, Kcnj8, Kcnd3,
237 Kcnh3, Kcns3); hormone encoding genes (Ghrh, Gnrh1, Nucb2) along with other neuronal genes

238 such as, Prss12 (encoding for Neurotrypsin)[61], Uchl1 (encoding for pan-neuronal marker
239 PGP9.5)[62], Cplx2 (encoding for Complexin 2)[63], Gpm6a (encoding for neuronal membrane glyco-
240 protein M6-A)[64], and Vamp2 (encoding for Synaptobrevin 2)[65] (Suppl. Fig 5). Owing to the small
241 size of the NENs cluster, a comparative analysis between these two neuronal lineages for these
242 neuronally significant genes was not possible. However, the discovery of these neuronally signif-
243 icant genes in the MENs cluster, and the subsequent validation of a set of them provides evidence
244 for the neuronal nature of MENs. Further examination of the MENs cluster yielded additional
245 MENs-specific marker genes Slpi, Aebp1, Clic3, Fmo2, Smo, Myl7, and Slc17a9, whose expres-
246 sion by adult enteric neurons has not been previously described and which we also validated (Fig
247 4b).

248 Next, we examined the MENs cluster for expression of a mesenchymal gene that would under-
249 score the mesodermal nature of MENs. Decorin (Dcn) is a gene coding for a chondroitin-dermatan
250 sulphate proteoglycan, which is expressed by mesoderm-derived cells, including fibroblasts and
251 smooth muscle cells[66]. Decorin was found to be highly expressed in the MENs cluster in our data
252 (Fig 5a), and not by the neurons in the Zeisel et al. database (Fig 5b)[48]. We used a validated
253 antibody against DCN[67] and found that this protein, known to be specifically expressed by meso-
254 derm-derived cells, is expressed specifically by tdTomato-negative small intestinal myenteric neu-
255 rons of the Wnt1-cre:*Rosa26*-tdTomato lineage fate mapping mouse (Fig 5c).

256 These data show that the MENs scRNAseq cluster, which can be identified by its co-expression
257 of neuronal markers (Elavl2, Pde10a, Hand2, etc), validated cell surface marker (Cdh3), and the
258 mesodermal marker Dcn is the same as the population of Hu-expressing neurons that do not
259 express tdTomato in the Wnt1-cre:*Rosa26*-tdTomato neural crest lineage fate mapping mouse.
260 We thus establish the distinct nature of MENs based on the co-expression of many neuronally
261 significant genes and of mesodermal genes by this cell population of Wnt1-cre:*Rosa26*-tdTomato-
262 negative neuron. Our experimental strategy of performing scRNAseq on LM-MP cells without any

263 pre-enrichment helps detects this newly characterized cell type. However, it does not allow us to
264 compare and contrast the transcriptomic profiles of MENs and NENs – especially given that we
265 do not know the true size of NENs represented in our dataset. This is exemplified by the fact that
266 cells within the Neuroglia cluster showed expression of glial genes such as Sox10 as well as
267 neuronal genes such as Ncam1, Hand2 and Stmn2, suggesting that NC-derived neurons may be
268 present within both the smaller NENs cluster as well as the larger Neuroglia cluster (Fig 4b).

269 **Detection of MENs in other murine and human datasets.** Since Phox2b, the transcription fac-
270 tor expressed by all ENS cells, shows significant higher expression in some neurons than in all
271 ENS glial cells[68], May-Zhang et al.[50] reasoned that flow sorted nuclei of Phox2b-CFP^{high} cells from
272 a Phox2b-CFP reporter mouse would provide for an enriched population of ENS neurons that can
273 be used for single nuclei RNA sequencing (snRNAseq). They first performed bulk-RNAseq on
274 Phox2b-CFP^{+} nuclei that were flow sorted based on CFP-expression level into CFP^{low} and CFP^{high}
275 fractions, of which the CFP^{low} fraction was found enriched with glial-specific gene expression pro-
276 file. May-Zhang et al.[50] used this to provide a rationale for performing snRNAseq on Phox2b-
277 CFP^{high} nuclei, which they presumed to consist of all enteric neurons. Since, MENs make up
278 roughly half of all adult ENS neurons, we hypothesized that they should also express Phox2b. By
279 using a PHOX2b-specific antibody, we validated the expression of this important transcription
280 factor in MENs (Fig 5d). Next, we tested whether we could detect some of the genes that show
281 enriched expression in MENs (namely, Smo, Aebp1, Cdh3, Fmo2, Il18, Slpi, Upk3b, Msln, Hand2)
282 in the Phox2b^{+} bulkRNAseq data from May-Zhang et al.[50], and found that not only were these
283 genes expressed by their Phox2b^{+} cells, but expression of these genes was also significantly
284 enriched in the Phox2b-CFP^{low} fraction (Fig 5e) that was not used for subsequent snRNAseq
285 experiments. These data provide evidence that MENs express Phox2b, both transcriptomically,
286 as well as at the protein level. We next queried whether any MENs were represented in the May-
287 Zhang et al.'s snRNAseq data generated on Phox2b-CFP^{high} nuclei, given that they reported on

288 the presence of a cluster of adult enteric neurons that expressed mesenchymal markers. We
289 again tested whether the MENs-expressed genes, such as Decorin, etc were also expressed by
290 the 'mesenchymal' neurons in the May-Zhang et al.[50] dataset. We found a high degree of similarity
291 between the top genes expressed by the MENs cluster in our scRNAseq dataset and the 'mes-
292 enchymal' neurons in the May-Zhang et al.'s snRNAseq dataset (Table 1, Suppl. Fig 4d). Further-
293 more, examination of the top genes shows that this Decorin-expressing neuronal sub-population
294 is significantly different from the other Calcb-expressing neuronal populations, which we presume
295 to be the CGRP-expressing NENs (Table 1).

296 To confirm that the 'mesenchymal' neurons identified by May-Zhang et al.[50] are MENs, we used
297 an agnostic bioinformatics projection-based approach which we have previously published[69]. This
298 approach allows us to learn latent space representations of gene expression patterns using single
299 cell transcriptomic data, generating patterns that correspond to cell-type-specific gene expression
300 signatures[69]. We can then project other single cell and bulk RNA transcriptomic datasets into
301 these learned patterns to accurately quantify the differential use of these transcriptional signatures
302 in target data across platforms, tissues, and species[69]. In this instance, gene expression patterns
303 were learned on our murine single cell transcriptomic data using non-negative matrix factorization
304 (NMF) dimensionality reduction and the data was decomposed into 50 distinct NMF-patterns[69,70]
305 (Fig 6a). Four NMF patterns were identified that were specific to MENs (Fig 6a, b; Suppl. Fig 4e).
306 We next projected the snRNAseq dataset from May-Zhang et al.[50] into the four MEN-specific
307 patterns and found that all these patterns specifically labeled the cluster of 'mesenchymal' neu-
308 rons in the May-Zhang et al. dataset of the adult ileal ENS (Fig 6b). Further, upon clustering the
309 nuclei based on their projection weights from the four MEN-specific patterns, we identified a clus-
310 ter of nuclei that showed higher usage of all four patterns, when compared to all the other nuclei
311 sequenced in the dataset (Suppl. Fig 4f). The genes that define this cluster of cells are similar to
312 the top-expressed genes that define our MENs cluster (Suppl. Fig 4g, Table 1). This approach,

313 together with the high similarities in the top-expressed genes, establishes that cluster of neurons
314 annotated as 'mesenchymal' neurons by May-Zhang et al. are indeed MENs. Further, one of the
315 markers used by May-Zhang et al. to describe their mesenchymal neuronal cluster was the gene
316 Myh11[50], which is known to be expressed by mesoderm-derived smooth muscle cells in the adult
317 gut[71]. To test whether Myh11 is expressed by MENs, we immunolabeled the small intestinal LM-
318 MP tissue from an adult Wnt1-cre:*Rosa26*-tdTomato mouse with a monoclonal antibody against
319 MYH11 (Invitrogen) and found that tdTomato-negative and Hu^+ neurons exclusively immuno-
320 labeled for MYH11 (Suppl. Fig. 6a). We confirmed that a subpopulation of adult enteric neurons
321 expressed Myh11 by immunolabeling small intestinal LM-MP tissues from a tamoxifen treated
322 Myh11-cre^{ERT2}:*Rosa26*-YFP transgenic mouse line with anti-YFP/GFP and anti-Hu antibodies
323 (Suppl. Fig. 6b). Anti-MYH11 antibodies labeled circular smooth muscle in the human duodenum,
324 where it did not immunolabel nerve fibers and some submucosal neurons immunostained with
325 antibodies against the pan-neuronal marker PGP9.5 but showed immunolabeling against
326 PGP9.5-expressing myenteric neurons in the adult healthy small intestinal tissue (Supp. Fig 6c,
327 d). Thus, we confirm that the MENs identified by us correspond to the cluster of 'mesenchymal
328 neurons' observed by May-Zhang et al. As compared to our scRNAseq dataset, where MENs
329 comprise of a significantly large numbers of cells, the MENs cluster in the May-Zhang et al. da-
330 taset is significantly smaller, possibly due to the fact that a large number of MENs were left unse-
331 quenced in their Phox2b-CFP^{low} fraction.

332 Similarly, Drokhlyansky et al.[49] using MIRACL-seq found a small cluster of cells that express the
333 MENs-signature genes (Cdh3, Dcn, Slpi, Aebp1, Wt1, Msln, Fmo2). However, the neuronal nature
334 of these cells was not correctly identified as the study used a gene signature profile specific for
335 neural crest-derived neurons (derived from their experiment with enriched Wnt1-cre2:*Rosa26*-
336 tdTomato-expressing neural crest-derived cells). As a result, this cluster of cells – which shows
337 similarity to the MENs transcriptomic profile, was instead annotated as *Mesothelial*. This

338 ‘mesothelial’ cluster in the Drokhlyansky et al.[49] dataset shows similar gene expression profile as
339 that of the cluster of ‘mesenchymal neurons’ from the May-Zhang et al.[50] dataset (Table 1), espe-
340 cially given that many of the marker genes for both clusters are similar (Lrrn4, Rspo1, Msln,
341 Upk3b, Upk1b, Gpm6a, Wnt5a, Gpc3, Sulf1, Muc16). The ‘mesothelial’ cluster also expresses
342 neuronally significant genes such as Gabra3 (GABA receptor A subunit 3[72]), Prss12 (Neurotryp-
343 sin[61,73]), Synpr (Synaptoporin[74]), Trpv4 (Transient receptor potential cation channel subfamily V
344 member 4[75]), and Nxph1 (Neurexophillin-1[76]). Unfortunately, a deeper interrogation of this dataset
345 was not possible due to the size and the manner in which the original data was processed[49]. In
346 addition, MENs were not represented in the snRNAseq carried out in Wright et al.[22], which was
347 based solely on neural crest-derived cells.

348 In contrast to these snRNAseq based studies, the Marklund Lab in two studies performed single
349 cell RNA-sequencing (scRNAseq) on juvenile ENS cells, first on tdTomato$^+$ cells from P21 Wnt1-
350 cre:*Rosa26*:tdTomato lineage fate mapping mice in Zeisel et al.[48] and then from the newly char-
351 acterized Baf53b-cre:*Rosa26*-tdTomato BAC-transgenic mouse line[77] in Morarach et al.[51]. Barring
352 2 small clusters (ENC5 and ENC11), the other neuronal clusters identified in Morarach et al.[51]
353 mapped to the neural crest-derived clusters identified earlier by them in Zeisel et al.[48]. The gene
354 expression signature of these two clusters (ENC5: Sst, Calb2; ENC11: Npy, Th, Dbh) did not
355 match the signature of our MENs cluster or that of the cluster of mesenchymal neurons in the
356 May-Zhang et al.[50] study (Table 1). We reasoned that the lack of MENs in the Morarach et al.[51]
357 data may be driven by the non-comprehensive nature of Baf53b-cre in this BAC transgenic mouse
358 line labeling all neurons. On immunolabeling LM-MP tissues from two P21 Baf53b-cre:*Rosa26*-
359 tdTomato mice with antibodies against Hu, we enumerated 1312 Hu$^+$ cells in the ileum (759 from
360 mouse 1 and 553 from mouse 2), 5758 Hu$^+$ cells in the proximal colon (3411 from mouse 1 and
361 2347 from mouse 2), and 3352 Hu$^+$ cells in the distal colon (1894 from mouse 1 and 1458 from
362 mouse 2), and found that a significant population of myenteric neurons did not express tdTomato

363 (Suppl. Fig. 6e, f). Given this non-comprehensive nature of the Baf53b-cre BAC transgenic line in
364 labeling all myenteric neurons, and the congruence between the transcriptomic profiles of cells
365 analyzed using the Baf53b-cre and the neural crest-specific Wnt1-cre lines, we infer that molec-
366 ular taxonomy performed on enteric neurons in the Morarach et al.[51] dataset is restricted to NENs.

367 In a recent report, Elmentaite et al.[78] performed scRNAseq on dissociated single cells from the
368 human gut at fetal, juvenile, and adult ages and catalogued multiple intestinal cell-types to gen-
369 erate a comprehensive gut cell atlas. Canonical enteric neurons, while adequately represented in
370 the fetal ages, were not found in the juvenile and adult ages which were dominated by mesen-
371 chymal and other cell types[78]. Given that our scRNAseq approach of sequencing diverse cell
372 types from the murine gut wall without any marker-based pre-selection was similar to this ap-
373 proach in human tissue, we reasoned that MENs would also be represented in their description
374 of mesenchymal cell clusters, especially in the juvenile and adult ages. To detect putative MENs
375 in this human gut cell atlas data, we projected the entire human mesenchymal cell scRNAseq
376 dataset into the four murine MEN-specific NMF patterns and detected putative human MENs
377 clusters (Suppl. Fig 4h). Since our identification of MENs and the generation of MEN-specific NMF
378 patterns was based on post-natal healthy murine tissue, we next projected data from only post-
379 natal healthy mesenchymal clusters into the four MEN-specific NMF patterns (Fig 6b). The four
380 patterns identified a population of cells within the post-natal intestinal mesenchymal cell clusters
381 suggesting that these cells are putative MENs in the human gut (Fig 6b). These putative MENs,
382 which map to Cluster 1 in our representation of the intestinal mesenchymal cells from the post-
383 natal gut cell atlas data (Fig 7a) were annotated previously by Elmentaite et al. as transitional
384 stromal cells (Fig 7b). We next tested and found that the MENs marker Dcn (Fig 7c) along with
385 pan-neuronal Uchl1 among other neuronal markers Hand2, Stx3, Slc17a9, Pde10a and Tubb2b
386 (Fig 7d) that we earlier showed to be expressed by adult murine MENs, were expressed by the
387 putative MENs in the adult human gut.

388 We hypothesized that the reason these cells were not annotated as enteric neurons was due to
389 the use of a NENs-restricted gene list. Apart from the NENs marker Ret, such gene lists often
390 contain the pre-synaptic gene Snap25, a component of the SNARE complex, which is widely
391 assumed to be a pan-neuronal marker in the adult ENS[48,49,79,80]. While we have previously ob-
392 served the NENs-specific nature of RET, our transcriptomic data suggests that MENs either do
393 not express Snap25 or do so in very small amounts (Suppl. Fig 4d). We tested the expression of
394 SNAP-25 by NENs and MENs in the myenteric ganglia of an adult Wnt1-cre:*Rosa26*-tdTomato
395 mouse and found that SNAP-25 expressing neurons expressed tdTomato, but not the MENs-
396 marker MHCst, suggesting the NEN-specific expression of this canonical marker for synaptic neu-
397 rons (Fig 8a). Next, we used a validated Snap25-Gcamp knock-in mouse line[81-83], where
398 GCamp/GFP is knocked in at the Snap25 locus and hence is expressed by Snap25-expressing
399 cells, to confirm that the expression of Snap25 is indeed restricted to a subset of myenteric neu-
400 rons in the adult LM-MP layer. By using antibodies against Hu and against GFP, we found that
401 the expression of Snap25-GFP is indeed restricted to a subset of adult myenteric neurons (Fig
402 8b). Finally, by immunolabeling adult small intestinal LM-MP of Snap25-Gcamp mice with anti-
403 bodies against MHCst and against GFP, we confirmed the lack of Snap25 expression by a pop-
404 ulation of MENs (Fig 8c). The low or lack of expression of Ret, Snap-25, Elavl3 and Elavl4 in
405 MENs as observed both by us and May-Zhang et al.[50] may help explain why these canonical gene
406 lists missed the correct identification and annotation of MENs' neuronal nature in human da-
407 tasets[78]. Next, we examined the expression of MENs markers MHCst, MET, SLC17A9, and
408 DECORIN in LM-MP tissues from adult humans with no known gut motility disorder and found
409 them to be expressed by a population of myenteric neurons in normal adult human ENS (Fig 9;
410 Suppl. Fig 7a, b, c). Thus, our bioinformatic approaches and immunofluorescence analyses of
411 MEN-specific markers in adult human gut together shows that the human gut similarly contains a
412 population of MENs.

413 We next tried sub-clustering the MENs cell cluster in our scRNAseq data to study whether indi-
414 vidual subclusters could be discriminated on the basis of MENs markers or other genes. However,
415 at the current sequencing depth, these clusters did not yield meaningful information on specific
416 marker genes that could be used to define them (Suppl. Fig 8a, b).

417 **The proportion of mesoderm-derived neurons expands with age to become the dominant**
418 **population in the aging ENS**. Since the ENS at birth consists solely of NENs[13], we next studied
419 the birth-date and eventual expansion of the MEN lineage in the post-natal gut. Using Wnt1-
420 cre:*Rosa26*-tdTomato mouse line, we enumerated the tdTomato$^-$ MENs in LM-MP at different
421 ages and found a significant age-associated increase in MENs proportions (Fig 10a, b, c; One-
422 way ANOVA, $F = 117.6$, DFn, DFd = 5, 12; $p < 0.0001$). At P11, MENs were found only in few
423 isolated myenteric ganglia (Fig 10a) and together represented only ~5% of all myenteric neurons
424 (tdTomato$^-$ neurons: 4.12% ± 2.98 SEM; n = 1327 Hu$^+$ neurons counted from 3 mice), suggesting
425 that they originate shortly before this age. The proportion of MENs in myenteric ganglia rises
426 sharply thereafter: by P22, they account for ~30% of all neurons (tdTomato$^-$ neurons: 29.63% ±
427 1.229 SEM; n = 742 neurons counted from 3 mice); and at P60 they represent ~45% of all neurons
428 (tdTomato$^-$ neurons: 46.38% ± 4.62 SEM; n = 700 neurons counted from 3 mice). During the adult
429 ages, the proportions of MENs in the adult ENS remains relatively stable as at P180, MENs con-
430 tinue to represent roughly half of all myenteric neurons (tdTomato$^-$ neurons: 57.29% ± 3.62 SEM;
431 n = 586 neurons counted from 3 mice). However, MENs dominate the proportions of the aging
432 ENS as at the very old age of 17 months (P510), the ENS is populated almost exclusively by
433 MENs (Fig 10b; tdTomato$^-$ neurons: 95.99% ± 1.62 SEM; n = 996 neurons counted from 3 mice).
434 Thus, the proportions of NENs and MENs in the myenteric ganglia can be used as a biomarker
435 for deducing ENS age, as a healthy ENS dominant in NENs would be juvenile, one with roughly
436 equal proportions would be adult, and an aging ENS is dominated by MENs.

437 We next tested whether the representation of MEN-specific transcriptomic signatures show a sim-
438 ilar increase during the maturation and aging of the human gut. We tested whether the represen-
439 tation of the four MEN-specific NMF patterns (Fig 5a) increased with age in the human tran-
440 scriptomic data from Elmentaite et al.[78]. We grouped the transcriptomic data from the wide-range
441 of healthy post-natal specimens of the gut cell atlas into three groups: Juvenile (containing data
442 on 2910 cells represented by 10 samples within the age range of 4 – 12 years), Adult (containing
443 data on 3696 cells represented by 36 samples within the age range of 20 – 50 years), and Aging
444 (containing data on 2848 cells represented by 37 samples within age range of 60 – 75 years) and
445 tested whether the representation of the four MEN-specific patterns changed significantly be-
446 tween these age groups. Barring pattern 16 which showed a non-significant increase in projection
447 weights between the Juvenile and Aging samples (One-way ANOVA, F = 2.10, DFn, DFd = 2, 8,
448 p = 0.18), projection weights of MEN-specific pattern 27 (One-way ANOVA, F = 16.08, DFn, DFd
449 = 2, 8, p = 0.0016), pattern 32 (One-way ANOVA, F = 8.13, DFn, DFd = 2, 8, p = 0.01) and pattern
450 41 (One-way ANOVA, F = 9.818, DFn, DFd = 2, 8, p = 0.007) all show significant age-associated
451 increase in the human gut tissue (Fig 10d, every datapoint refers to mean projected pattern weight
452 for cells within a defined age or age range). This suggests that analogous to the age-associated
453 increase in MENs we observed in murine gut (Fig 10b), the proportions of MENs in the human
454 gut also might increase with age. We also found that the representation of MENs cluster (Cluster
455 1) in the post-natal human gut cell atlas data expanded with maturation and age (Suppl. Fig 7d)

456 **GDNF and HGF levels regulate the populations of the neural crest-derived and the meso-**
457 **derm-derived neurons, respectively, in the maturing ENS.** GDNF-RET signaling is responsi-
458 ble for proliferation and neurogenesis from NC-derived ENS precursor cells during development
459 as well as for the survival of Ret-expressing enteric neurons[84-87]. Similarly, HGF signaling has
460 been shown to be essential for the proliferation of mesoderm-derived cells[88]. Since the expression
461 of the HGF receptor MET and the GDNF receptor RET is exclusive to MENs and NENs

462 respectively, we studied the correlation between age and levels of HGF and GDNF in LM-MP (Fig
463 10e, f). Given that both GDNF, as well as HGF expression is found in the LM-MP layer[44,89,90], we
464 used LM-MP tissue to study how the levels of these two trophic factors change in and around the
465 ENS tissue during maturation. We found that in agreement with a previous report[88], GDNF protein
466 levels are markedly reduced between the P10 and the P30 ages and remains reduced thereafter
467 up to the P90 age (Fig 10g; n = 3 mice/age-group, F = 6.821, DFn, DFd = 1, 7, p = 0.0348, One
468 way ANOVA). In addition, expression of Gdnf transcripts show significant reduction between the
469 ages of P30 and P90 (Fig 10h; n = 6 mice/age-group, P30: 1.070 ± 0.179 SEM, P90: 0.539 ±
470 0.129 SEM, p = 0.037, Student's t-test). On the other hand, HGF expression increases progres-
471 sively between P10 and P90 ages (Fig 10i, j: n = 3 mice/age-group, Protein levels: F = 8.820,
472 DFn, DFd = 1, 7, p = 0.02; mRNA levels: F = 36.98, DFn, DFd = 1, 16, p < 0.0001, One way
473 ANOVA). The ratio of HGF to GDNF expression in ileal LM-MP tissue shows significant increase
474 from the age of P10 to P90 (Suppl. Fig 9a, F = 48.60, DFn, DFd = 1, 7, p = 0.0002, One way
475 ANOVA), and HGF expression is consistently higher than GDNF expression in the full thickness
476 small intestinal tissue from adult and aging mice in the Tabula muris data[91] (Suppl. Fig 9b). We
477 then queried the plasma proteome levels from the LonGenity cohort of 1,025 aging individuals
478 and found that HGF levels correlated positively, while GDNF and RET levels correlated negatively
479 with age (Suppl. Fig 9c)[92], suggesting parallels between our data from murine intestine and hu-
480 man plasma proteome data.

481 Since GDNF tissue levels are correlated with NENs proportions, we hypothesized that GDNF
482 signaling regulates NENs proportions in maturing and adult ENS. On administration of GDNF or
483 saline to cohorts of P10 Wnt1-cre:*Rosa26*-tdTomato mice over 10 days[84,93], we found that GDNF
484 treatment promoted the juvenile phenotype by enhancing the proportions of tdTomato^{+} NENs and
485 correspondingly reduced the proportion of tdTomato^{-} MENs in P20 mice to a level similar to that
486 seen at the P10 age, while retaining the MENs proportions in saline-treated control mice remained

487 at a level expected of its age (Fig 10k; Controls: %MENs: 25.87 ± 4.37 SEM of 1350 neurons
488 from 3 mice; GDNF: %MENs: 3.86 ± 0.07 SEM of 1301 neurons from 3 mice; p = 0.0072; Stu-
489 dent's t-test). Consistent with a previous report[84], the GDNF-driven expansion of NENs and as-
490 sociated contraction of MENs conserved the total neuronal numbers (Fig 10k; Controls: neu-
491 rons/ganglia = 20.60 ± 4.00 SEM; GDNF: neurons/ganglia = 24.39 ± 6.96 SEM; p = 0.52; Stu-
492 dent's t-test).

493 Since HGF tissue levels increase with age, we hypothesized that increasing HGF signaling drives
494 the expansion of MENs in the maturing gut. HGF administration to cohorts of P10 Wnt1-
495 cre:*Rosa26*-tdTomato mice over 10 days promoted an increase in the tdTomato$^-$ MENs popula-
496 tion in P20 mice to levels previously observed in P60 mice, while tissues from saline-treated con-
497 trol mice exhibited a MENs:NENs ratio that is expected at P20 (Fig 10l; Controls: %MENs: 27.40
498 ± 5.49 SEM of 1970 neurons from 5 mice; HGF: %MENs: 49.37 ± 5.52 SEM of 1704 neurons
499 from 5 mice; p = 0.02, Student's t-test). Similar to GDNF treatment, HGF treatment also did not
500 cause any significant change in total neuronal numbers (Fig 10l; Controls: neurons/ganglia =
501 20.35 ± 2.22 SEM; HGF: neurons/ganglia = 18.21 ± 0.69 SEM; p = 0.38, Student's t-test).

502 **Transcriptomic evidence of MENs genesis.** As the proportions of MENs in the myenteric plexus
503 rise significantly between the ages of P10 and P30, we reasoned that this phase was accompa-
504 nied by significant neurogenesis of MENs. To provide transcriptomic evidence that MENs popu-
505 lations indeed expand during this phase, using 10X Genomics v3.1, we again performed unbiased
506 scRNAseq and agnostic clustering, this time on unsorted cells from the myenteric plexus layer of
507 two male mice of P21 age, when the MENs population is still expanding (Suppl. Fig 10a). Using
508 NMF-generated MENs patterns to run projectR-based analyses (Suppl. Fig 10b) and by using the
509 NENs and Neuroglia-specific markers, we again annotated the neuroglia, the NENs, and the
510 MENs as before and found that at this age, we were able to sequence a similar number of MENs
511 and NENs (~500 cells) along with a large number (~800) of neuroglia cells (Fig 11a). The

512 expression of Met was again detected in the MENs cluster, as well as in a small subset of Ret-
513 expressing NENs in the P21 cluster (Suppl. Fig 10c). MENs showed significantly higher UMI per
514 cell, when compared to neural crest-derived cells (NENs and neuroglial cells) (Suppl. Table 4,
515 One-way ANOVA; $F = 187.4$, DFn, DFd = 2, 1877, $p < 0.0001$), which we expected given the
516 larger size of MENs[94] (Suppl. Fig 4a). By immunolabeling LM-MP tissue from 3 P21 Wnt1-
517 cre:*Rosa26*-tdTomato male mice with antibodies against MET, we found that proportions of MET-
518 expressing neurons at this age were significantly higher in the population of tdTomato-negative
519 MENs than in the population of tdTomato$^+$ NENs (of 152 MET-immunolabeled neurons across 3
520 mice, 81.51 ± 1.55 S.E.M. were tdTomato-negative MENs). The Met and Ret co-expressing NENs
521 cluster in our data were described as populations of neural crest-derived Chat$^+$ Calcb$^+$ neurons
522 by Zeisel et al.[48] at the P21 age (Suppl. Fig 10d), where they were annotated as ENT6, 8, and 9
523 clusters (and which correspond to clusters ENC1, 3, 4, 7, 6, and 7 in the Morarach et al.[51] data-
524 base). These Met- and Ret-co-expressing neurons were also described by Avetisyan et al.[44] as
525 fetal-born neural crest-derived neurons that respond to both GDNF and HGF. By contrast, MENs
526 do not express Ret and hence are the only cell population that can respond to solely to HGF. This
527 data provides further evidence on the HGF-induced expansion of MENs during the juvenile phase.

528 We next performed *in silico* analyses on the MENs cluster using our recently published Tricycle
529 software[95], which is capable of inferring continuous cell-cycle position and can be applied to da-
530 tasets with multiple cell types, across species and experimental conditions, including sparse data
531 and shallow sequenced droplet-based dataset - thus allowing us to find evidence of cell cycling
532 in the MENs subset. P21 MENs scRNAseq data was projected into universal cell cycle principal
533 components (PCs) defined by the expression of 500 cell-cycle correlated genes and the continu-
534 ous cell cycle position (theta) was measured as the angle from the origin (Fig 11b). Based on
535 expression of 500 cell-cycle correlated genes, cells between 0.5π and 1.5π show hallmarks of
536 being cycling cells (Fig 11b). Our analyses showed that a significant number of cells in the MENs

537 cluster (213 out of 510) were present between 0.5 and 1.5π, which represents the mitotic position
538 in the continuous cell-cycle phase (Fig 11c). We confirmed our analyses by observing that the
539 expression of the cell cycle gene Top2a in the cells of the MENs cluster was highly correlated
540 with this phase (Fig 11d). Next, we found that a key cell cycle regulator gene Ect2 (epithelial cell
541 transforming 2), which encodes for the guanine nucleotide exchange factor protein ECT2, which
542 activates RhoA in a narrow zone at the cell equator in anaphase during cell division[96], was ex-
543 pressed in the MENs cluster and its expression was highly correlated with the cell's mitotic posi-
544 tion on the Tricycle plot (Fig 11e). We then used antibodies against ECT2 to immunolabel the LM-
545 MP from P21 mice and found expression of this key cell cycle regulator protein in DECORIN-
546 expressing and MHCst-expressing MENs at this age (Fig 11f, g). Thus, the Tricycle-based com-
547 putational analyses found evidence of cell cycling in the MENs cluster and identified a key cell
548 cycle gene Ect2 as a marker for putative MENs precursor cells.

549 **Reduced GDNF-RET signaling accelerates ENS aging to cause intestinal dysfunction.**
550 Since reduced GDNF or RET levels are associated with intestinal dysfunction in patients[80,97,98],
551 we hypothesized that alterations in GDNF-RET signaling unrelated to those seen with normal
552 aging, would cause dysfunction. To test this hypothesis, we studied lineage proportions and in-
553 testinal function in a mouse model of reduced RET signaling. Ret-null heterozygous mice, which
554 have been previously used to study the effect of reduced RET signaling in the adult ENS, have
555 normal ENS structure but altered gut physiology[84]. A similar mouse model with a Ret^{CFP} allele has
556 a CFP reporter inserted at its *Ret* locus rendering it null[99]. $Ret^{+/CFP}$ (or $Ret^{+/-}$) mice carrying a
557 single copy of the Ret gene showed significant reduction in Ret transcript and RET protein ex-
558 pression in the early post-natal murine gut[99]. Similarly, we found significantly reduced Ret tran-
559 script expression in the adult LM-MP of $Ret^{+/-}$ mice compared to age-matched wildtype $Ret^{+/+}$ mice
560 (Suppl. Fig 10e). In these mice, using antibodies against CFP/GFP, Hu, and MHCst, we confirmed
561 that the NENs marker Ret-CFP, and the MENs marker MHCst were expressed by different

562 neuronal subpopulations (Fig 12a). Using the adult $Ret^{+/-}$ mice, we tested the effect of partial Ret
563 loss on ENS lineages at two adult ages: 9 weeks (~P60) and 16 weeks (~P110). Using antibody
564 against CFP/GFP to detect CFP^{+} RET-expressing neurons, we found that $Ret^{+/-}$ mice show a
565 significant reduction in the proportions of Ret-CFP^{+} NENs (Fig 12b; 9 weeks: %CFP^{+} neurons:
566 24.91 ± 5.42 SEM of 837 neurons from 3 mice; 16 weeks: %CFP^{+} neurons: 13.13 ± 0.98 SEM of
567 1227 neurons from 5 mice; p = 0.03, Student's t-test). We observed a corresponding significant
568 increase in the proportions of $MHCst^{+}$ MENs with age in $Ret^{+/-}$ mice (Fig 12c; 9 weeks: %MENs:
569 58.74 ± 7.33 SEM of 644 neurons from 3 mice; 16 weeks: %MENs: 82.84 ± 3.58 SEM of 935
570 neurons from 5 mice, One-way ANOVA, p = 0.014), while control $Ret^{+/+}$ mice showed no signifi-
571 cant age-associated change in the proportions of MENs (Fig 12c; 9 weeks: %MENs: 43.27 ± 3.24
572 SEM of 780 neurons from 3 mice; 16 weeks: %MENs: 54.48 ± 4.07 SEM of 1276 neurons from 5
573 mice, One-way ANOVA, p = 0.36), which is consistent with our previous results that MENs pro-
574 portions in wildtype animals are relatively stable in this time window. The expedited loss of NENs
575 in $Ret^{+/-}$ mice confirms that depletion of endogenous RET signaling in the adult ENS accelerates
576 the aging-associated loss of NENs.

577 Having previously shown that aging mice have intestinal dysmotility[100], we tested whether the
578 increased loss of NENs in the $Ret^{+/-}$ ENS, concomitant with the expansion of MENs accelerated
579 ENS aging, causes an early onset of aging-associated intestinal dysmotility. We studied whole
580 gut transit time (WGTT) in a cohort (n = 8) of adult $Ret^{+/-}$ mice and their littermate control (n = 10)
581 $Ret^{+/+}$ mice over 7 weeks, between 9 and 16 weeks of age. While 9-week adult $Ret^{+/-}$ mice were
582 similar to control $Ret^{+/+}$ mice, WGTT between the two genotypes diverged with age. Consistent
583 with a prior report[84], 16-week old $Ret^{+/-}$ mice displayed significantly delayed intestinal transit

584 compared to age-matched control $Ret^{+/+}$ mice (Fig 12d; WGTT (in min) $Ret^{+/+}$: 121.4 ± 4.01 SEM;
585 $Ret^{+/-}$: 157.3 ± 14.62 SEM, p = 0.048; Student's t-test).

586 **GDNF reverts aging in the ENS to normalize intestinal motility.** Along with others, we have
587 previously shown that aging is associated with slowing of intestinal motility[101,102]. We hypothesized
588 that this may be a consequence of the replacement of the juvenile NENs population by MENs and
589 therefore GDNF supplementation, by restoring a more balanced MENs:NENs ratio, may prevent
590 age related changes in motility. We studied 17-month-old male mice (at an age where NENs
591 constitute only ~5% of all myenteric neurons; Fig 10c) before and after they received 10 days of
592 intraperitoneal injection of GDNF or saline (n=5 for each cohort). While the two cohorts showed
593 no significant difference in their intestinal transit times at baseline (WGTT (in min) Control: 192.8
594 ± 11.55 SEM; GDNF: 202.4 ± 7.60 SEM, p = 0.50, Student's t-test), GDNF treatment caused
595 significant improvement in intestinal transit (Fig 13a, WGTT (in min) Control: 175.0 ± 8.89 SEM;
596 GDNF: 101.0 ± 8.91 SEM, p = 0.0004, Student's t-test), reaching levels previously observed in
597 healthy mice (Fig 12d).

598 GDNF treatment significantly reduced the proportions of $MHCst^{+}$ MENs (Fig 13b; Suppl. Fig 11a,
599 b; Control: %MENs: 88.76 ± 1.48 SEM of 909 neurons from 5 mice; GDNF: %MENs: 74.12 ± 5.98
600 SEM of 799 neurons from 5 mice; p = 0.045; Student's t-test) while increasing the numbers of
601 RET^{+} NENs (Fig 13c; Suppl. Fig 11c, d; Control: RET^{+} neurons: 1.35 ± 0.05 SEM in forty-two 40X
602 fields from 4 mice; GDNF: RET^{+} neurons: 3.19 ± 0.56 SEM in forty-one 40X fields from 4 mice, p
603 = 0.017; Student's t-test). Consistent with our earlier observation, GDNF treatment did not change
604 the average neuronal numbers in the ileal myenteric ganglia (Control: 17.56 ± 1.82 SEM neurons
605 per ganglia, GDNF: 16.01 ± 1.22 SEM neurons per ganglia, p = 0.49, Student's t-test).

606 **The two neuronal lineages in human disease.** In addition to the detection of MENs in the adult
607 healthy gut by bioinformatic and immunofluorescence means (Fig 4, 5, 6, 7), we next examined

608 the relevance of the two neuronal lineages NENs and MENs in human disease. For this, we tested
609 whether gut dysfunction associated with pathological reductions in NENs-signaling mechanisms
610 are also associated with increased abundance of MENs. We mined previously generated and
611 publicly available transcriptomic data from intestinal tissues from humans with normal gut motility
612 (controls) and from patients with obstructed defecation (OD) associated with enteric neuropa-
613 thy.[100]. In this dataset, Kim et al. have previously shown that OD patients have significantly re-
614 duced intestinal expression of Gdnf and Ret[100]. Again, using our transfer learning tool *Pro-*
615 *jectR*[69,103], which allowed us to query bulk-RNAseq data across species to estimate relative use
616 of MENs-specific NMF-patterns generated earlier, we tested whether the usage of MENs-specific
617 NMF-patterns was significantly altered between transcriptomes of OD patients and healthy hu-
618 mans (n = 3/group)[100]. This projection analysis indicated that 2 of the 4 MENs-specific NMF-pat-
619 terns showed significantly higher usage in OD samples compared to controls (Fig 14a, Suppl. Fig
620 12; Student's t-test, $p < 0.05$), providing evidence that the enteric neuropathy in these patients is
621 associated with a relative increase in MENs-specific transcriptional signatures. We further queried
622 the differential gene expression analysis performed by Kim et al and found that in addition to Gdnf
623 and Ret (as reported by them) other important NEN genes (Snap25 and Nos1) were also signifi-
624 cantly downregulated while the MEN marker genes identified in this study (Clic3, Cdh3, Slc17a9)
625 (Fig 14b) were significantly upregulated.

626 **Discussion**

627 Current dogma states that the adult ENS is exclusively derived from neural crest precursors that
628 populate the gut during fetal development[104]. The results of this study indicate a much more com-
629 plex system, one in which the fetal and early life "juvenile" ENS consisting of neural crest-derived
630 enteric neurons (NENs) is incrementally replaced during maturation by mesoderm-derived enteric
631 neurons (MENs). Eventually, the aging ENS consists almost exclusively of the neurons of the
632 MEN lineage. Using a combination of floxed transgenic reporters bred into multiple lineage fate

633 mapping transgenic mice, this study also provides the first definitive evidence of a significant
634 mesodermal contribution to any neural tissue. Previously, the mesoderm and especially the Lat-
635 eral Plate Mesoderm (LPM) was known to give rise to diverse cell-types within the viscera, includ-
636 ing several in the gut[105], and our study shows that cells of this embryonic derivation also give rise
637 to ENS neurons. A previous report on a dual origin of the ENS described adult enteric neurons
638 from Foxa2$^+$ or Sox17$^+$ precursors[14] and inferred that these were endodermal in origin. However,
639 Foxa2 and Sox17 are also expressed by mesoderm-derived cells[25-28]. By contrast, using two NC-
640 lineage-traced mouse lines (Wnt1-cre and Pax3-cre), two lineage-traced mouse lines marking
641 mesodermal derivatives (Tek-cre, and Mesp1-cre), and robust adult mesoderm markers, we iden-
642 tify a population of Mesp1-derived MHCst- and MET-expressing adult enteric neurons, which
643 makes up the entire non-NC-derived population of myenteric neurons. These results provide ro-
644 bust evidence that the second source of adult enteric neurons is the mesoderm, and not the
645 endoderm.

646 **Distinct neuronal nature of MENs**. While the developmental origins of neurons have been
647 thought to be restricted to the neural tube and the neural crest, many neurons – such as placode-
648 derived neurons, have been known to be derived from non-neural tube, non-neural crest devel-
649 opmental lineages[106]. Similarly, while supposed pan-neuronal markers, such as Snap25, are ex-
650 pressed specifically by neurons, not all neurons express Snap25[107]. Indeed, release of neuro-
651 transmitters may occur independently of Snap25[108-113], suggesting that the expression of this pro-
652 tein is not central to neuronal functions. These present us with important context based on which,
653 one can study the data generated using multiple lines of evidence to infer the neuronal nature of
654 MENs. *Firstly*, we show that MENs are intra-ganglionic cells, which conditionally express report-
655 ers under mesoderm-specific lineage fate mapping models and are labeled with antibodies
656 against the neuronal marker Hu. *Secondly,* MENs show expression of important ENS neurotrans-
657 mitter-encoding or generating proteins CGRP, NOS1, and ChAT. *Thirdly,* with our single cell

658 transcriptomic analysis, where we used the markers Calcb, Met, and Cdh3 that we had validated
659 to identify and annotate the MEN cell cluster, we discovered an additional set of neuronal-specific
660 marker genes (Pde10a, Vsnl1, Stmn2, Stx3, Tubb2b, Slc17a9, Hand2, Gpr88, Elavl2, Ntf3) which
661 were found to be expressed widely or selectively within MENs. These markers include both novel
662 as well as established enteric neuronal markers[2,60,114]. *Fourthly*, further transcriptomic analyses
663 of the MENs scRNAseq cluster identifies the expression of many other neuronally significant
664 genes – including those encoding for ion channels, neurotransmitter receptors, hormones, cal-
665 cium channels, etc. – which provide a further glimpse into the diverse neuronal functions of MENs.
666 *Finally*, our analyses shows that MENs express the pan-ENS-expressed gene Phox2b, and that
667 our MENs scRNAseq cluster maps to a neuronal cluster in the May-Zhang et al.[50] database, which
668 is annotated as a 'mesenchymal neuron' cluster[50]. Our data, together with our analyses of publicly
669 available data, thus provides evidence on the neuronal nature of MENs. While the co-expression
670 of aforementioned pan-neuronal markers establishes the neuronal nature of MENs, the expres-
671 sion of set of key genes in MENs suggests putative specialized functional roles of these subpop-
672 ulations when they co-exist with NENs in adults. These include the expression of genes associ-
673 ated with putative sensory (Calcb)[115], neuromodulatory (Ntf3)[116], secretory (Cftr)[117], immunomod-
674 ulatory (Il18)[2], hormone regulating (Ghrh)[118], extracellular matrix (ECM)-modulating (Dcn), and
675 motility-regulating roles (Slc17a9 or VNUT)[119]. These MEN-enriched or MEN-specific expression
676 profiles suggest that MENs perform various roles in the regulation of diverse gastrointestinal func-
677 tions. While the current scRNAseq data is restricted in providing meaningful cell clusters that can
678 inform the true functional diversity of MENs, future work will provide detailed analyses and func-
679 tional characterization of MENs.

680 Beyond establishing the neuronal nature of MENs, our analyses also help establish the distinct
681 neuronal nature of MENs. Based on the lineage fate mapping experiments with multiple combi-
682 nations of neural crest and mesoderm lineage fate mapping mice models and based on the

683 expression of mesoderm-specific markers such as MHCst and Decorin, we identified that MENs
684 are a population of mesoderm-derived cells. MHCst is a subset of myosin heavy chain isoforms
685 that has been previously shown to be specifically expressed by a subset of mesoderm-derived
686 muscle cells[120]. While prior reports do not clarify the nature of the exact epitope and the gene
687 responsible for MHCst, the expression of the smooth muscle myosin heavy chain protein MYH11
688 specifically in MENs suggests that the epitope detected by the anti-MHCst antibody in MENs is
689 of the mesoderm specific protein MYH11 protein.

690 Further, our bioinformatic analyses of the human gut cell atlas data generated by Elmentaite et
691 al.[78] also shows the existence of a putative MENs-like cell cluster in the human gut, which shows
692 a similar co-expression of mesenchymal and neuronal markers as observed by us in our MENs
693 cluster and by May-Zhang et al.[50] in their 'mesenchymal neuronal' cluster. Indeed, Elmentaite et
694 al.[78] identified this supposed mesenchymal cluster by the expression of the mesoderm-specific
695 gene Decorin. Further, by observing the co-expression of neuronal and mesoderm-specific mark-
696 ers in human gut tissue, we validate the presence of neurons that express mesoderm-specific
697 markers or MENs in adult human tissue.

698 **Detection and identification of MENs in other datasets.** Recent studies have significantly in-
699 creased our understanding of the molecular nature of various classes of enteric neurons. How-
700 ever, these studies differ significantly in their methods and tools used, which have precluded them
701 from detecting or correctly identifying the developmental origins of MENs. While May-Zhang-et
702 al.[50] observed the presence of a small neuronal cluster that expressed mesenchymal marker
703 genes, their study did not further interrogate the developmental origins of the 'mesenchymal' en-
704 teric neurons. Drokhlyansky et al.[49] in their unbiased MIRACL-seq analyses and Elmentaite et
705 al.[78] in their human gut cell atlas datasets detected the MENs cluster but could not correctly iden-
706 tify their neuronal nature, possibly owing to the expression of mesenchymal genes in this cluster,
707 and also due to the absent or lower than expected expression of canonical neural markers such

708 as Ret and Snap25. In contrast to these studies that performed single cell or nuclear tran-
709 scriptomic studies that were unbiased by lineage markers, other transcriptomic datasets from
710 Drokhlyansky et al.[49], Wright et al.[22], and Zeisel et al.[48] were generated using enriched neural
711 crest-derived cells, which contributed to the absence of MENs in these datasets. An important
712 outlier to these studies is Morarach et al.[51] from the Marklund group, which utilized the newly
713 characterized BAC-transgenic line Baf53b-cre to label and flow sort enteric neuronal cells for
714 subsequent single cell RNA sequencing. Our analysis of ileal and colonic tissue from this line
715 shows that it does not comprehensively label all enteric neurons. While this may seem at odds
716 from the Morarach et al.[51] report, this apparent difference in the behavior of this transgenic line
717 can be explained by the fact that in contrast to the established and accepted practice of counting
718 all Hu-immunolabeled neurons employed by us and others[22,50,121], the Morarach et al. study re-
719 stricted the enumeration to only include neurons that showed only cytoplasmic and not nuclear
720 expression of Hu. Neuronal Hu proteins (HuB, HuC, and HuD) show both nuclear and cytoplasmic
721 localization[122], and since the Morarach et al.[51] study only enumerated cytoplasmic Hu-expressing
722 neurons, their characterization of this transgenic mouse line was performed using only a subset
723 of all neurons. In addition, compared to Drokhlyansky et al.[49], Wright et al.[22], and May-Zhang-et
724 al.[50] whose protocols for neuronal enrichment were based on flow sorting neuronal nuclei, the
725 Marklund group (in both Zeisel et al.[48] and Morarach et al.[51]) performed flow sorting of late post-
726 natal enteric neuronal cells, which can cause significant stress on neuronal cells. These factors,
727 together with the BAC transgenic nature of the Baf53b-cre line, may have contributed to the lack
728 of MENs in the Morarach et al.[51] data. Further, all neuronal cells described in the Morarach et al.[51]
729 study express Snap25 (which we show is not expressed by all adult enteric neurons), and mostly
730 map to known neural crest-derived cell clusters identified in Zeisel et al.[48]. This suggests that the
731 rich transcriptomic atlas of enteric neurons generated by deep transcriptomic profiling of Baf53b-
732 cre-derived neurons carried out by Morarach et al.[51] is restricted only to the NENs, which comprise
733 of half of all adult enteric neurons. Thus, prior experimental data could not establish the true

734 developmental identity, correct annotation, and transcriptomic definition of a population of meso-
735 derm-derived neurons or MENs in murine and human tissue.

736 By contrast, we were able to correctly identify the MENs cluster in unbiased scRNAseq of adult
737 murine LM-MP cells and use it to both identify and validate the expression of MENs-specific mark-
738 ers in the adult murine LM-MP tissue, as well as use bioinformatic analyses to identify the MENs
739 in publicly available murine data from May-Zhang et al.[50] and human data from Elmentaite et al.[78].
740 This allowed us to show the expression of MENs markers MHCst, MET, DCN, and SLC17A9 in
741 many enteric neurons in adult humans, suggesting that the mesoderm-derived ENS may be a
742 feature common to mice and humans alike. MENs in both species can readily be identified by
743 their expression of MENs-specific markers, thus providing a convenient tool to further identify and
744 study these neurons.

745 **Development of MENs and MENgenesis.** The presence of small population of MENs in the gut
746 at the post-natal age day 10 (P10) and their expansion during maturation suggests that key
747 timepoints in their development correspond with the post-natal development of the ENS. Im-
748 portantly, since MENs populations are expanding at this age, performing scRNAseq-based bioin-
749 formatic analyses of the juvenile LM-MP cells not only provided us with the computational evi-
750 dence of significant cell cycling in the MENs cluster at this age, but also provided us with the
751 information on Ect2, a cell-cycle marker expressed by cycling putative MENs precursor cells. Ect2
752 transcripts were found expressed by cycling cells within the MENs cluster at the P21 age, which
753 also showed significant enrichment in the expression of the cell-cycle gene Top2a. Except for a
754 cluster of cells annotated as proliferating glial cells that show expression of the cell cycle gene
755 Top2a, Ect2 gene expression is not detected in other murine myenteric neural crest-derived cells
756 in the scRNAseq study performed by Zeisel et al.[48] at the P21 juvenile age. Our anatomical ob-
757 servation on the expansion of the MEN population in the adolescent gut along with the computa-
758 tional evidence of cell cycling in the MENs cluster at this age, and the detection and validation of

759 Ect2 gene expression in a subset of MENs provide evidence of significant MENgenesis during
760 the juvenile phase. ECT2 expression was found in MHCst- and DCN-expressing myenteric cells
761 at this age, suggesting that many of these are proliferating MEN-precursor cells, and may not be
762 terminally differentiated functional neurons.

763 The rapidly expanding MEN population is 10-11 days old in the P21 post-natal gut (as they origi-
764 nate in the gut just before P10 post-natal age) and thus, the age at which these cells partake in
765 regulation of diverse gastrointestinal functions is yet unknown. This important issue precludes us
766 from using the two MENs transcriptomic datasets to compare how MENs functions change with
767 age. Prior studies have reported on the differing birthdates of various neural crest-derived enteric
768 neuronal sub-populations in the developing fetal gut[9,51,123]. Similar studies need to be performed
769 in the future to understand the birthdates of the various subpopulations that comprise MENs, and
770 to ascertain when do they become functional. A recent study by Parathan et al.[121] highlighted
771 important neuronal and neurochemical changes in the adolescent gut. Further studies on how the
772 ENS matures and ages thus need to be performed in the context of NENs and MENs to truly
773 understand how shared and distinct functions of these two lineages change with maturation and
774 age. A crucial aspect of this work will require further identifying the molecular markers for the
775 Ect2-expressing proliferating MEN progenitor cells. Our earlier work showed that Nestin-express-
776 ing neural progenitor cells are neural crest-derived cells that contribute to steady state neurogen-
777 esis in the adult ENS[19], thus suggesting that MENs are derived from Ect2-expressing non-Nestin^{+}
778 precursor cells.

779 **Use of scRNAseq to identify MENs.** The use of single cell and single nucleus transcriptomic
780 approaches provides an important tool that has been recently used to perform molecular taxon-
781 omy of fetal and post-natal enteric neurons and glial cells[22,48,50,51]. In addition to performing deep
782 sequencing that allows for cluster-based molecular taxonomy, these tools can also be utilized for
783 identification of novel cell types, where prior information on their presence and marker expression

784 is unknown[52,95,124-126]. Compared to the other studies that utilized this tool to study the ENS, we
785 used the single cell transcriptomics to both confirm the presence of MENs and identify more MEN-
786 specific markers; as well as to use the MEN-specific transcriptomic signature to query their pres-
787 ence in other murine and human datasets. In contrast to its use for performing molecular taxon-
788 omy, which requires deep sequencing of an enriched cell population, our strategy of opting for a
789 lower read depth (shallow sequencing) is efficient, practical, and economical for discovering and
790 identifying novel celltypes[52]. In addition, even if a gene is being expressed at a medium - low
791 level, there is a certain probability that it will not be detected by scRNAseq in both deep and
792 shallow sequencing approaches. This is important since the older v2.0 10X Genomics chemistry
793 (used for our 6-month dataset) captures only 10-14% of the cellular transcriptome, and that from
794 the newer v3.1 chemistry (for our P21 data) captures only a third of the transcriptome from a
795 suspension of homogenous single cells[127,128]. While a partial solution to this issue is to increase
796 sequencing depth, beyond a certain point, this strategy leads to diminishing returns as the fraction
797 of PCR duplicates increases with deeper sequencing. While getting insights into cellular hetero-
798 geneity of MENs is important for furthering our understanding of how they regulate diverse gut
799 functions, the transgenic mice that can specifically label only MENs or all enteric neurons to allow
800 for their enrichment are currently not available[49,48,22,51,68,50]. Without the availability of MENs-spe-
801 cific transgenic models, the scRNAseq strategy employed by us is the only currently available tool
802 for querying the transcriptome of MENs. These reflect significant bottlenecks that have disallowed
803 the comprehensive and an in-depth characterization of all enteric neurons in all the current studies
804 on the adult ENS.

805 **Expression of MET and RET by MENs and NENs.** Since our scRNAseq data highlighted the
806 lineage-specific nature of the expression of Ret and Met in the adult ENS, we studied whether
807 these genes regulated the origin, expansion, and maintenance of the neuronal populations that
808 express them. The expression of MET by MENs in the mature adult ENS is consistent with an

809 earlier study by Avetisyan et al. that reported that a deletion of Met in the Wnt1-cre expressing
810 NC-lineage did not alter the abundance of MET^+ neurons in the adult ENS[44]. If Met was expressed
811 solely by neural crest-derived cells, then the loss of MET by enteric neurons would have been
812 expected since the conditional deletion of Met gene in this floxed Met transgenic animal has been
813 observed to cause a significant or comprehensive loss of MET protein expression in other or-
814 gans[129,130,131,132]. While at first glance, observations of the mutually exclusive nature of RET and
815 MET provided by us and by Avetisyan et al.[44] in the adult gut might not agree with Zeisel et al.'s[48]
816 observed co-expression of Ret and Met transcripts in NENs at the P21 developmental stage, our
817 observation that a small proportion of NENs in the P21 gut express MET helps provide an expla-
818 nation. Our P21 data and the data from Zeisel et al.[48] are consistent with one of the observations
819 made by Avetisyan et al.[44], who showed the existence of a population of fetal neural crest-derived
820 enteric neurons that are co-dependent on GDNF and HGF and hence would express both RET
821 and MET. In contrast to these observations made in the fetal and juvenile ENS, the anatomical
822 observations made by Avetisyan et al.[44] in the adult ENS (where MET immunoreactivity in the
823 adult enteric neurons is exclusive of Ret expression) suggests that the population of fetal-derived
824 Ret and Met co-expressing neurons is lost after maturation. Compared to the P21 scRNAseq data
825 from Zeisel et al.[48] that shows that all Met-expressing neural crest-derived neurons co-express
826 Calcb (CGRP), Ret, and Chat, Avetisyan et al.'s anatomical data in the adult gut shows that de-
827 spite accounting for a third of all enteric neurons and expressing CGRP, MET-expressing adult
828 enteric neurons do not co-express Ret and only a small proportion of these MET^+ neurons co-
829 express ChAT. Thus, Avetisyan et al.'s data agrees with our data on the adult ENS which shows
830 exclusive expression of RET and MET by NENs and MENs, respectively, and that while MENs
831 consist of a large proportion of CGRP-expressing MET^+ neurons, they contain only a small pop-
832 ulation of ChAT-expressing neurons. Along with Avetisyan et al.'s data, our data suggests that
833 the adult small intestinal myenteric plexus contains a significant proportion of neurons that do not
834 immunolabel with antibodies against NOS1 or ChAT. This observation is consistent with earlier

835 data from Parathan et al.[121] who showed that ~35-40% of small intestinal myenteric neurons from
836 6-week-old mice did not immunolabel with antibodies against NOS1 or ChAT.

837 Since they do not express the neural crest-marker RET, MENs are the only neuronal population
838 that respond to HGF alone. In this study, we show that MENs are dependent on HGF-MET sig-
839 naling in a manner analogous to the requirement of GDNF-RET signaling by NENs. While our
840 study does not discount that the exogenous HGF supplementation in juvenile mice may alter
841 proportions of RET and MET-co-expressing neurons within the NENs subpopulation, our report
842 focuses on HGF's ability to drive the expansion of MENs population in the ENS. Similarly, Ret
843 haploinsufficiency-mediated loss of the NEN lineage causes a proportional increase in the MEN
844 lineage, while maintaining overall neuronal numbers. Conservation of neuronal number, despite
845 significant shifts in the proportions of the two neuronal lineages suggests the presence of yet
846 unknown quorum sensing signaling mechanisms between the two lineages that reciprocally reg-
847 ulate their populations to maintain the structure of the post-natal ENS. This again implies the
848 existence of a yet undefined precursor cell responsible for the expansion of the MEN population
849 in a manner analogous to what we have previously described for NENs[19].

850 **Relevance to aging and human disease.** While it is known that Gdnf expression in the mature
851 gut is significantly downregulated[44,84,93,133], the functional consequences of this loss have been
852 unclear[84]. We found that reduced GDNF-RET signaling drives the age-dependent loss of NENs
853 as this loss can be slowed or reversed by GDNF supplementation and accelerated by further
854 reduction of Ret expression. In aging animals, GDNF-driven resuscitation of NENs was associ-
855 ated with a functional normalization of age-associated delay in intestinal transit. Our results iden-
856 tify a novel role for GDNF in maintaining or resuscitating the canonical NEN population, while
857 preserving overall enteric neuronal numbers. In the last few years, studies have focused on iden-
858 tifying juvenile protective factors (JPFs), the loss of which correlates with or drives maturation-
859 and aging-associated phenotypes[134]. In this context, GDNF may therefore qualify as a JPF or a

860 *senolytic* as its presence maintains the dominance of NENs in maturing ENS, corresponding to a
861 juvenile phenotype; and its re-introduction promotes and resuscitates the genesis of NENs in
862 adult and aging gut to restore healthy gut function. The exact nature of the cells that respond to
863 GDNF re-introduction and generate NENs is yet unknown, but it can be hypothesized that these
864 may include Nestin^{+} enteric neural stem cells and/or GDNF-responsive Schwann cells[19,135]. In
865 addition to its effect on resuscitating NENs, acute administration of GDNF also augments peri-
866 staltic motility by increasing neuronal activity[22,136]. Since the aging gut has a very small number
867 of RET-expressing GDNF-responsive NENs, we assume that GDNF-driven normalization of in-
868 testinal motility would first increase the proportions of RET-expressing NENs and then augment
869 their activation. This further emphasizes the importance of using GDNF or similar RET agonists
870 in the treatment of age-associated intestinal dysmotility.

871 While Avetisyan et al. showed that MET expression highly correlated with CGRP-expression in
872 the adult murine myenteric plexus[44], MET co-expression by all MHCst^{+} human enteric neurons in
873 our data and by all PGP9.5^{+} neurons in human enteric neurons by Avetisyan et al.[44] suggests that
874 MET-expression in the human ENS may not be restricted to CGRP-expressing IPANs. In addition,
875 recent data shows that our understanding of the nature of markers that can correctly identify
876 IPANs in the murine and human ENS is still evolving[50,137], suggesting that ascribing function to
877 neurons using a single marker may be incorrect.

878 The detection of MENs cluster in the post-natal and adult scRNAseq data in the gut cell atlas
879 generated by Elmentaite et al.[78], their increasing representation with age, and the subsequent
880 validation of the MEN-specific markers MHCst, MET and SLC17A9 in a subset of adult human
881 ENS neurons shows that our findings may be of clinical importance. Many gastrointestinal motility
882 functions are compromised with advancing age, resulting in clinically significant disorders[138] Alt-
883 hough the exact mechanisms will need to be worked out, our results indicate that a MENs-pre-
884 dominant ENS is associated with significant differences in gut motility. The progressive nature of

885 the change in enteric neuronal lineages with age may have pathological implications for the el-
886 derly gut when the balance is overwhelmingly in favor of MENs. Understanding the forces that
887 regulate parity between these two different sources of neurogenesis therefore holds the promise
888 of arresting or reverting progressive loss of gut motility with increasing age. Our results may also
889 have implications for the pathogenesis of disordered motility unrelated to aging, as downregula-
890 tion of Gdnf and Ret expression has been associated with diverticular disease and obstructed
891 defecation in adult patients[97,100,139]. GWAS analyses further showed that Gdnf gene was in the
892 eQTL associated with increased incidence of diverticular disease[140]. It is in this context that the
893 identification of SNAP-25 as a NENs marker gene and the transcriptomic pattern analyses of
894 patients with chronic obstructed defecation are significant. Expression of Snap25 is upregulated
895 by GDNF and is significantly downregulated in gut tissues of patients with diseases associated
896 with significant reduction in GDNF-RET signaling (diverticular disease and obstructed defeca-
897 tion)[80,97,100]. Thus, while earlier thought to be a pan-neuronal[49,141], establishing the identity of
898 SNAP-25 as a NEN lineage-restricted marker provides us not only with an important tool to query
899 proportions of NENs in murine and human tissue but also suggests the NENs-limited nature of
900 prior observations based on Snap25 transgenic animals[79,141]. Gut dysmotility disorders that pre-
901 sent with conserved ENS neuronal numbers[97] have puzzled investigators on the etiology of the
902 disease. Our results suggest an explanation based on NENs-to-MENs lineage shifts that conserve
903 overall enteric neuronal numbers with variable effects on function.

904 In conclusion, using multiple lines of evidence, we show that the ENS of the juvenile and mature
905 mammalian gut is dominated by two different classes of neurons that have distinct ontogenies
906 and trophic factors, associated with functional differences. The shift in neuronal lineage may rep-
907 resent a functional adaptation to changes in nutrient handling, microbiota or other physiological
908 factors associated with different ages. Further research in the functional differences between the
909 neuronal lineages and factors that regulate the parity between these two nervous systems in

910 humans during the lifetime will be important to advance our understanding of the adult ENS and

911 the treatment of age-related and other pathological disorders of gut motility.

912 **Acknowledgements**

913 We would like to thank Dr. Chulan Kwon (JHU) for his kind gift of the Mesp1-cre mice, Dr. Jeremy
914 Nathans (JHU) for his kind gift of the Tek-EGFP, Tek-cre and *Hprt*-tdTomato lineage-traced mice
915 and his support, and Dr. Vanda Lennon (Mayo Clinic) for her kind gift of the ANNA1 anti-Hu anti-
916 sera. We thank Dr. Akira Sawa (JHU) for his help with the *Rosa26*-EGFP mouse line, and Dr
917 Meera Murgai (NCI) for her help with the Myh11-cre^{ERT2}:*Rosa26*-YFP mouse tissues. We thank
918 Dr. Xinzhong Dong (JHU) and Dr. Mark Donowitz (JHU) for their support. The microscopy was
919 performed on the Ross Imaging Core at the Hopkins Conte Digestive Disease Center at the Johns
920 Hopkins University (P30DK089502) using the Olympus FV 3000rs (procured with the NIH-NIDDK
921 S10 OD025244 grant) and we thank Dr. George McNamara for his help with confocal training and
922 imaging. The 10X Genomics Chromium processing for scRNAseq was performed at the GRCF
923 Core and the sequencing was performed at the CIDR core at the Johns Hopkins University. S.K.
924 was funded through a grant from the Ludwig Foundation, a grant from the NIA (R01AG066768),
925 a pilot award from the Hopkins Digestive Diseases Basic & Translational Research Core Center
926 grant (P30DK089502), and a pilot award from the Diacomp initiative through Augusta University.
927 L.A.G was funded in part by a Johns Hopkins Catalyst Award and a grant from the NIA
928 (R01AG066768). J.S. was funded through the Maryland Genetics, Epidemiology, and Medicine
929 training program sponsored by the Burroughs Welcome Fund. P.J.P. was funded through the
930 Hopkins Conte Digestive Disease Center at the Johns Hopkins University (P30DK089502),
931 NIDDK (R01DK080920), the Maryland Stem Cell Research Foundation (MSCRF130005), and a
932 grant from the AMOS family.

933 **Author contributions**

934 S.K., and P.J.P. conceived the study; S.K., M.A., M.L, L.A.G. and P.J.P. designed the research
935 studies; S.K. L.B, C.Z, A.S., A.B., and M.S. conducted the experiments; S.K., Z.H., M.K., J.L.,

936 L.B., S.B., E.V., J.S., S.N., M.S., G.L., and L.A.G. acquired and analyzed the data; S.K., and P.J.P

937 drafted the manuscript.

938 **Methods**

939 *Animals*:

940 Experimental protocols were approved by The Johns Hopkins University's Animal Care and Use
941 Committee in accordance with the guidelines provided by the National Institutes of Health. Pres-
942 ence of vaginal plug was ascertained as 0.5 days post-fertilization and this metric was used to
943 calculate age of mice. Only male mice were used for the studies detailed in this report. The Wnt1-
944 cre:*Rosa26*-tdTomato lineage-traced line was generated as detailed before by breeding the
945 B6.Cg-Tg(*Wnt1-cre*) with the Ai14 transgenic mouse line (Jax #: 007914) containing the *Rosa26*-
946 tdTomato transgene[19,142,143]. The Wnt1-cre line used in this study is the well validated line for
947 studying neural crest derivatives previously used by us and others[18,19,22,48,144], and not the Wnt1-
948 cre2 line used by Drokhlyansky et al.[49]. We again validated the fidelity of this line by observing
949 whether any aberrant recombination occurred in our Wnt1-cre:*Rosa26*-tdTomato line by studying
950 the intestinal mucosal tissue and found that the line behaved expectedly to label neural crest-
951 derivatives and epithelial cells (Suppl. Fig 1i). Pax3-cre:*Rosa26*-tdTomato lineage-traced line was
952 generated by breeding the Ai9 transgenic mouse line (Jax #: 007909) with the Pax3-cre trans-
953 genic mouse (Jax #: 005549). The Wnt1-cre:*Hprt*-tdTomato mouse was generated by breeding
954 our aforementioned Wnt1-cre transgenic mouse line with the *Hprt*-tdTomato transgenic mouse
955 line (Jax #: 021428, kind gift from Prof. Jeremy Nathans). Mesp1-cre:*Rosa26*-tdTomato mice
956 were generated by breeding the Mesp1-cre transgenic mice[145] (gift from Dr. Chulan Kwon, JHU)
957 with the Ai14 transgenic mice. Mesp1-cre:*Rosa26*-GFP mice were generated by breeding the
958 Mesp1-cre transgenic mice with the *Rosa26*-EGFP transgenic mouse line (gift from Dr. Akira
959 Sawa, JHU). Neither the *Rosa26*-tdTomato (Ai14) line nor the *Rosa26*-EGFP line showed any
960 reporter expression in the absence of a cre driver (Suppl. Fig 1j, k). $Ret^{+/CFP}$ mice (MGI:3777556)
961 were inter-bred to get a colony of adult $Ret^{+/+}$ and $Ret^{+/CFP}$ mice. $Ret^{CFP/CFP}$ mice died at or

962 before term. Tek-cre:*Hprt*-tdTomato mice were generated by breeding Tek-cre transgenic mice
963 (also known as Tie2-cre; Jax #: 004128) with the *Hprt*-tdTomato transgenic mouse line. 17-month-
964 old male C57BL/6 mice from the aging mouse colony of the National Institute of Aging were pro-
965 cured for the GDNF-treatment experiment.

966 *Human Tissues:*

967 Human tissues were obtained under IRB protocol IRB00181108 that was approved by Institutional
968 Review Board at the Johns Hopkins University. Pathological normal specimens of human duode-
969 num and colon were obtained post-resection. Tissues were obtained from adult donors and were
970 de-identified such that the exact age, gender, and ethnicity of the donors was unknown.

971 *Tissue preparation*:

972 Mice were anesthetized with isoflurane and sacrificed by cervical dislocation. A laparotomy was
973 performed, and the ileum was removed and lavaged with PBS containing penicillin-streptomycin
974 (PS; Invitrogen), then cut into 1-cm-long segments and placed over a sterile plastic rod. A super-
975 ficial longitudinal incision was made along the serosal surface and the LM-MP was peeled off
976 from the underlying tissue using a wet sterile cotton swab [19] and placed in Opti-MEM medium
977 (Invitrogen) containing Pen-Strep (Invitrogen). The tissue was then laid flat and fixed within 30
978 minutes of isolation with freshly prepared ice cold 4% paraformaldehyde (PFA) solution for 45
979 minutes in the dark to preserve fluorescence intensity and prevent photo-bleaching. All LM-MP
980 tissues post-isolation were fixed within 30 minutes of their isolation. After the fixation, the tissue
981 was removed and stored in ice cold sterile PBS with Pen-Strep for immunofluorescence staining
982 and subsequent microscopy.

983 For human tissues, duodenal tissue from adult human patients (n = 3 patients), who did not have
984 any prior history of chronic intestinal dysmotility, that was removed by Whipple procedure was
985 obtained. A colonic sample from a pathologically normal colonic resection from an adult donor

986 suffering from colon carcinoma who similarly did not have prior history of chronic intestinal dys-
987 motility was also obtained. The resected tissue was placed in ice cold Opti-MEM medium (Invi-
988 trogen) containing Pen-Strep (Invitrogen). The mucosal and sub-mucosal tissue was dissected
989 out in the medium under light microscope and the muscularis layer containing myenteric plexus
990 tissue was obtained. The tissue was laid out between two glass slides and fixed overnight in ice
991 cold 4% PFA after which it was removed and stored in ice cold sterile PBS with Pen-Strep for
992 immunofluorescence staining, optical clarification, and subsequent microscopy.

993 *Immunohistochemistry*:

994 For murine tissue: The fixed LM-MP tissue was washed twice in ice-cold PBS in the dark at 16°C.
995 The tissue was then incubated in blocking-permeabilizing buffer (BPB; 5% normal goat serum
996 with 0.3% Triton-X) for 1 hour. While staining for antibodies that were mouse monoclonal, 5%
997 normal mouse serum was added to the BPB. The tissue was then removed from the BPB and
998 was incubated with the appropriate primary antibody at the listed concentration (Table S1) for 48
999 h at 16°C in the dark with shaking at 55 rpm. Following incubation with primary antibody, the
1000 tissue was washed three times (15-min wash each) in PBS at room temperature in the dark. The
1001 tissue was then incubated in the appropriate secondary antibody at room temperature for 1 hour
1002 while on a rotary shaker (65 rpm). The tissue was again washed three times in PBS at room
1003 temperature, counterstained with DAPI to stain the nuclei, overlaid with Prolong Antifade Gold
1004 mounting medium, cover-slipped, and imaged.

1005 Immunostaining for ChAT was performed using fixed and unpeeled murine tissues from adult
1006 male Wnt1-cre:*Rosa26*-tdTomato mice. The intestinal segments were obtained by perfuse fixing
1007 the mouse with ice-cold PBS and then freshly prepared 4% PFA solution. Once the intestine was
1008 harvested, the ileum was flushed with cold HBSS with 0.4 mol/L N-acetyl-l-cysteine and then PBS
1009 to remove luminal contents. After, the tissue was fixed in 4% PFA overnight. The fixed tissue was
1010 then immersed in 2% Triton-X 100 solution for 2 d at 15°C for permeabilization. The tissue was

1011 immunostained with antibodies against Hu (ANNA1) and against ChAT (rabbit, Abnova). The pri-
1012 mary antibody was then diluted (1:100) in the dilution buffer (0.25% Triton X-100, 1% normal goat
1013 serum, and 0.02% sodium azide in PBS) and incubated for 1 day at 15°C. An Alexa Fluor 647-
1014 conjugated goat anti-rabbit secondary antibody (1:200, Invitrogen) and an Alexa Fluor 488-con-
1015 jugated goat anti-human secondary antibody (1:200, Invitrogen) were then used to reveal the
1016 immunopositive structure. Finally, the labeled specimens were immersed in FocusClear solution
1017 (CelExplorer) for optical clearing before being imaged by laser confocal microscopy using a Zeiss
1018 LSM 510 META. The LSM 510 software and the Avizo 6.2 image reconstruction software (VSG)
1019 were used for the 2D and 3D projection of the confocal micrographs. The Avizo software was
1020 operated under a Dell T7500 workstation and the "Gaussian Filter" function of Avizo was used for
1021 noise reduction of the micrographs.

1022 Colchicine treatment: For CGRP immunostaining, mice were injected with Colchicine at a con-
1023 centration of 5 mg/Kg body weight 16 hours (overnight) before they were sacrificed. The mice
1024 were housed singly during this time and adequate gel packs were provided. Food and water were
1025 provided *ad libitum*. On the following day, the mice were sacrificed, and their LM-MP tissues were
1026 harvested as detailed above.

1027 For human tissue: The fixed muscularis layer containing myenteric plexus tissue was removed
1028 from ice cold PBS and incubated in blocking-permeabilizing buffer (BPB; 5% normal goat serum,
1029 5% normal mouse serum with 0.3% Triton-X) for 4 hours. The tissue was then removed from the
1030 BPB and was incubated with the appropriate primary antibody at the listed concentration (Table
1031 S1) for 5 days at 16°C in the dark with shaking at 55 rpm. Following incubation with primary
1032 antibody, the tissue was washed five times (15-min wash each) in PBS at room temperature in
1033 the dark. The tissue was then incubated in the appropriate secondary antibody at 16°C in the dark
1034 with shaking at 55 rpm for 2 days. The tissue was again washed in dark for five times in PBS that
1035 contained DAPI at room temperature. After the final wash, the tissue was suspended in tissue

1036 clarification buffer CUBIC[146] for 1 hour at 4°C in the dark after which it was overlaid with Prolong
1037 Antifade Gold mounting medium, cover-slipped, and imaged. Briefly, the CUBIC optical clarifica-
1038 tion buffer was made by mixing 2.5 g of urea (25% by wt), 2.5 g of N, N, N´, N´-tetrakis (2-hydroxy-
1039 propyl) ethylenediamine (25% by wt), 1.5 g of Triton X-100 (15% by wt) in 35 ml of Distilled Water.
1040 The solution was shaken till the ingredients were dissolved and yielded a clear viscous solution.

1041 *Microscopy*:

1042 Except for ChAT microscopy, all other imaging was done by using the oil immersion 63X objective
1043 on the Leica SP8 confocal microscope and by using the oil immersion 40X objective on the Olym-
1044 pus Fluoview 3000rs confocal microscope with resonance scanning mode. For thick tissues, such
1045 as human tissues, the Galvano mode of the Olympus Fluoview 3000rs microscope that enabled
1046 higher resolution imaging and averaging was used. Images obtained were then analyzed using
1047 Fiji (https://fiji.sc/).

1048 Live tissue imaging of the mouse gut tissue was performed by harvesting small intestinal tissue
1049 from an adult Wnt1-cre:*Rosa26*-tdTomato mouse and immediately putting it in OptiMEM solution.
1050 The tissue was then immediately put on a chamber slide containing OptiMEM and imaged in live
1051 tissue culture conditions of the EVOS M7000 microscope under the 20X objective.

1052 *Enumeration of neurons*:

1053 Enumeration of tdTomato^{+} and tdTomato^{-} neurons was performed on tissue with native tdTomato
1054 fluorescence. The native tdTomato fluorescence in fixed tissue was intense, thus there was no
1055 need to increase fluorescent signal using anti-RFP/tdTomato antibodies.

1056 Enumeration of enteric neurons to study alterations to ENS neuronal numbers was performed by
1057 following the well-established protocol[147-150] of counting the numbers of neurons in myenteric gan-
1058 glia and comparing them between animals for statistically significant differences. Identification of

1059 myenteric ganglia was performed according to our pre-determined method published earlier[19].
1060 Briefly, contiguous clusters of neurons were defined as a ganglion and the total numbers of neu-
1061 rons within these clusters were enumerated as numbers of myenteric neurons per ganglion. As a
1062 rule, clusters of 3 neurons or more were deemed to consist of a ganglion and our enumeration
1063 strategy did not count extra-ganglionic neurons. We imaged ~10 ganglia per tissue for our enu-
1064 meration and each group studied had n ≥ 3 mice. Identification and enumeration of neurons and
1065 detection of co-localization was performed manually by trained laboratory personnel. Fig 1d com-
1066 prises of the data from 6 P60 mice, which includes data from the 3 mice that were used for the
1067 development experiment presented in Fig 8c.

1068 *Protein isolation and detection:*

1069 After the LM-MP tissue was isolated, it was weighed and placed in a sterile 1.5 ml microfuge tube.
1070 1X RIPA buffer (Cell Signaling Technology) with Halt Protease Inhibitor Cocktail (Thermo Scien-
1071 tific) at 5X concentration, Phosphatase Inhibitor Cocktails II and III (Sigma-Aldrich) at 2X concen-
1072 trations were added to the tissue lysate buffer. Tissue was disrupted using 1.0 mm silica beads
1073 in Bullet Blender 24 (Next Advance) for 5 mins at highest setting. The lysate was incubated at
1074 4°C with shaking for 30 mins, centrifuged at 14,000rpm for 20 mins and the supernatant was
1075 taken and stored in -80°C in aliquots. Protein concentration was estimated using Bradford assay
1076 solution (Biorad) following the manufacturer's protocol. For immunoblotting, 40 µg of protein was
1077 loaded per well of 4%-20% gradient denaturing gel (Biorad). Protein marker used was Precision
1078 Plus Dual Color standards (Biorad). After fractionating the proteins, they were blotted onto Im-
1079 munBlot PVDF membrane (Biorad) overnight at 4°C at 17V for 12-16 hours. After blotting, mem-
1080 brane was blocked with Odyssey TBS blocking buffer (Li-Cor) for 1 hour at room temperature with
1081 shaking. Incubation with primary antibodies were carried out at 4°C with shaking for 24 hours.
1082 Following binding, the blot was washed 4 times with TBS-T (Tris Buffered Saline with 0.5%
1083 Tween) for 15 mins each with shaking at room temperature. Secondary antibody incubation was

1084 carried out in dark at room temperature for 1.5 hours with shaking. The blot was then washed 4
1085 times for 15 mins each and imaged on Odyssey CLx system (Li-Cor).

1086 Part of the aforementioned protocol was also followed for detecting HuB protein (recombinant
1087 Human ELAVL2, 1-346aa, from Biosource; Catalogue number MBS205995). The protein was
1088 loaded in two amounts (0.5 µg and 1.25 µg) in separate lanes of a 4-20% gradient denaturing gel
1089 (Biorad) along with protein marker Precision Plus Dual Color standards (Biorad). After fractionat-
1090 ing the proteins, they were blotted onto ImmunBlot PVDF membrane (Biorad) overnight at 4°C at
1091 17V for 12-16 hours. After blotting, membrane was blocked with Odyssey TBS blocking buffer (Li-
1092 Cor) for 1 hour at room temperature with shaking. Incubation with primary antibodies were carried
1093 out at 4°C with shaking for 24 hours. Following binding, the blot was washed 4 times with TBS-T
1094 (Tris Buffered Saline with 0.5% Tween) for 15 mins each with shak-ing at room temperature.
1095 Secondary antibody incubation was carried out in dark at room tempera-ture for 1.5 hours with
1096 shaking. The blot was then washed 4 times for 15 mins each and imaged on Odyssey CLx system
1097 (Li-Cor).

1098 Antibody used to detect RET was a well validated antibody used previously for detecting RET in
1099 ENS[151] and was further validated by us using a western blot on total proteins isolated from murine
1100 small intestinal LM-MP (Suppl Figure 8e). Antibodies used are detailed in the Supplementary
1101 Table 1.

1102 *RNA isolation and quantitative detection of specific transcripts:*

1103 The isolated tissue was stored in RNALater Solution (Ambion). RNA was isolated using RNeasy
1104 Mini Kit (Qiagen) following manufacturer's protocol. RNA quantification was carried out using
1105 Epoch Microplate Spectrophotometer (BioTek). cDNA synthesis was carried by SuperScript IV
1106 VILO Master Mix (Invitrogen). Quantitative Real-time PCR was carried out using Taqman Gene

1107 Expression Master Mix (Applied Biosystems) and Roto-Gene Q (Qiagen). The probes used are
1108 listed in Supplementary Table 1.

1109 *Single Cell RNA sequencing and analyses:*

1110 Single cell preparation from murine ileal tissues: Ileal tissues from male littermate C57/BL6
1111 wildtype mice were isolated by peeling as previously described. The tissues were then dissociated
1112 in Digestion Buffer containing 1 mg/ml Liberase (Sigma-Aldrich) in OptiMEM. Tissues from mouse
1113 1 were dissociated in the Digestion buffer containing Liberase TH and tissues from mouse 2 were
1114 dissociated in the Digestion buffer containing Liberase TL. Dissociation was performed at 37°C
1115 for 30 minutes on a rotary shaker, after which the cells were centrifuged at 200g for 7 minutes,
1116 and the pellet was resuspended in ice cold sterile PBS. The cell suspension was passed through
1117 a 40 µm cell sieve and the resulting filtered cell suspension was again centrifuged at 200g for 7
1118 minutes. This process of cell centrifugation and filtration was repeated two more times, after which
1119 the cells were resuspended in 1 ml ice cold sterile PBS. The repeated steps of serial cell washes
1120 and filtration removed clumps and debris and the viability of the resulting cell suspension was
1121 estimated to be >90% using Trypan Blue dye test. The cells were then processed through 10X
1122 Genomics Chromium V2.0 system (for the 6-month-old murine tissues) and 10X Genomics Chro-
1123 mium V3.1 system (for the P21 murine tissues) according to the manufacturer's suggested work-
1124 flow. The processing was done at the GRCF Core Facility at the Johns Hopkins University. The
1125 pooled libraries were sequenced on an Illumina HiSeq 2500 (for 6-month-old tissues) and Illumina
1126 Novaseq (for P21 tissues) to an average depth of 3.125×10^8 reads per sample library. The se-
1127 quencing was performed at the CIDR core facility at the Johns Hopkins University.

1128 For processing data from scRNAseq on 6-month-old murine LM-MP tissues: Pre-processing of
1129 FASTQs to Expression Matrices: FASTQ sequence files were processed following a Kallisto
1130 Bustools workflow compatible with downstream RNA velocity[152]. References required for pseudo-
1131 alignment of transcripts were obtained using the get_velocity_files (functionality of BUSpaRSE

1132 (https://github.com/BUStools/BUSpaRse)), with “L=98” for 10X Genomics v2.0 sequencing chem-
1133 istry. Reads were pseudo-aligned to an index built from Ensembl 97 transcriptome annotation
1134 (Gencode vM22; GRCm38). Across two samples processed, a total of 578,529,125 reads were
1135 successfully pseudo-aligned. Barcodes within a Hamming distance of one to known 10X Ge-
1136 nomics v2.0 barcodes were corrected. Reads were classified as “spliced” or “unspliced” by their
1137 complement to the target list of intronic sequences and exonic sequences, respectively, and sub-
1138 sequently quantified separately into expression count matrices. Spliced counts are used for all
1139 analyses.

1140 Single cell gene expression analysis: scRNA-seq count matrices were analyzed using Monocle3.
1141 11,123 high-quality cells were identified as meeting a 200 UMI minimum threshold with a mito-
1142 chondrial read ratio of less than 20%; droplets that did not meet these criteria were excluded from
1143 the analysis. Mitochondrial counts were determined as the sum of reads mapping to 37 genes
1144 annotated to the mitochondrial genome. All genes with non-zero expression were included for
1145 downstream analysis. Raw counts were first scaled by a cell-size scaling factor and subsequently
1146 log10 transformed with a pseudo-count of 1. Normalized values are used in place of raw counts
1147 unless otherwise noted.

1148 Prior to UMAP dimensionality reduction, batch effects between the two biological replicates were
1149 assessed and corrected via the mutual nearest neighbors (MNN) algorithm as implemented by
1150 Batchelor in Monocle3[153]. 15 clusters of cells in the UMAP embedding were identified by Leiden
1151 community detection. 30 marker genes for each cluster were identified based on greatest pseudo
1152 R^2 values and used for supervised annotation of cell types by searching UniProt, Allen Cell Atlas
1153 and through literature search with Pubmed.

1154 NC-derived cell clusters were identified by expression of NC markers Ret and Sox10. MEN cluster
1155 was identified by its expression of CGRP-coding Calcb, Met, and Cdh3. The pan-MENs protein
1156 marker MHCst was identified by labeling with an antibody S46 which labels all members of the

1157 MHCst family[41]. Since the antibody does not identify a single gene product, MHCst immunostain-
1158 ing could not be used to identify a specific gene marker for use in the annotation of the MEN
1159 cluster. For further analysis into the MENs population, the full LM-MP dataset was subset to in-
1160 clude only the 2,223 cells annotated as MENs. These cells were re-processed as above, but with
1161 a reduced PCA dimensionality of k=20 as input for the UMAP embedding. 5 clusters of cells in
1162 the UMAP embedding were identified by Leiden community detection (k= 10, resolution = 5e -4).

1163 P20 LM-MP scRNA processing and analysis: Pre-processing of FASTQs to Expression Matrices:
1164 FASTQ sequence files were processed following a Kallisto Bustools workflow compatible with
1165 downstream RNA velocity. References required for pseudo-alignment of transcripts were ob-
1166 tained using the get_velocity_files (functionality of BUSpaRSE
1167 (https://github.com/BUStools/BUSpaRse)), with "L=91" for 10X Genomics v3.1 sequencing chem-
1168 istry. Reads were processed following the same steps as the six month LMMP dataset. Spliced
1169 counts are used for all analyses.

1170 Single cell gene expression analysis: scRNA-seq count matrices were analyzed using Monocle3.
1171 11,264 high-quality cells were identified as meeting a 600 UMI minimum threshold with a mito-
1172 chondrial read ratio of less than 20%; droplets that did not meet these criteria were excluded from
1173 the analysis. Mitochondrial counts were determined as the sum of reads mapping to 37 genes
1174 annotated to the mitochondrial genome. All genes with non-zero expression were included for
1175 downstream analysis. Raw counts were first scaled by a cell-size scaling factor and subsequently
1176 log10 transformed with a pseudo-count of 1. Normalized values are used in place of raw counts
1177 unless otherwise noted.

1178 NC-derived and MENs cell clusters were identified by expression of established marker genes.
1179 Further, the identity of MENs was confirmed by a projection analysis using MENs-specific patterns
1180 learned in the six month dataset. To investigate differences in division potential within the ENS,
1181 the data was subset to NENs, neuroglia, and MENs for computational cell cycle analysis (NENs:

1182 n = 526; neuroglia: n = 844; MENs: n = 510). Continuous scores for cell cycle position (0-2π) were
1183 calculated via Tricycle by projecting each cell into the default reference space. The relevance of
1184 these scores was confirmed by profiling the scores' correlation with expression of genes with
1185 known variation over the cell cycle. Lastly, each cell was unambiguously characterized as "non-
1186 cycling" (0-0.5π or 1.5-2π) or "cycling" (0.5-1.5π) by binarizing Tricycle scores.

1187 External datasets: Spliced and unspliced count matrices for mesenchymal subset of the Gut Cell
1188 Atlas were obtained from https://www.gutcellatlas.org/[78], and existing annotations were used
1189 when available. SnRNAseq counts matrices from May-Zhang et al.[50] were downloaded from GEO
1190 GSE153192. Bulk RNAseq dataset from the Human Obstructed defecation study by Kim et al.[100]
1191 was obtained from GEO GSE101968.

1192 Pattern discovery and ProjectR analyses: Pattern discovery was utilized to identify sets of co-
1193 expressed genes that define cell-type specific transcriptional signatures. The normalized expres-
1194 sion matrix was decomposed via non-negative matrix factorization (NMF) as implemented in the
1195 R package *NNLM*, with k=50 and default parameters. Cell weights for each pattern were grouped
1196 by assigned cell-type and represented by heatmap. Pattern vectors were hierarchically clustered
1197 by a Euclidian distance metric, implemented in ComplexHeatmap[154]. These patterns were then
1198 tested on the bulk RNA-Seq expression matrix for the Human Obstructed Defecation study[100].
1199 The log2 expression (log2(rpkm + 1)) from this study was projected onto the NMF patterns using
1200 projectR[69]. Students' t tests were performed on the projection weights from the Control and OD
1201 groups to test for differences between them. For the projection of datasets generated by May-
1202 Zhang et al.[50] and Elmentaite et al.[78], log10-transformed normalized counts were projected.

1203 **Analysis of May-Zhang et al. dataset**

1204 Raw UMI count matrices for the single-nucleus RNA sequencing of enteric neurons performed by
1205 May-Zhang et al.[50] from the ileum of adult mice were obtained from GEO (GSE153192). The

1206 DropletUtils package (v1.10.3)[155,156] was used to compute barcode ranks, knee, and inflection
1207 point statistics for all the samples. All barcodes in the 10X genomics libraries with total UMI greater
1208 than the inflection point were considered to be cell-containing droplets and retained for further
1209 analysis. The inDrop libraries were filtered to retain all barcodes with UMI greater than 200. The
1210 filtered matrices were combined to form a SingleCellExperiment object.

1211 Cell-specific scaling factors accounting for composition biases were computed using com-
1212 puteSumFactors (scran v1.18.7)[157]. The raw UMI counts were then scaled using the scaling fac-
1213 tors and log 2 transformed after addition of a pseudo count of 1 using logNormCounts (scater
1214 v1.18.6)[158]. Batch effects between the samples were corrected using fastMNN (batchelor
1215 v1.6.3)[153].

1216 Unsupervised clustering was performed using a graph-based clustering technique. The graph
1217 was obtained using buildSNNgraph (scran v1.18.7)[157] and the louvain algorithm implemented in
1218 the igraph package (v1.2.7)[159] was used to identify communities. Differential expression testing
1219 was performed between all pairs of clusters using findMarkers (scran v1.18.7)[157]. One-sided
1220 Welch's t-test was used to identify genes that were upregulated in a cluster as compared to any
1221 others in the dataset. Benjamini-Hochberg method was applied (to combined p-values) to correct
1222 for multiple testing and the genes were ranked by significance. The top ranked genes were used
1223 as marker genes for the clusters. The log fold change from the pairwise comparison with the
1224 lowest p-value was used as the summary log fold change.

1225 The log normalized counts from this dataset were then projected into the NMF patterns learned
1226 on our scRNAseq data. This was performed using transfer learning implemented in projectR
1227 (v1.6.0). The projection weights corresponding to the four MEN-specific patterns were then clus-
1228 tered using graph-based clustering and visualized by UMAP (uwot v0.1.10)(
1229 https://github.com/jlmelville/uwot).

1230 *Whole gut transit time analyses*:

1231 Whole-gut transit time (WGTT) for every mouse was analyzed by the method using the carmine
1232 red protocol[19]. Mice were placed in individual cages and deprived of food for 1 hour before receiv-
1233 ing 0.3 mL 6% (wt/vol) carmine solution in 0.5% methylcellulose by oral gavage into the animal's
1234 stomach. The time taken for each mouse to produce a red fecal pellet after the administration of
1235 carmine dye was recorded in minutes. The experiment was terminated at 210 minutes post-ga-
1236 vage and the WGTT of any mice that did not expel the red dye at the termination was marked at
1237 the value of 210 min. The mean difference in whole gut transit time (in minutes) between both the
1238 $Ret^{+/+}$ and $Ret^{+/-}$ mice cohorts, and the GDNF and Saline-treated Control cohorts were analyzed
1239 statistically.

1240 *In vivo Injections:*

1241 GDNF injection: Similar to prior report that gave sub-cutaneous injections of GDNF to post-natal
1242 mice[93], we took 6 littermate 10 day old (P10) male Wnt1-cre:*Rosa26*-tdTomato mice and divided
1243 into two subgroups, GDNF and Control. Each mouse in the GDNF group was injected sub-cuta-
1244 neously with 50 µl of 2mg/ml of GDNF (Peprotech Catalogue #: 450-44) every other day, while
1245 the Control group was injected with 50 µl of sterile saline. The mice were given 5 doses and then
1246 sacrificed on P20, after which their LM-MP tissues were isolated as detailed above. The tissues
1247 were then immunostained with antibodies against Hu and imaged. In a separate experiment, adult
1248 (P60) mice were also injected sub-cutaneously with GDNF (100 µl of 100 µg/ml of GDNF). The
1249 mice were given 5 doses over a course of 10 days and then sacrificed on P70, after which their
1250 LM-MP tissues were isolated as detailed above. For studying the effect of GDNF on aging mice,
1251 two cohorts of 17-month-old male C57BL/6 mice (n=5 mice/cohort) were obtained from the aging
1252 colony of the National Institute of Aging. Before the start of dosing, the whole gut transit time was
1253 assayed. The animals were then injected daily sub-cutaneously either with 100 µl of saline

1254 (Control) or 100 µl of GDNF (500 µg/ml) for 10 consecutive days, after which the mice were sac-
1255 rificed, and their LM-MP tissues were isolated as detailed above. The tissues were then im-
1256 munostained with antibodies against Hu and imaged.

1257 HGF injection: Similar to prior report that gave sub-cutaneous injections of HGF to post-natal
1258 mice, we took 6 littermate 10 day old (P10) male Wnt1-cre:*Rosa26*-tdTomato mice and divided
1259 into two subgroups, HGF and Control. Each mouse in the HGF group was injected sub-cutane-
1260 ously with 100 µl of 2mg/ml of HGF (Peprotech Catalogue #:315-23) every other day, while the
1261 saline group was injected with 100 µl of sterile saline. The mice were given 5 doses and then
1262 sacrificed on P20, after which their LM-MP tissues were isolated as detailed above. The tissues
1263 were then immunostained with antibodies against Hu and imaged.

1264 *Statistics:*

1265 Data was analyzed using Graphpad Prism 8.3.1 and R using Unpaired Students t-test, Simple
1266 Linear Regression, and Ordinary One-Way ANOVA.

1267 *Data:*

1268 All raw data are provided in Supplementary Table 2 and 3. We imaged atleast 10 ganglia per
1269 tissue for our enumeration and each group studied had n ≥ 3 mice. Raw single cell RNA sequenc-
1270 ing data is archived on the NCBI GEO server and can be accessed under the accession numbers
1271 GSE156146 and GSE213604.

1272 *Code:*

1273 Code generated for the scRNA/snRNA analyses is available at https://github.com/jared-
1274 slosberg/6month_ENS/.

1275

1276 **Figures**

1277 **Figures**

1278 **Fig 1: Half of all adult small intestinal myenteric neurons are derived from a non-neural**
1279 **crest lineage.**

1280 **(a)** Enteric glia, labeled with GFAP (green) in the myenteric plexus from an adult Wnt1-
1281 cre:*Rosa26*-tdTomato mouse. Inset is magnified in color segregated panels, showing $GFAP^+$ glia
1282 co-expressing tdTomato (red, red arrows). Nuclei are labeled with DAPI (blue). Scale bar = 10
1283 μm.

1284 **(b)** 2 dimensional representation of a 3 dimensional stack of images shows enteric neurons, la-
1285 beled with Hu (green), in the myenteric plexus from an adult Wnt1-cre:*Rosa26*-tdTomato mouse.
1286 Enteric neurons either express tdTomato (red arrow) or not (white arrows). Nuclei are labeled with
1287 DAPI (blue). Scale bar = 10 μm.

1288 **(c)** Orthogonal views of the image **(b)** shows the lack of tdTomato expression in a particular Hu-
1289 immunolabeled enteric neuron.

1290 **(d)** Quantification of $tdTomato^+$ and $tdTomato^-$ neurons in the myenteric ganglia of 6 P60 Wnt1-
1291 cre:*Rosa26*-tdTomato mice. Data represents Mean ± SEM.

1292 **Fig 2: Mesoderm-lineage-tracing and marker expression provide evidence of the mesoder-**
1293 **mal-derivation of half of all adult small intestinal myenteric neurons.**

1294 **(a)** Small intestinal LM-MP from adult male Tek-cre:*Hprt*-tdTomato shows the presence of Tek-
1295 derived and hence mesoderm-derived tdTomato$^+$ (red) Hu$^+$ (green) neurons (white arrows) and
1296 non-mesoderm-derived tdTomato$^-$ neurons (green arrows). Vascular cells depict higher fluores-
1297 cence intensity (yellow arrow) than cells in the ganglia. Nuclei are labeled with DAPI. Scale bar =
1298 10 μm.

1299 Cardiac and small intestinal tissues from **(b)** heart and **(c)** small intestinal LM-MP layer of adult
1300 male Mesp1-cre:*Rosa26*-tdTomato mice shows the presence of variable tdTomato expression in
1301 cells of these tissues. While cardiomyocytes in heart and cells within the myenteric ganglia (white
1302 arrows) exhibit lower tdTomato fluorescence, similar to the tissues from Tek-cre:*Hprt*-tdTomato
1303 mice in (a), the vascular cells exhibit higher fluorescence intensity (yellow arrows). Scale bar =
1304 10 μm.

1305 **(d)** Small intestinal LM-MP from adult male Mesp1-cre:*Rosa26*-tdTomato mouse shows the pres-
1306 ence of mesoderm-derived tdTomato$^+$ (red) Hu$^+$ (green) neurons (white arrows) and non-meso-
1307 derm-derived tdTomato$^-$ neurons (green arrows). Nuclei are labeled with DAPI. Scale bar = 10
1308 μm.

1309 **(e)** Small intestinal LM-MP from adult male Mesp1-cre:*Rosa26*-EGFP mouse, when im-
1310 munostained with antibodies against GFP and against Hu, shows the presence of mesoderm-
1311 derived EGFP$^+$ (green) Hu$^+$ (red) neurons (white arrows) and non-mesoderm-derived EGFP$^-$
1312 neurons (red arrows). Nuclei are labeled with DAPI. Scale bar = 10 μm.

1313 **(f)** Quantification of tdTomato-expressing and non-expressing neurons in the myenteric ganglia
1314 of 3 P60 Mesp1-cre:*Rosa26*-tdTomato mice. Data represents Mean ± SEM.

1315 MHCst immunolabeling exclusively marks all the **(g)** mesoderm-derived adult Hu^+ (green) neu-
1316 rons in the small intestinal LM-MP of Mesp1-cre:*Rosa26*-tdTomato mice; and **(h)** all the non-NC-
1317 derived neurons in the small intestinal LM-MP of Wnt1-cre:*Rosa26*-tdTomato mice (white arrows).
1318 MHCst does not label $tdTomato^+$ NC-derived cells (yellow arrows). Nuclei are stained with DAPI
1319 (blue). Scale bar = 10 μm.

1320 **Fig 3: Cellular and molecular phenotyping of MENs and NENs.**

1321 MET immunostaining (green) labels **(a)** Wnt1-cre:*Rosa26*-tdTomato$^-$ MENs and **(b)** a population
1322 of Mesp1-cre:*Rosa26*-tdTomato$^+$ MENs (white arrow) while not labeling all MENs (red arrow).

1323 **(c)** RET immunostaining (green) only labels Wnt1-cre:*Rosa26*-tdTomato$^+$ NENs (green arrow)
1324 and not tdTomato$^-$ MENs (white arrows).

1325 **(d)** NOS1 is expressed by both tdTomato$^+$ NENs (red, white arrows) and tdTomato$^-$ MENs (blue
1326 arrows) in an adult Wnt1-cre:*Rosa26*-tdTomato mouse, but most MENs do not express NOS1
1327 (marked by *).

1328 **(e)** NEN lineage contains significantly higher proportions of NOS1$^+$ neurons compared to MEN
1329 lineage in Wnt1-cre:*Rosa26*-tdTomato mice. Data represent mean ± S.E.M. $p < 0.0001$; Fisher's
1330 exact test.

1331 **(f)** ChAT is expressed by both tdTomato$^+$ NENs (red, white arrows) and tdTomato$^-$ MENs (blue
1332 arrows) in an adult Wnt1-cre:*Rosa26*-tdTomato mouse.

1333 **(g)** NEN lineage contains significantly higher proportions of ChAT$^+$ neurons compared to MEN
1334 lineage in Wnt1-cre:*Rosa26*-tdTomato mice. Data represent mean ± S.E.M. $p < 0.0001$; Fisher's
1335 exact test.

1336 **(h)** Both tdTomato$^+$ (red) and tdTomato$^-$ neurons in the myenteric plexus of an adult Wnt1-
1337 cre:*Rosa26*-tdTomato mouse (Hu, green) express CGRP (blue) Inset showing a tdTomato$^-$
1338 CGRP$^+$ neuron (white arrow) is magnified on the right.

1339 **(i)** MEN lineage contains significantly higher proportions of $CGRP^+$ neurons compared to NEN

1340 lineage in Wnt1-cre:*Rosa26*-tdTomato male mice. Data represent mean ± S.E.M. $p < 0.0001$;

1341 Fisher's exact test.

1342 Nuclei in **(b) and (c)** are labeled with DAPI (blue). Scale bar for all images denotes 10 μm.

1343 **Fig 4: scRNAseq-analyses identifies the distinct transcriptomic profile of the MENs.**

1344 **(a)** UMAP representation of 11,123 sequenced high-quality cells that were identified as meeting
1345 a 200 UMI minimum threshold with a mitochondrial read ratio of less than 20%. Clusters were
1346 annotated by markers that were found to be cell-type specific by searching UniProt, Allen Cell
1347 Atlas and Pubmed databases. Cells of the neural crest lineage were then identified as NENs by
1348 their expression of neural crest marker gene Ret and Neuroglia by their expression of Ncam1 and
1349 Sox10, or as MENs by co-expression of Calcb (CGRP), Cdh3, and Met genes.

1350 **(b)** Visualization of expression of select MEN-specific and neuronal markers using quasi-violin
1351 plots. “Max value” represents the scale for the log-normalized expression of each gene.

1352 **(c)** Validation of the MENs-specific marker genes discovered in the scRNAseq analyses by im-
1353 munohistochemistry and confocal microscopy of small intestinal LM-MP from adult male Wnt1-
1354 cre:*Rosa26*-tdTomato mice. Expression of neuronal markers STX3, VSNL1, STMN2, HAND2,
1355 GPR88, PDE10A, ELAVL2, and TUBB2B (Gray, green arrows) was found in tdTomato^{-} MENs.
1356 Immunostaining of the proteins AEBP1, CFTR, CLIC3, NT-3, SLPI, SMO, IL-18, SLC17A9, FMO2
1357 and MYL7 (green; green arrows) was found to be localized to tdTomato^{-} MENs. tdTomato^{+} (red)
1358 NC-cells did not immunostain for these markers (red arrows). Panel also shows Wnt1-
1359 cre:*Rosa26*-tdTomato tissue with no primary controls (stained with AlexaFluor 488 and AlexaFluor
1360 647 antibodies). Figures with * annotations are 2D representation of 3D stacks of images. Nuclei
1361 in some panels were labeled with DAPI (blue). Scale bar denotes 10 μm.

1362 **Fig 5: MENs express the mesenchymal gene Decorin and the ENS-specific gene Phox2b.**

1363 **(a)** Sparkline representation plot of the top 90 percentile of expressed genes in the various
1364 scRNAseq cell clusters from the adult murine LM-MP tissue of a 6-month-old mouse shows that
1365 the MENs cluster, which expresses the genes Cdh3, Pde10a, and Hand2, also expresses signif-
1366 icant amounts of the mesenchymal gene Decorin (Dcn). Darker colors of the sparkline plot repre-
1367 sent higher expression.

1368 (b) Sparkline representation plot of the neural crest-derived enteric neurons from the Zeisel et al.
1369 dataset shows that the Decorin gene is not found expressed by most neural crest-derived enteric
1370 neurons.

1371 (c) 2 dimensional representation views and orthogonal view of a myenteric ganglion from the
1372 small intestinal LM-MP of adult male Wnt-cre:*Rosa26*-EGFP mouse, where tdTomato (red) is
1373 expressed by neural crest-derived cells, when immunostained with antibodies against DECORIN
1374 (grey) shows that the DECORIN-expressing myenteric cells (green arrows) do not express
1375 tdTomato and hence are non-neural crest-derived MENs. Nuclei are labeled with DAPI. Scale bar
1376 = 10 μm.

1377 (d) Representative image of a myenteric ganglion from the small intestinal LM-MP of adult male
1378 Wnt-cre:*Rosa26*-EGFP mouse, where tdTomato (red) is expressed by neural crest-derived cells,
1379 when immunostained with antibodies against PHOX2b (green) shows that the PHOX2b-expres-
1380 sion is found in myenteric cells that do not express tdTomato (green arrows, and hence are not
1381 neural crest-derived cells, or MENs) as well as in tdTomato-expressing neural crest-derived NENs
1382 (red arrow). Nuclei are labeled with DAPI. Scale bar = 10 μm.

1383 (e) Volcano plot of gene expression profiles of Phox2b-expressing cells, which were sorted based
1384 on their CFP expression level, shows that the expression of MENs marker genes Smo, Aebp1,

1385 Cdh3, Fmo2, Il18, Slpi, Upk3b, Msln, and Hand2 is significantly enriched in the Phox2b-CFP^{low}

1386 fraction. Red dotted line shows the $p_{adjusted}$ value of 0.05.

1387

1388 **Fig 6: Computational analyses using *projectR* identifies MENs in publicly available murine**
1389 **and human transcriptomic datasets.**

1390 **(a)** Heatmap of cell weights for the patterns learned by NMF (k=50). Hierarchical clustering was
1391 calculated using Euclidean distance. Multiple clusters annotated as the same cell type are
1392 merged. The four most specific MENs patterns (16, 27, 32 and 41) are selected.

1393 **(b)** In addition to using the four MEN-specific NMF patterns to label the MENs cluster in our
1394 scRNAseq dataset (plots in top row), two other transcriptomic datasets: May-Zhang et al.'s murine
1395 ileal ENS snRNAseq dataset[50] (plots in second row), and Elmentaite et al.'s gut mesenchymal
1396 scRNAseq dataset[78] (plots in third row), were projected into the defined four MEN-specific pattern
1397 space using *ProjectR*. Raw projected cell weights were visualized using previously learned UMAP
1398 embedding. The cell clusters that show high pattern usage are shown bounded by the red square.
1399 Plots in the final row shows projection of healthy post-natal mesenchymal cells from Elmentaite
1400 et al's data[78] into the four MEN-specific NMF patterns, which again show a population of cells
1401 showing high MEN-specific pattern utilization.

1402

1403 **Fig 7. Detection of MENs in human single cell RNA sequencing data.**

1404 **(a)** UMAP representation of scRNAseq data from Elmentaite et al.'s healthy post-natal mesen-
1405 chymal cells from the human gut[78].

1406 **(b)** Breakdown for previously published annotated features of the post-natal health subset of the
1407 gut cell atlas as presented in Elmentaite et al.[78].

1408 **(c)** Expression of the MENs marker gene Dcn in the UMAP representation of healthy post-natal
1409 data from Elmentaite et al.[78]., which was annotated as clusters of mesenchymal cells.

1410 **(d)** Expression of neuronal marker genes Slc17a9, Stx3, Uchl1, Tubb2b, Pde10a, and Hand2 in
1411 the UMAP representation of healthy post-natal data from Elmentaite et al.[78], which was annotated
1412 as clusters of mesenchymal cells.

1413 **Fig 8: Validation of SNAP-25 as a NENs marker**

1414 **(a)** SNAP-25 expression is restricted to the neural crest lineage in the adult myenteric ganglia.
1415 SNAP-25 expression (green) co-localizes with tdTomato (red) but not with the MENs marker
1416 MHCst (cyan) as observed in 2D and orthogonal views of a myenteric ganglia from a Wnt1-
1417 cre:*Rosa26*-tdTomato mouse that was immunolabeled with antibodies against MHCst and SNAP-
1418 25. Nuclei were labeled with DAPI (blue). Scale bar denotes 10 μm.

1419 **(b)** In the adult male Snap25-Gcamp knock-in mice, the expression of Snap25-Gcamp/GFP
1420 (green) is restricted to a subset of Hu-expressing (red) myenteric neurons in the adult murine
1421 small intestinal myenteric ganglia (yellow arrows), while many neurons (red arrows) do not show
1422 any detectable expression of Snap25. Nuclei were labeled with DAPI (blue). Scale bar denotes
1423 10 μm.

1424 **(c)** Orthogonal views of z-stack of an image of the myenteric ganglion from the small intestinal
1425 LM-MP tissue from an adult male Snap25-Gcamp knock-in mice shows that the expression of
1426 Snap25-Gcamp/GFP (green) is exclusive of the expression of the MENs marker MHCst (red).
1427 Nuclei were labeled with DAPI (blue). Scale bar denotes 10 μm.

1428 **Fig 9: Observation of MENs marker expression in the adult human myenteric ganglia**

1429 **(a)** Hu-expressing small intestinal myenteric neurons (green) from the normal human duodenal
1430 tissue, when immunolabeled with antibodies against the MENs marker DECORIN (red) identifies
1431 putative human MENs (red arrows) and NENs (green arrows) by presence or absence of
1432 DECORIN immunolabeling. Scale bar denotes 10 μm.

1433 **(a)** Hu-expressing small intestinal myenteric neurons (green) from the normal human duodenal
1434 tissue, when immunolabeled with antibodies against the MENs marker MHCst (red) and MET
1435 (blue) identifies putative human MENs (red arrows) and NENs (green arrows) by presence or
1436 absence of these MENs markers. Scale bar denotes 10 μm.

1437 **(c)** Immunolabeling myenteric tissue with antibodies against the MENs markers SLC17A9 (green,
1438 green arrows) and MHCst (red) shows SLC17A9 expression in a subset of MHCst-expressing
1439 (red) neurons. Subset of MHCst-expressing cells do not express SLC17A9 (red arrow). Nuclei
1440 are labeled with DAPI (blue) in the normal human duodenal tissue. Scale bar denotes 10 μm.

1441 **Fig 10: GDNF and HGF signaling regulate age-dependent changes in NENs and MENs pro-**
1442 **portions.**

1443 **(a, b)** Immunostaining myenteric plexus tissue from juvenile and mature Wnt1-cre:*Rosa26*-
1444 tdTomato mice with antibodies against the pan-neuronal marker Hu (green).

1445 **(c)** Age-associated loss of NENs and gain of MENs in the small intestinal LM-MP of maturing and
1446 aging Wnt1-cre:*Rosa26*-tdTomato mice. Data represent mean ± S.E.M.

1447 **(d)** Mean ± SEM of the four MEN-specific pattern weights in the human mesenchymal cell popu-
1448 lations from Elmentaite et al.[78], wherein data from age ranges of 4 – 12 years was clubbed to-
1449 gether as Juvenile (Juv), data from age ranges of 20 – 50 years was clubbed together as Adult
1450 (Ad), and data from age ranges of 60 – 75 years was clubbed together as Aged (Ag). Every
1451 datapoint refers to mean projected pattern weight for cells within a defined age or age range,
1452 where Juv data comprise of ages 4, 6, 9, 10, 12 years; Ad data comprise of age ranges 20 - 25,
1453 25 – 30, and 45-50 years; and finally Ag data comprise of age ranges 60 – 65, 65 – 70, and 70 –
1454 75 years. One-way ANOVA ** = $p < 0.01$).

1455 **(e)** Western blot analyses of GDNF (green) and the house-keeping protein β-actin (red) expres-
1456 sion in LM-MP tissues from mice of ages P10, P30, and P90. (n = 3 mice per group; each sample
1457 is a biological replicate). Fluorescent intensities of the two bands of GDNF (that correspond to
1458 ~25 kD bands of protein marker) were quantified together. The lower band of GDNF is present
1459 only in the P10 tissues and disappears in P30 and P90 adult murine tissues.

1460 **(f)** Western blot analyses of HGF (green) and the house-keeping protein β-Actin (red) expression
1461 in LM-MP tissues from mice of ages P10, P30, and P90. (n = 3 mice per group; each sample is a
1462 biological replicate). Fluorescent intensities of the two bands of HGF (that are between 50 kD and
1463 37 kD bands of the protein marker) were quantified together.

1464 **(g)** The normalized fluorescent intensity of GDNF protein to house-keeping protein β-Actin com-
1465 pared between the three age groups. GDNF presence was highest in P10 group and was signifi-
1466 cantly reduced in P30 and P90 groups. Data represent mean ± S.E.M. One-way ANOVA **** $p <$
1467 0.001.

1468 **(h)** Age-dependent decrease in Gdnf mRNA transcript expression (normalized to the house-keep-
1469 ing gene Hprt) in the myenteric plexuses of P30 and P90 old mice. Data represent mean ± S.E.M.
1470 Student's t-test *$p < 0.05$.

1471 **(i)** The normalized fluorescent intensity of HGF protein to house-keeping protein β-Actin was
1472 compared between the three age groups. HGF expression significantly increased from P10
1473 through P90. Data represent mean ± S.E.M. One-way ANOVA *$p < 0.05$.

1474 **(j)** Age-dependent increase in Hgf mRNA transcript expression (normalized to the house-keeping
1475 gene Hprt) in the myenteric plexuses of P10, P30, and P90 old mice. Data represent mean ±
1476 S.E.M. One-way ANOVA * $p < 0.05$, *** $p < 0.01$, **** $p < 0.001$.

1477 **(k)** Percent proportions of tdTomato$^-$ MENs and mean Hu$^+$ neurons/ganglia in LM-MP of cohorts
1478 of Wnt1-cre:*Rosa26*-tdTomato mice that were dosed with GDNF or Saline from P10 to P20 age.
1479 Data represent mean ± S.E.M. Student's t-test ** $p < 0.01$.

1480 **(l)** Percent proportions of tdTomato$^-$ MENs and mean Hu$^+$ neurons/ganglia in LM-MP of cohorts
1481 of Wnt1-cre:*Rosa26*-tdTomato mice that were dosed with HGF or Saline from P10 to P20 age.
1482 Data represent mean ± S.E.M. Student's t-test * $p < 0.05$.

1483

1484 **Fig 11: Ect2-expression labels a population of cycling MENs**

1485 **(a)** UMAP representation of the cells of the MENs, NENs, and Neuroglia clusters from scRNAseq
1486 of cells from the small intestinal LM-MP tissue of two post-natal day 21 (P21) mice.

1487 **(b)** Tricycle analyses of ENS cell-types with their cell cycle positions. The continuous cell cycle
1488 position (theta) is measured as the angle from the origin. Anti-clockwise representation of cells
1489 that are represented between 1.5π and 0.5π space on the embedding are increasingly present
1490 within the quiescent G1/G0 cell cycle phase. In contrast, cells that are represented between the
1491 0.5π and 1π space on the embedding are present within the S phase, and those within the 1π
1492 and 1.5π space are present within the G2M phase.

1493 **(c)** Cells within the P21 MENs cluster were projected into Tricycle software. 213 of the 504 P21
1494 MENs were present between the 0.5π and 1.5π space on the embedding and hence were inferred
1495 to be undergoing cell cycling.

1496 **(d, e)** Expression of cell-cycle correlated genes Top2a and Ect2 in MENs shows significant ex-
1497 pression of these two genes in cells of the P21 MENs cluster that are present between the values
1498 of 0.5π and 1.5π in the Tricycle embedding. Loess curve fittings (black) represent the dynamics
1499 of gene expression over the cell cycle (theta).

1500 Orthogonal views of small intestinal myenteric ganglia from a P21 wildtype mouse when im-
1501 munostained with antibodies against ECT (green) and against MENs markers **(f)** DECORIN (red)
1502 and **(g)** MHCst (red), shows that ECT2 is expressed in a subset of MENs at this age. Nuclei are
1503 labeled with DAPI (blue). Scale bar denotes 10 μm.

1504 **Fig 12: Reduced RET signaling accelerates ENS aging to cause pathology**

1505 **(a)** Hu immunostaining (green) LM-MP tissues from 16-week-old $Ret^{+/CFP}$ ($Ret^{+/-}$) mouse shows
1506 mutually exclusive expression of Ret-CFP (cyan, green arrow) and MHCst (red, red arrow) MENs.
1507 Nuclei are stained with DAPI (blue). Scale bar = 10 μm.

1508 **(b)** Quantification of Ret-CFP^{+} neurons from 9- and 16-week-old $Ret^{+/-}$ mice show age-associated
1509 loss of Ret-CFP^{+} neurons. Data represent mean ± S.E.M. Student's t-test * $p < 0.05$.

1510 **(c)** Quantification of $MHCst^{+}$ MENs shows significant increase in their proportions in $Ret^{+/-}$ mice
1511 but not in $Ret^{+/+}$ mice with age. Data represent mean ± S.E.M. One way ANOVA * $p < 0.05$, ** p
1512 < 0.01, *** $p < 0.001$).

1513 **(d)** Measures of whole gut transit time (WGTT) in cohorts of $Ret^{+/-}$ and $Ret^{+/+}$ mice MENs show
1514 significant slowing of whole gut transit of $Ret^{+/-}$ but not $Ret^{+/+}$ mice with age. Data represent mean
1515 ± S.E.M. One way ANOVA * = $p < 0.05$.

1516 **Fig 13: GDNF normalizes altered intestinal motility by increasing NENs proportions in the**
1517 **aging gut.**

1518 **(a)** Measures of whole gut transit time (WGTT) in GDNF (treated with GDNF) and Control (treated
1519 with Saline) cohorts of 17-month-old mice taken before the start of treatments and after the end
1520 of 10 consecutive days of treatment shows that the two groups are matched in their transit times
1521 before treatment, but GDNF treatment significant decreases average transit times when com-
1522 pared to the control cohort. Data represent mean ± S.E.M. Student's t-test *** = $p < 0.001$.

1523 **(b)** Quantification of percent $MHCst^+$ MENs per Hu-labeled neurons in myenteric ganglia in the
1524 GDNF and Control cohorts shows significant decrease in their proportions in GDNF-treated cohort
1525 but not in saline-treated control cohort. Data represent mean ± S.E.M. Student's t-test ** $p < 0.01$.

1526 **(c)** Quantification of numbers of RET^+ NENs per 40X field views of myenteric ganglia shows
1527 significant increase in their numbers in GDNF cohort mice when compared with Control cohort
1528 mice. Data represent mean ± S.E.M. Student's t-test * $p < 0.05$.

1529 **Fig 14: Patients with chronic gut dysmotility show significant shifts in their normal propor-**
1530 **tions of the two neuronal lineages.**

1531 **(a)** ProjectR-based projection of bulkRNAseq data from intestinal specimens of patients with nor-
1532 mal motility and patients with obstructive defecation (OD), a chronic condition of intestinal dys-
1533 motility, into the 50 different NMF patterns learnt earlier, shows that the MEN-specific NMF pat-
1534 terns 32 and 41 were significantly upregulated in bulk-RNAseq of OD patients compared to con-
1535 trols. Data represent mean ± S.E.M. One way ANOVA. Data mined from raw data generated by
1536 Kim et al.[100]

1537 **(b)** OD patients show a significant decrease in the expression of important NENs-associated
1538 genes such as Ret, Gdnf, Snap-25, Nos1, Klhl1, and Chat, while showing a significant increase
1539 in the expression of important MENs-specific genes such as Clic3, Upk3a, Cdh3, Slpi, and
1540 Slc17a9. Data taken from Kim et al.[100]

1541 **Suppl Figure 1: Presence and absence of tdTomato reporter expression in the myenteric**
1542 **ganglia of adult neural crest lineage-traced mice**

1543 **(a)** Hu-immunostained Wnt1-cre:*Rosa26*-tdTomato LM-MP tissue, where tdTomato-expression
1544 (red) marks neural crest-derived cells, and Hu (green) labels myenteric neurons, we observed the
1545 presence of higher intensity fluorescence (red arrows) and lower intensity fluorescence (orange
1546 arrows) in various tdTomato$^+$ neurons. The myenteric ganglia also contained Hu$^+$ neurons that
1547 did not express tdTomato (green arrow) and these neurons alone were deemed to be non-neural
1548 crest-derived neurons. Scale bar denotes 10 μm.

1549 **(b)** Reporter non-expressing Hu-immunolabeled neurons (green, green arrows) can be ob-
1550 served both through the expression of the tdTomato reporter (red), as well as on antibody label-
1551 ing of the tdTomato reporter (gray).

1552 **(c)** Freshly harvested small intestinal tissue from Wnt1-cre:*Rosa26*-tdTomato mice when im-
1553 aged under 20X magnification of a live tissue fluorescence microscope shows the presence of
1554 cells that express tdTomato (red) and those that don't.

1555 **(d)** Cells showing hyper-aggregation of the tdTomato reporter can be found in freshly harvested
1556 full-thickness small intestinal myenteric plexus in tissues imaged under 20X magnification of a
1557 live tissue fluorescence microscope.

1558 **(e)** Myenteric ganglia from fixed LM-MP tissue of adult Wnt1-cre:*Rosa26*-tdTomato mice show
1559 show hyper-aggregation of tdTomato (white arrow) when imaged using a confocal microscope.
1560 Nuclei are stained with nuclear marker DAPI (blue). Scale bar denotes 10 μm.

1561 **(f)** Cells showing hyper-aggregation of tdTomato (red, red arrow) show no detectable nuclear
1562 labeling with DAPI (blue) or of pan-neuronal marker Hu (green, green arrow). Scale bar denotes
1563 10 μm.

1564 In addition, interrogation of two other neural crest-specific lineage-traced mouse lines confirms
1565 our observations with Wnt1-cre:*Rosa26*-tdTomato mice. **(g)** In Wnt1-cre:*Hprt*-tdTomato adult
1566 male mice, tdTomato expression (red) is present only in a subset of Hu-immunolabeled (green)
1567 neurons (red arrows) while it is not detected in other Hu-expressing neurons (green). Similarly,
1568 **(h)** only a subpopulation of Hu^+ adult enteric neurons (green) is derived from the neural crest, as
1569 seen by its co-expression of tdTomato (red, red arrows) in the Pax3-cre:*Rosa26*-tdTomato mice
1570 while other neurons that do not express tdTomato (white arrows) are inferred to be not derived
1571 from the neural crest. Scale bar denotes 10 μm.

1572 **(i)** Orthogonal views of small intestinal villus from a Wnt1-cre:*Rosa26*-tdTomato mouse that
1573 shows presence of tdTomato-expressing (red) neural crest-derived fibers inside the villus but a
1574 complete lack of tdTomato-expression by intestinal epithelial cells. Nuclei are labeled with DAPI
1575 (blue). Scale bar denotes 10 μm.

1576 **(j)** Representational image of the myenteric plexus from a *Rosa26*-tdTomato mouse without any
1577 cre driver showing that in absence of cre recombinase to drive tdTomato expression, there is a
1578 lack of tdTomato expression in this layer. Nuclei are labeled with DAPI (blue). Scale bar denotes
1579 10 μm.

1580 **(k)** Representational image of the myenteric plexus from a *Rosa26*-EGFP mouse without any cre
1581 driver showing that in absence of cre recombinase to drive EGFP expression, there is a lack of
1582 EGFP expression in this layer. Nuclei are labeled with DAPI (blue). Scale bar denotes 10 μm.

1583 **(l)** Western blot image showing detection of two different loading amounts of the recombinant
1584 HuB protein by the rabbit polyclonal antibody against HuC/D (abcam). Molecular Weight marker
1585 with defined band sizes indicated on the right.

1586

1587 **Suppl Figure 2: Tek-expressing and Mesp1-expressing mesodermal lineage contributes to**
1588 **adult enteric neurons.**

1589 **(a)** Adult small intestinal LM-MP layer from a male Tek-EGFP mouse, where EGFP expression
1590 (green) labels Tek-expressing cells was immunostained with specific antibodies against the pan-
1591 neuronal marker PGP9.5 (red) and imaged under a confocal microscope. The Tek-EGFP expres-
1592 sion did not label any cells within the myenteric plexus marked by PGP9.5 expression showing
1593 that adult small intestinal myenteric neurons did not express Tek. Nuclei are labeled with DAPI
1594 (blue). Scale bar denotes 10 μm.

1595 **(b)** We observed the presence of higher intensity fluorescence (red arrows) and lower intensity
1596 fluorescence (green arrow) in various tdTomato^{+} cells in a section of heart tissue from a 6-month-
1597 old Mesp1-cre:*Rosa26*-tdTomato adult male mouse, where tdTomato (red) labels Mesp1-derived
1598 cells of the mesodermal lineage that includes cardiomyocytes and vasculature. Nuclei are stained
1599 by DAPI (blue). Scale bar denotes 10 μm.

1600 **(c)** Adult small intestinal LM-MP layer from a 6-month-old male Mesp1-cre:*Rosa26*-tdTomato
1601 mouse, where tdTomato (red) cells are mesoderm-derived cells, was immunostained with specific
1602 antibodies against the pan-neuronal marker Hu (green) and imaged under a confocal microscope.
1603 tdTomato-expressing cells outside the ganglia (red arrows) were brighter than tdTomato+ neu-
1604 rons inside the ganglia (green arrows). Nuclei are labeled with DAPI (blue). Scale bar denotes 10
1605 μm.

1606 **(d)** Adult small intestinal LM-MP layer from a 2-month old male Mesp1-cre:Rosa26-EGFP mouse,
1607 where EGFP cells are mesoderm-derived, was immunostained with specific antibodies against
1608 the reporter EGFP (green) and the pan-neuronal marker Hu (red) and imaged under a confocal
1609 microscope. A population of Hu-immunolabeled neurons were also labeled with antibodies
1610 against EGFP (green arrows) while other neurons were not (red arrows), suggesting the

1611 derivation of EGFP$^+$ neurons from the Mesp1-expressing mesoderm. **(e)** No primary control for
1612 the Anti-GFP immunostaining showed very weak EGFP expression in the fixed LM-MP tissue
1613 from these animals. Nuclei were labeled with DAPI (blue). Scale bar = 10 μm. Consistent with the
1614 observations made with the tdTomato reporter in this transgenic line, the Mesp1-cre:*Rosa26*-
1615 EGFP animals also show a brighter reporter signal in the vasculature and a dimmer reporter signal
1616 in the myenteric neurons.

1617 **(f)** MHCst$^+$ (cyan) labels all tdTomato$^+$ (red) Hu$^+$ (green) adult neurons (white arrows) but not the
1618 tdTomato$^-$ neurons (yellow arrow) in the mesoderm-specific Tek-cre:*Hprt*-tdTomato lineage-
1619 traced lines. Nuclei are stained with DAPI (blue). Scale bar = 10 μm.

1620 **Suppl Figure 3: Validation of MENs-specific markers by immunohistochemistry and con-**
1621 **focal microscopy.**

1622 Small intestinal LM-MP from several adult 5-month-old male Wnt1-cre:*Rosa26*-tdTomato mice,
1623 where tdTomato-expression (red) labels neural crest-derived cells, was used to ascertain and
1624 validate the expression of the novel MENs marker and of known neuronal marker genes.

1625 **(a)** The myenteric ganglion shown in Fig 2h is presented here as a merged image (where MHCst
1626 immunostaining and tdTomato-expression are shown together) and with MHCst immunostaining
1627 without tdTomato signal to better appreciate the presence of MHCst-expressing neurons in the
1628 ganglia. MHCst-specific antibody S46 (green) was found to label tdTomato non-expressing cells
1629 within the myenteric ganglia as well as cells outside of the myenteric ganglia. Neural crest-derived
1630 cells within the myenteric ganglia expressed tdTomato. Nuclei are labeled with DAPI (blue). Scale
1631 bar denotes 10 µm.

1632 The immunostaining of the MENs-markers elucidated through scRNAseq analyses: **(b)** CDH3, **(c)**
1633 AEBP1, **(d)** SLPI, **(e)** CFTR, **(f)** NT-3, **(g)** CLIC3, **(h)** FMO2, **(i)** IL-18, **(j)** MYL-7, and **(k)** SLC17A9
1634 (all immunolabeled cells in these panels are green; green arrows) was found to be localized to or
1635 enriched in cells without tdTomato expression, while the tdTomato^{+} cells were found to show not
1636 to express these MENs-specific markers (red arrow). In addition, we also immunolabeled the
1637 myenteric ganglia from this transgenic mouse line with known neuronal markers (gray) and with
1638 antibodies against the pan-neuronal marker Hu (green) to show that the neuronal markers Elavl2
1639 or HuB **(l)**, GPR88 **(m)**, HAND2 **(n)**, PDE10A **(o)**, TUBB2B **(p)** and VSNL1 **(q)** were expressed
1640 by both tdTomato^{+} (red arrow) and tdTomato^{-} Hu^{+} neurons. Orthogonal views of images where
1641 3D image z-stacks were obtained are provided for better visualization of marker expression in the
1642 3D space. Nuclei in these tissues were labeled with DAPI (blue). Scale bar denotes 10 µm.

1643 **Suppl Figure 4: scRNAseq metrics**

1644 **(a)** MENs are significantly larger in size as compared to the NENs, as the mean Feret's Diameter
1645 of the Wnt1-cre:*Rosa26*-tdTomato^{-} MENs is significantly more than that of the Wnt1-
1646 cre:tdTomato^{+} NENs. Student's t-test; ** p value < 0.01.

1647 **(b, c)** UMAP representation of sequenced cells generated from 10X Genomics Chromium-derived
1648 libraries from the two mouse samples, taken from separate littermate adult male mice, shows
1649 similar representation of their cells across the various clusters.

1650 **(d)** Quasiviolin plot of expressed genes provide a comparison of important MEN-specific and neu-
1651 ronal genes between the NENs and MENs clusters in the adult ileal May-Zhang et al. dataset and
1652 the NENs, Neuroglial, and MENs clusters in our scRNAseq dataset.

1653 **(e)** Top genes that are pattern drivers for the four MEN-specific NMF patterns along with their
1654 gene weights.

1655 **(f)** The four MEN-specific patterns were together used to label a group of cells (True) that together
1656 showed increased usage of the MEN-specific patterns, when compared to other cell types (False)
1657 in the adult ileal snRNAseq dataset from May-Zhang et al.[50].

1658 **(g)** Top-expressed genes in the group of cells **(f)** that showed higher utilization of the MEN-spe-
1659 cific patterns, compared to other cells in the dataset.

1660 **(h)** Representation of the four MEN-specific NMF patterns in the UMAP of our data and the pro-
1661 jection of the May-Zhang et al.[50] murine ileal dataset and the entire gut mesenchymal single cell
1662 RNA seq dataset by Elmentaite et al.[78] into the MEN-specific patterns highlights cell clusters that
1663 show higher usage of the four NMF patterns. Bottom row shows increasing usage of these pat-
1664 terns with age in the entire mesenchymal gut cell atlas data.

1665 **Suppl Figure 5: Expression of neuronally significant genes by MENs**

1666 Sparklines plot of gene expression in various cell clusters, as revealed by single cell transcriptom-
1667 ics of diverse LM-MP cells from small intestinal tissue of two 6-month-old mice, show that expres-
1668 sion of some genes is enriched in the MENs cluster, when compared to the other major clusters
1669 of cells in the dataset. Lower to higher expression in the plot is represented by yellow to blue
1670 gradient. Subsequent analyses shows that proteins coded by these genes are neuronally signifi-
1671 cant.

1672

1673 **Suppl Figure 6: Expression of mesodermal marker MYH11, and reporter expression under**
1674 **the Baf53b-cre transgenic line in post-natal myenteric neurons**

1675 **(a)** Orthogonal views of a myenteric ganglion of an adult Wnt1-cre:*Rosa26*-tdTomato mouse,
1676 where tdTomato (red) is expressed by neural crest-derived cells, shows that immunolabeling with
1677 a MYH11-specific antibody (green) labels tdTomato non-expressing cells. Nuclei are labeled with
1678 DAPI (blue). Scale bar denotes 10 µm.

1679 **(b)** Representative image of the myenteric plexus layer from a Myh11-cre^{ERT2}:*Rosa26*-YFP adult
1680 male mouse, which was dosed with tamoxifen for two consecutive weeks, and which when im-
1681 munostained with antibodies against YFP/GFP (green) and the pan-neuronal marker Hu (red),
1682 shows the presence of YFP-expressing neurons (green arrows) in the myenteric ganglia that also
1683 contains YFP negative neurons (red arrow). Nuclei are labeled with DAPI (blue). Scale bar de-
1684 notes 10 µm.

1685 **(c)** Immunostaining of healthy human adult duodenal tissue with antibodies against the pan-neu-
1686 ronal marker PGP9.5 (green) and MYH11 (red), shows that in the circular muscularis layer of the
1687 tissue, MYH11 labels the smooth muscle and not the PGP9.5 immunostained nerve fibers and
1688 cell bodies. Scale bar denotes 10 µm.

1689 **(d)** Immunostaining of healthy human adult duodenal tissue with antibodies against the pan-neu-
1690 ronal marker PGP9.5 (green) and MYH11 (red), shows that in the myenteric ganglia, MYH11
1691 immunolabels a subset of PGP9.5-expressing myenteric neurons (white arrows). Scale bar de-
1692 notes 10 µm.

1693 **(e)** Representative image of a myenteric ganglion from a Baf53b-cre:*Rosa26*-tdTomato adult male
1694 mouse, where tdTomato (red) is expressed by Baf53b expressing cells or those derived from
1695 Baf53-expressing cells, when immunostained with antibodies against the pan-neuronal marker
1696 Hu (green), shows the presence of neurons that express tdTomato (white arrows) along with

1697 neurons that do not express tdTomato (green arrows). Nuclei are labeled with DAPI (blue). Scale
1698 bar denotes 10 μm.

1699 **(f)** Graphical representation of the proportions of tdTomato-expressing Hu^+ myenteric neurons in
1700 the LM-MP tissue of two male P21 Baf53b-cre:*Rosa26*-tdTomato mice shows that myenteric gan-
1701 glia from ileum, proximal colon, and distal colon contain significant proportions of neurons that do
1702 not express tdTomato under the Baf53b-cre transgenic line.

1703

1704 **Suppl Figure 7: Putative mesoderm-derived enteric neurons (MENs) are present in adult**
1705 **human myenteric ganglia.**

1706 **(a, b)** The mesodermal specific markers, MET and MHCst are expressed by a subpopulation of
1707 human enteric neurons. Myenteric ganglia from normal duodenal tissue of 2 different adult human
1708 subjects express the pan-neuronal marker Hu (green), with distinct subpopulations positive and
1709 negative for MET (blue) and MHCst (red). MET and MHCst-expressing neurons (red arrows) in
1710 the human ENS are assumed to be mesoderm-derived enteric neurons (MENs) and those not
1711 expressing these MENs markers (green arrows) are presumably NENs. Nuclei are labeled with
1712 DAPI (gray). Scale bar = 10 μm.

1713 **(c)** The mesodermal specific marker DECORIN is expressed by a subpopulation of human enteric
1714 neurons. Myenteric ganglia from normal human duodenal tissue when immunostained with anti-
1715 bodies against the pan-neuronal marker Hu (green) and DECORIN (red) shows the presence of
1716 DECORIN-expressing myenteric neurons, which are assumed to be MENs. Nuclei are labeled
1717 with DAPI (blue). Scale bar = 10 μm.

1718 **(d)** Distribution of the various mesenchymal clusters of the post-natal healthy gut cell atlas data
1719 (generated by Elmentaite et al.[78]) by donor age. For the age of each donor, the proportion of cells
1720 annotated as belonging to each cluster is shown. Proportions of Cluster 1 are observed to expand
1721 with age.

1722 **Suppl Fig 8: Sub-clustering MENs in the scRNAseq dataset generated from 6-month-old**

1723 **mice.**

1724 **(a)** Sub-clustering the MENs cluster from our scRNAseq dataset into 5 distinct clusters **(b)** was

1725 found to be not based on the expression of cluster-specific marker genes.

1726

1727 **Suppl Fig 9: HGF and GDNF ratios in maturing and adult murine gut.**

1728 **(a)** Ratio of HGF:GDNF values in fluorescence intensities of their western blots (normalized to
1729 their own house-keeping protein Beta Actin) from the small intestinal LM-MP of post-natal mice
1730 at different ages during their maturation.

1731 **(b)** Ratio of HGF:GDNF expression values from the full thickness small intestinal tissue of adult
1732 mice taken from the Tabula muris database[91].

1733 **(c)** Analyses of human plasma proteome from 1,025 individuals was performed by Sathyan et
1734 al.[92] and the correlation of various plasma proteomes with aging was calculated. Of the genes
1735 that showed significant correlation with age ($p < 0.05$), we found that the HGF levels in human
1736 plasma correlated positively with age (above 0), while the levels of GDNF and RET correlated
1737 negatively with age (below 0).

1738 **Suppl Fig 10: Identification of the MENs cluster in the P21 scRNAseq data and expression**
1739 **of Ret in NENs and in the Ret heterozygous mice.**

1740 **(a)** UMAP representation of all the cell clusters generated from scRNAseq performed on all cells
1741 from the P21 murine LM-MP.

1742 **(b)** Projection of scRNAseq from the P21 murine LM-MP cells into the four MEN-specific NMF
1743 patterns generated using scRNAseq on 6-month-old murine LM-MP cells shows higher usage of
1744 the four NMF patterns in the putative MENs cluster in the P21 dataset (black arrow).

1745 **(c)** Expression of the genes Ret and Met in the MENs and NENs clusters in the scRNAseq of P21
1746 LM-MP cells shows that while Met-expression is detected in both MENs and a subset of NENs,
1747 the MET-expressing NENs subset shows significant expression of Ret, while the MENs do not
1748 express Ret.

1749 **(d)** Sparklines plot of gene expression of various neuronally significant genes in the scRNAseq
1750 data from Zeisel et al., which was generated using flow sorted Wnt1-cre:*Rosa26*-tdTomato^{+} cells
1751 from a P21 mouse, shows that Met expression is observed in the clusters ENT6, 8, and 9 which
1752 also show expression of CGRP-expressing gene Calcb, the neural crest-specific gene Ret, Cho-
1753 line acetyltransferase-expressing gene Chat and the pan-neuronal marker PGP9.5-expressing
1754 gene Uchl1.

1755 **(e)** Fold change in transcript abundance of the gene Ret in the small intestinal LM-MP tissue from
1756 Ret wildtype (Ret WT) and Ret heterozygous (Ret Het) littermate adult mice shows that Ret tran-
1757 scripts are significantly less abundant in the tissue of Ret Het mice, when compared to those from
1758 Ret WT mice. Ret transcript expression in every sample was normalized to the expression of the
1759 house keeping gene Hprt. Student's t-test; * p value < 0.05.

1760 **Suppl Fig 11: Effect of GDNF treatment on MHCst-expressing MENs and RET-expressing**
1761 **NENs in aging mice**

1762 Representative image of MHCst (red) and Hu (green)-immunostained myenteric ganglia of **(a)**
1763 saline-treated control and **(b)**. GDNF-treated 17-month-old mice show MHCst^{+} (yellow arrows)
1764 and MHCst^{-} neurons. Note the reduction in MHCst-immunostaining on inter-ganglionic fibers in
1765 the 17-month-old mice when treated with GDNF, compared to control mice. Nuclei are stained
1766 with DAPI (blue). Scale bar indicates 10 µm.

1767 Representative image of RET-immunostained (green) myenteric ganglia of **(c)**. saline-treated
1768 control and **(d)**. GDNF-treated 17-month-old mice. Nuclei are stained with DAPI (blue). Scale bar
1769 indicates 10 µm.

1770 **(e)** Western blot image of a 4-20% gel performed using the RET antibody on total protein lysate
1771 from small intestinal LM-MP layer from post-natal mice shows the expected band between150
1772 and 250 kDa of RET protein.

1773 **Suppl Fig 12: Projection of the bulk RNA sequencing data of intestinal tissue from Con-**
1774 **trol and Patients with Obstructed Defecation into our murine scRNAseq-derived NMF pat-**
1775 **terns using *projectR*.**

1776 Transcriptomic data from intestinal tissues of patients with normal intestinal motility and those
1777 with obstructed defecation (OD) was procured from GEO (GSE101968). Non-negative matrix fac-
1778 torization (NMF), as implemented in the R package *NNLM* (https://github.com/linxihui/NNLM),
1779 was performed on the murine scRNAseq data using k=50 and default parameters; and cell
1780 weights for each pattern were grouped. Using projectR, the log2 expression (log2(rpkm + 1)) from
1781 the human bulk RNA sequencing data from control and OD patients were projected into the mu-
1782 rine scRNAseq-derived NMF patterns. The mean projection weights from Control and OD groups
1783 were tested for statistically significant differences using Students' t tests.

References

1 Kulkarni, S. *et al.* Advances in Enteric Neurobiology: The "Brain" in the Gut in Health and Disease. *J Neurosci* **38**, 9346-9354, doi:10.1523/JNEUROSCI.1663-18.2018 (2018).

2 Jarret, A. *et al.* Enteric Nervous System-Derived IL-18 Orchestrates Mucosal Barrier Immunity. *Cell* **180**, 50-63 e12, doi:10.1016/j.cell.2019.12.016 (2020).

3 Uesaka, T., Young, H. M., Pachnis, V. & Enomoto, H. Development of the intrinsic and extrinsic innervation of the gut. *Dev Biol* **417**, 158-167, doi:10.1016/j.ydbio.2016.04.016 (2016).

4 Obermayr, F., Hotta, R., Enomoto, H. & Young, H. M. Development and developmental disorders of the enteric nervous system. *Nature reviews. Gastroenterology & hepatology* **10**, 43-57, doi:10.1038/nrgastro.2012.234 (2013).

5 Hao, M. M. & Young, H. M. Development of enteric neuron diversity. *J Cell Mol Med* **13**, 1193-1210, doi:10.1111/j.1582-4934.2009.00813.x (2009).

6 Anderson, R. B., Newgreen, D. F. & Young, H. M. Neural crest and the development of the enteric nervous system. *Adv Exp Med Biol* **589**, 181-196, doi:10.1007/978-0-387-46954-6_11 (2006).

7 Young, H. M. & Newgreen, D. Enteric neural crest-derived cells: origin, identification, migration, and differentiation. *Anat Rec* **262**, 1-15, doi:10.1002/1097-0185(20010101)262:1<1::AID-AR1006>3.0.CO;2-2 (2001).

8 Young, H. M., Hearn, C. J. & Newgreen, D. F. Embryology and development of the enteric nervous system. *Gut* **47 Suppl 4**, iv12-14; discussion iv26, doi:10.1136/gut.47.suppl_4.iv12 (2000).

9 Bergner, A. J. *et al.* Birthdating of myenteric neuron subtypes in the small intestine of the mouse. *J Comp Neurol* **522**, 514-527, doi:10.1002/cne.23423 (2014).

10 Uesaka, T., Nagashimada, M. & Enomoto, H. Neuronal Differentiation in Schwann Cell Lineage Underlies Postnatal Neurogenesis in the Enteric Nervous System. *J Neurosci* **35**, 9879-9888, doi:10.1523/JNEUROSCI.1239-15.2015 (2015).

11 Espinosa-Medina, I. *et al.* Dual origin of enteric neurons in vagal Schwann cell precursors and the sympathetic neural crest. *Proc Natl Acad Sci U S A* **114**, 11980-11985, doi:10.1073/pnas.1710308114 (2017).

12 Burns, A. J. Migration of neural crest-derived enteric nervous system precursor cells to and within the gastrointestinal tract. *Int J Dev Biol* **49**, 143-150, doi:10.1387/ijdb.041935ab (2005).

13 Laranjeira, C. *et al.* Glial cells in the mouse enteric nervous system can undergo neurogenesis in response to injury. *The Journal of clinical investigation* **121**, 3412-3424, doi:10.1172/JCI58200 (2011).

14 Brokhman, I. *et al.* Dual embryonic origin of the mammalian enteric nervous system. *Dev Biol* **445**, 256-270, doi:10.1016/j.ydbio.2018.11.014 (2019).

15 Sohal, G. S., Ali, M. M. & Farooqui, F. A. A second source of precursor cells for the developing enteric nervous system and interstitial cells of Cajal. *Int J Dev Neurosci* **20**, 619-626 (2002).

16 Habeck, M. VENT cells--a load of hot air? *Drug Discov Today* **8**, 332-333 (2003).

17 Saffrey, M. J. Cellular changes in the enteric nervous system during ageing. *Dev Biol* **382**, 344-355, doi:10.1016/j.ydbio.2013.03.015 (2013).

18 Becker, L., Kulkarni, S., Tiwari, G., Micci, M. A. & Pasricha, P. J. Divergent fate and origin of neurosphere-like bodies from different layers of the gut. *Am J Physiol Gastrointest Liver Physiol* **302**, G958-965, doi:10.1152/ajpgi.00511.2011 (2012).

19 Kulkarni, S. *et al.* Adult enteric nervous system in health is maintained by a dynamic balance between neuronal apoptosis and neurogenesis. *Proc Natl Acad Sci U S A* **114**, E3709-E3718, doi:10.1073/pnas.1619406114 (2017).

1829 20 Antal, M., Beneduce, B. M. & Regehr, W. G. The substantia nigra conveys target-dependent
1830 excitatory and inhibitory outputs from the basal ganglia to the thalamus. *J Neurosci* **34**, 8032-
1831 8042, doi:10.1523/JNEUROSCI.0236-14.2014 (2014).
1832 21 Freyer, L., Aggarwal, V. & Morrow, B. E. Dual embryonic origin of the mammalian otic vesicle
1833 forming the inner ear. *Development* **138**, 5403-5414, doi:10.1242/dev.069849 (2011).
1834 22 Wright, C. M. *et al.* scRNA-Seq Reveals New Enteric Nervous System Roles for GDNF, NRTN, and
1835 TBX3. *Cell Mol Gastroenterol Hepatol* **11**, 1548-1592 e1541, doi:10.1016/j.jcmgh.2020.12.014
1836 (2021).
1837 23 King, P. H., Redden, D., Palmgren, J. S., Nabors, L. B. & Lennon, V. A. Hu Antigen Specificities of
1838 ANNA-I Autoantibodies in Paraneoplastic Neurological Disease. *Journal of Autoimmunity* **13**, 435-
1839 443, doi:https://doi.org/10.1006/jaut.1999.0337 (1999).
1840 24 Honig, G., Liou, A., Berger, M., German, M. S. & Tecott, L. H. Precise pattern of recombination in
1841 serotonergic and hypothalamic neurons in a Pdx1-cre transgenic mouse line. *J Biomed Sci* **17**, 82,
1842 doi:10.1186/1423-0127-17-82 (2010).
1843 25 Bardot, E. *et al.* Foxa2 identifies a cardiac progenitor population with ventricular differentiation
1844 potential. *Nat Commun* **8**, 14428, doi:10.1038/ncomms14428 (2017).
1845 26 Burtscher, I., Barkey, W., Schwarzfischer, M., Theis, F. J. & Lickert, H. The Sox17-mCherry fusion
1846 mouse line allows visualization of endoderm and vascular endothelial development. *genesis* **50**,
1847 496-505, doi:10.1002/dvg.20829 (2012).
1848 27 Wilm, B., Ipenberg, A., Hastie, N. D., Burch, J. B. & Bader, D. M. The serosal mesothelium is a major
1849 source of smooth muscle cells of the gut vasculature. *Development* **132**, 5317-5328,
1850 doi:10.1242/dev.02141 (2005).
1851 28 Kawaguchi, M., Bader, D. M. & Wilm, B. Serosal mesothelium retains vasculogenic potential. *Dev*
1852 *Dyn* **236**, 2973-2979, doi:10.1002/dvdy.21334 (2007).
1853 29 Herrick, S. E. & Mutsaers, S. E. Mesothelial progenitor cells and their potential in tissue
1854 engineering. *Int J Biochem Cell Biol* **36**, 621-642, doi:10.1016/j.biocel.2003.11.002 (2004).
1855 30 Chan, Sunny S.-K. *et al.* Mesp1 Patterns Mesoderm into Cardiac, Hematopoietic, or Skeletal
1856 Myogenic Progenitors in a Context-Dependent Manner. *Cell Stem Cell* **12**, 587-601,
1857 doi:10.1016/j.stem.2013.03.004 (2013).
1858 31 Devine, W. P., Wythe, J. D., George, M., Koshiba-Takeuchi, K. & Bruneau, B. G. Early patterning
1859 and specification of cardiac progenitors in gastrulating mesoderm. *Elife* **3**,
1860 doi:10.7554/eLife.03848 (2014).
1861 32 Lescroart, F. *et al.* Early lineage restriction in temporally distinct populations of Mesp1 progenitors
1862 during mammalian heart development. *Nat Cell Biol* **16**, 829-840, doi:10.1038/ncb3024 (2014).
1863 33 Klotz, L. *et al.* Cardiac lymphatics are heterogeneous in origin and respond to injury. *Nature* **522**,
1864 62-67, doi:10.1038/nature14483 (2015).
1865 34 Chan, S. S. *et al.* Mesp1 patterns mesoderm into cardiac, hematopoietic, or skeletal myogenic
1866 progenitors in a context-dependent manner. *Cell Stem Cell* **12**, 587-601,
1867 doi:10.1016/j.stem.2013.03.004 (2013).
1868 35 Baup, D., Moser, M., Schurmans, S. & Leo, O. Developmental regulation of the composite CAG
1869 promoter activity in the murine T lymphocyte cell lineage. *Genesis* **47**, 799-804,
1870 doi:10.1002/dvg.20569 (2009).
1871 36 Alexopoulou, A. N., Couchman, J. R. & Whiteford, J. R. The CMV early enhancer/chicken beta actin
1872 (CAG) promoter can be used to drive transgene expression during the differentiation of murine
1873 embryonic stem cells into vascular progenitors. *BMC Cell Biol* **9**, 2, doi:10.1186/1471-2121-9-2
1874 (2008).
1875 37 Hu, X. *et al.* Reprogramming progressive cells display low CAG promoter activity. *Stem Cells* **39**,
1876 43-54, doi:10.1002/stem.3295 (2021).

38 Akagi, Y. *et al.* Transcriptional activation of a hybrid promoter composed of cytomegalovirus enhancer and beta-actin/beta-globin gene in glomerular epithelial cells in vivo. *Kidney Int* **51**, 1265-1269, doi:10.1038/ki.1997.172 (1997).

39 Agah, R. *et al.* Gene recombination in postmitotic cells. Targeted expression of Cre recombinase provokes cardiac-restricted, site-specific rearrangement in adult ventricular muscle in vivo. *The Journal of clinical investigation* **100**, 169-179, doi:10.1172/JCI119509 (1997).

40 Sokoloff, A. J., Li, H. & Burkholder, T. J. Limited expression of slow tonic myosin heavy chain in human cranial muscles. *Muscle Nerve* **36**, 183-189, doi:10.1002/mus.20797 (2007).

41 Stockdale, F. E. & Miller, J. B. The cellular basis of myosin heavy chain isoform expression during development of avian skeletal muscles. *Dev Biol* **123**, 1-9, doi:10.1016/0012-1606(87)90420-9 (1987).

42 Miller, J. B., Crow, M. T. & Stockdale, F. E. Slow and fast myosin heavy chain content defines three types of myotubes in early muscle cell cultures. *J Cell Biol* **101**, 1643-1650, doi:10.1083/jcb.101.5.1643 (1985).

43 Vaughan, S. K., Stanley, O. L. & Valdez, G. Impact of Aging on Proprioceptive Sensory Neurons and Intrafusal Muscle Fibers in Mice. *J Gerontol A Biol Sci Med Sci* **72**, 771-779, doi:10.1093/gerona/glw175 (2017).

44 Avetisyan, M. *et al.* Hepatocyte Growth Factor and MET Support Mouse Enteric Nervous System Development, the Peristaltic Response, and Intestinal Epithelial Proliferation in Response to Injury. *J Neurosci* **35**, 11543-11558, doi:10.1523/JNEUROSCI.5267-14.2015 (2015).

45 Rappolee, D. A., Iyer, A. & Patel, Y. Hepatocyte growth factor and its receptor are expressed in cardiac myocytes during early cardiogenesis. *Circ Res* **78**, 1028-1036, doi:10.1161/01.res.78.6.1028 (1996).

46 Hao, M. M., Bornstein, J. C. & Young, H. M. Development of myenteric cholinergic neurons in ChAT-Cre;R26R-YFP mice. *J Comp Neurol* **521**, 3358-3370, doi:10.1002/cne.23354 (2013).

47 Abraira, V. E. *et al.* The Cellular and Synaptic Architecture of the Mechanosensory Dorsal Horn. *Cell* **168**, 295-310 e219, doi:10.1016/j.cell.2016.12.010 (2017).

48 Zeisel, A. *et al.* Molecular Architecture of the Mouse Nervous System. *Cell* **174**, 999-1014 e1022, doi:10.1016/j.cell.2018.06.021 (2018).

49 Drokhlyansky, E. *et al.* The Human and Mouse Enteric Nervous System at Single-Cell Resolution. *Cell* **182**, 1606-1622.e1623, doi:https://doi.org/10.1016/j.cell.2020.08.003 (2020).

50 May-Zhang, A. A. *et al.* Combinatorial Transcriptional Profiling of Mouse and Human Enteric Neurons Identifies Shared and Disparate Subtypes In Situ. *Gastroenterology* **160**, 755-770 e726, doi:10.1053/j.gastro.2020.09.032 (2021).

51 Morarach, K. *et al.* Diversification of molecularly defined myenteric neuron classes revealed by single-cell RNA sequencing. *Nat Neurosci* **24**, 34-46, doi:10.1038/s41593-020-00736-x (2021).

52 Pollen, A. A. *et al.* Low-coverage single-cell mRNA sequencing reveals cellular heterogeneity and activated signaling pathways in developing cerebral cortex. *Nat Biotechnol* **32**, 1053-1058, doi:10.1038/nbt.2967 (2014).

53 Heanue, T. A. & Pachnis, V. Expression profiling the developing mammalian enteric nervous system identifies marker and candidate Hirschsprung disease genes. *Proceedings of the National Academy of Sciences* **103**, 6919, doi:10.1073/pnas.0602152103 (2006).

54 D'Autreaux, F., Morikawa, Y., Cserjesi, P. & Gershon, M. D. Hand2 is necessary for terminal differentiation of enteric neurons from crest-derived precursors but not for their migration into the gut or for formation of glia. *Development* **134**, 2237-2249, doi:10.1242/dev.003814 (2007).

55 Strick, C. A. *et al.* Alterations in gene regulation following inhibition of the striatum-enriched phosphodiesterase, PDE10A. *Neuropharmacology* **58**, 444-451, doi:10.1016/j.neuropharm.2009.09.008 (2010).

56 Bernstein, H. G. *et al.* Hippocampal expression of the calcium sensor protein visinin-like protein-1 in schizophrenia. *Neuroreport* **13**, 393-396, doi:10.1097/00001756-200203250-00006 (2002).
57 Massart, R., Guilloux, J. P., Mignon, V., Sokoloff, P. & Diaz, J. Striatal GPR88 expression is confined to the whole projection neuron population and is regulated by dopaminergic and glutamatergic afferents. *Eur J Neurosci* **30**, 397-414, doi:10.1111/j.1460-9568.2009.06842.x (2009).
58 Soo Hoo, L. *et al.* The SNARE Protein Syntaxin 3 Confers Specificity for Polarized Axonal Trafficking in Neurons. *PLoS One* **11**, e0163671, doi:10.1371/journal.pone.0163671 (2016).
59 Breuss, M. *et al.* The Expression of Tubb2b Undergoes a Developmental Transition in Murine Cortical Neurons. *J Comp Neurol* **523**, 2161-2186, doi:10.1002/cne.23836 (2015).
60 De Giorgio, R., Arakawa, J., Wetmore, C. J. & Sternini, C. Neurotrophin-3 and neurotrophin receptor immunoreactivity in peptidergic enteric neurons. *Peptides* **21**, 1421-1426, doi:10.1016/s0196-9781(00)00286-2 (2000).
61 Mitsui, S., Yamaguchi, N., Osako, Y. & Yuri, K. Enzymatic properties and localization of motopsin (PRSS12), a protease whose absence causes mental retardation. *Brain Res* **1136**, 1-12, doi:10.1016/j.brainres.2006.11.094 (2007).
62 Krammer, H. J., Karahan, S. T., Rumpel, E., Klinger, M. & Kuhnel, W. Immunohistochemical visualization of the enteric nervous system using antibodies against protein gene product (PGP) 9.5. *Ann Anat* **175**, 321-325, doi:10.1016/s0940-9602(11)80029-4 (1993).
63 Ono, S. *et al.* Regulatory roles of complexins in neurotransmitter release from mature presynaptic nerve terminals. *Eur J Neurosci* **10**, 2143-2152, doi:10.1046/j.1460-9568.1998.00225.x (1998).
64 Leon, A., Aparicio, G. I. & Scorticati, C. Neuronal Glycoprotein M6a: An Emerging Molecule in Chemical Synapse Formation and Dysfunction. *Front Synaptic Neurosci* **13**, 661681, doi:10.3389/fnsyn.2021.661681 (2021).
65 Hoogstraaten, R. I., van Keimpema, L., Toonen, R. F. & Verhage, M. Tetanus insensitive VAMP2 differentially restores synaptic and dense core vesicle fusion in tetanus neurotoxin treated neurons. *Scientific Reports* **10**, 10913, doi:10.1038/s41598-020-67988-2 (2020).
66 Neill, T., Schaefer, L. & Iozzo, R. V. Decorin: A Guardian from the Matrix. *The American Journal of Pathology* **181**, 380-387, doi:https://doi.org/10.1016/j.ajpath.2012.04.029 (2012).
67 Scott, P. G., Dodd, C. M. & Pringle, G. A. Mapping the locations of the epitopes of five monoclonal antibodies to the core protein of dermatan sulfate proteoglycan II (decorin). *Journal of Biological Chemistry* **268**, 11558-11564, doi:https://doi.org/10.1016/S0021-9258(19)50237-X (1993).
68 Corpening, J. C., Cantrell, V. A., Deal, K. K. & Southard-Smith, E. M. A Histone2BCerulean BAC transgene identifies differential expression of Phox2b in migrating enteric neural crest derivatives and enteric glia. *Dev Dyn* **237**, 1119-1132, doi:10.1002/dvdy.21498 (2008).
69 Stein-O'Brien, G. L. *et al.* Decomposing Cell Identity for Transfer Learning across Cellular Measurements, Platforms, Tissues, and Species. *Cell Syst* **8**, 395-411 e398, doi:10.1016/j.cels.2019.04.004 (2019).
70 Stein-O'Brien, G. L. *et al.* Enter the Matrix: Factorization Uncovers Knowledge from Omics. *Trends Genet* **34**, 790-805, doi:10.1016/j.tig.2018.07.003 (2018).
71 Lee, M. Y. *et al.* Smooth Muscle Cell Genome Browser: Enabling the Identification of Novel Serum Response Factor Target Genes. *PLOS ONE* **10**, e0133751, doi:10.1371/journal.pone.0133751 (2015).
72 Purves-Tyson, T. D., Brown, A. M., Weissleder, C., Rothmond, D. A. & Shannon Weickert, C. Reductions in midbrain GABAergic and dopamine neuron markers are linked in schizophrenia. *Mol Brain* **14**, 96, doi:10.1186/s13041-021-00805-7 (2021).
73 Mitsui, S. *et al.* A mental retardation gene, motopsin/neurotrypsin/prss12, modulates hippocampal function and social interaction. *Eur J Neurosci* **30**, 2368-2378, doi:10.1111/j.1460-9568.2009.07029.x (2009).

74 Singec, I. *et al.* Synaptic vesicle protein synaptoporin is differently expressed by subpopulations of mouse hippocampal neurons. *J Comp Neurol* **452**, 139-153, doi:10.1002/cne.10371 (2002).
75 Fichna, J. *et al.* Transient receptor potential vanilloid 4 inhibits mouse colonic motility by activating NO-dependent enteric neurotransmission. *J Mol Med (Berl)* **93**, 1297-1309, doi:10.1007/s00109-015-1336-5 (2015).
76 Born, G. *et al.* Modulation of synaptic function through the alpha-neurexin-specific ligand neurexophilin-1. *Proc Natl Acad Sci U S A* **111**, E1274-1283, doi:10.1073/pnas.1312112111 (2014).
77 Zhan, X. *et al.* Generation of BAF53b-Cre transgenic mice with pan-neuronal Cre activities. *genesis* **53**, 440-448, doi:https://doi.org/10.1002/dvg.22866 (2015).
78 Elmentaite, R. *et al.* Cells of the human intestinal tract mapped across space and time. *Nature* **597**, 250-255, doi:10.1038/s41586-021-03852-1 (2021).
79 Matheis, F. *et al.* Adrenergic Signaling in Muscularis Macrophages Limits Infection-Induced Neuronal Loss. *Cell* **180**, 64-78 e16, doi:10.1016/j.cell.2019.12.002 (2020).
80 Barrenschee, M. *et al.* SNAP-25 is abundantly expressed in enteric neuronal networks and upregulated by the neurotrophic factor GDNF. *Histochem Cell Biol* **143**, 611-623, doi:10.1007/s00418-015-1310-x (2015).
81 Shore, A. N. *et al.* Reduced GABAergic Neuron Excitability, Altered Synaptic Connectivity, and Seizures in a KCNT1 Gain-of-Function Mouse Model of Childhood Epilepsy. *Cell Reports* **33**, 108303, doi:https://doi.org/10.1016/j.celrep.2020.108303 (2020).
82 Steinmetz, N. A. *et al.* Aberrant Cortical Activity in Multiple GCaMP6-Expressing Transgenic Mouse Lines. *eNeuro* **4**, doi:10.1523/ENEURO.0207-17.2017 (2017).
83 Zatka-Haas, P., Steinmetz, N. A., Carandini, M. & Harris, K. D. Sensory coding and the causal impact of mouse cortex in a visual decision. *eLife* **10**, e63163, doi:10.7554/eLife.63163 (2021).
84 Gianino, S., Grider, J. R., Cresswell, J., Enomoto, H. & Heuckeroth, R. O. GDNF availability determines enteric neuron number by controlling precursor proliferation. *Development* **130**, 2187-2198, doi:10.1242/dev.00433 (2003).
85 Natarajan, D., Marcos-Gutierrez, C., Pachnis, V. & de Graaff, E. Requirement of signalling by receptor tyrosine kinase RET for the directed migration of enteric nervous system progenitor cells during mammalian embryogenesis. *Development* **129**, 5151-5160 (2002).
86 Taraviras, S. *et al.* Signalling by the RET receptor tyrosine kinase and its role in the development of the mammalian enteric nervous system. *Development* **126**, 2785-2797 (1999).
87 Rodrigues, D. M., Li, A. Y., Nair, D. G. & Blennerhassett, M. G. Glial cell line-derived neurotrophic factor is a key neurotrophin in the postnatal enteric nervous system. *Neurogastroenterology and motility : the official journal of the European Gastrointestinal Motility Society* **23**, e44-56, doi:10.1111/j.1365-2982.2010.01626.x (2011).
88 Amano, O. *et al.* Hepatocyte growth factor is essential for migration of myogenic cells and promotes their proliferation during the early periods of tongue morphogenesis in mouse embryos. *Dev Dyn* **223**, 169-179, doi:10.1002/dvdy.1228 (2002).
89 Brun, P. *et al.* Toll-like receptor 2 regulates intestinal inflammation by controlling integrity of the enteric nervous system. *Gastroenterology* **145**, 1323-1333, doi:10.1053/j.gastro.2013.08.047 (2013).
90 Jangphattananont, N. *et al.* Distinct Localization of Mature HGF from its Precursor Form in Developing and Repairing the Stomach. *Int J Mol Sci* **20**, doi:10.3390/ijms20122955 (2019).
91 Almanzar, N. *et al.* A single-cell transcriptomic atlas characterizes ageing tissues in the mouse. *Nature* **583**, 590-595, doi:10.1038/s41586-020-2496-1 (2020).
92 Sathyan, S. *et al.* Plasma proteomic profile of age, health span, and all-cause mortality in older adults. *Aging Cell* **n/a**, e13250, doi:10.1111/acel.13250.

93 Wang, H. *et al.* The timing and location of glial cell line-derived neurotrophic factor expression determine enteric nervous system structure and function. *J Neurosci* **30**, 1523-1538, doi:10.1523/JNEUROSCI.3861-09.2010 (2010).

94 Nadal-Ribelles, M. *et al.* Sensitive high-throughput single-cell RNA-seq reveals within-clonal transcript correlations in yeast populations. *Nat Microbiol* **4**, 683-692, doi:10.1038/s41564-018-0346-9 (2019).

95 Zheng, S. C. *et al.* Universal prediction of cell-cycle position using transfer learning. *Genome Biol* **23**, 41, doi:10.1186/s13059-021-02581-y (2022).

96 Schneid, S. *et al.* The BRCT domains of ECT2 have distinct functions during cytokinesis. *Cell Rep* **34**, 108805, doi:10.1016/j.celrep.2021.108805 (2021).

97 Barrenschee, M. *et al.* No neuronal loss, but alterations of the GDNF system in asymptomatic diverticulosis. *PLoS One* **12**, e0171416, doi:10.1371/journal.pone.0171416 (2017).

98 Rossi, V. *et al.* Chronic intestinal pseudo-obstruction in a child harboring a founder Hirschsprung RET mutation. *Am J Med Genet A* **170**, 2400-2403, doi:10.1002/ajmg.a.37787 (2016).

99 Uesaka, T., Nagashimada, M., Yonemura, S. & Enomoto, H. Diminished Ret expression compromises neuronal survival in the colon and causes intestinal aganglionosis in mice. *The Journal of clinical investigation* **118**, 1890-1898, doi:10.1172/JCI34425 (2008).

100 Kim, M. *et al.* Obstructed defecation-an enteric neuropathy? An exploratory study of patient samples. *Int J Colorectal Dis* **34**, 193-196, doi:10.1007/s00384-018-3160-1 (2019).

101 Sun, T. *et al.* Aging-dependent decrease in the numbers of enteric neurons, interstitial cells of Cajal and expression of connexin43 in various regions of gastrointestinal tract. *Aging (Albany NY)* **10**, 3851-3865, doi:10.18632/aging.101677 (2018).

102 Becker, L. *et al.* Age-dependent shift in macrophage polarisation causes inflammation-mediated degeneration of enteric nervous system. *Gut* **67**, 827-836, doi:10.1136/gutjnl-2016-312940 (2018).

103 Sharma, G., Colantuoni, C., Goff, L. A., Fertig, E. J. & Stein-O'Brien, G. projectR: an R/Bioconductor package for transfer learning via PCA, NMF, correlation and clustering. *Bioinformatics* **36**, 3592-3593, doi:10.1093/bioinformatics/btaa183 (2020).

104 Young, H. M. & Newgreen, D. Enteric neural crest-derived cells: Origin, identification, migration, and differentiation. *The Anatomical Record* **262**, 1-15, doi:10.1002/1097-0185(20010101)262:1<1::AID-AR1006>3.0.CO;2-2 (2001).

105 Prummel, K. D., Nieuwenhuize, S. & Mosimann, C. The lateral plate mesoderm. *Development* **147**, dev175059, doi:10.1242/dev.175059 (2020).

106 Carlson, B. M. in *Human Embryology and Developmental Biology (Fifth Edition)* (ed Bruce M. Carlson) 269-293 (W.B. Saunders, 2014).

107 Verderio, C. *et al.* SNAP-25 Modulation of Calcium Dynamics Underlies Differences in GABAergic and Glutamatergic Responsiveness to Depolarization. *Neuron* **41**, 599-610, doi:https://doi.org/10.1016/S0896-6273(04)00077-7 (2004).

108 Nouvian, R. *et al.* Exocytosis at the hair cell ribbon synapse apparently operates without neuronal SNARE proteins. *Nature Neuroscience* **14**, 411-413, doi:10.1038/nn.2774 (2011).

109 Grabs, D., Bergmann, M., Urban, M., Post, A. & Gratzl, M. Rab3 proteins and SNAP-25, essential components of the exocytosis machinery in conventional synapses, are absent from ribbon synapses of the mouse retina. *Eur J Neurosci* **8**, 162-168, doi:10.1111/j.1460-9568.1996.tb01177.x (1996).

110 Hellström, J., Arvidsson, U., Elde, R., Cullheim, S. & Meister, B. Differential expression of nerve terminal protein isoforms in VAChT-containing varicosities of the spinal cord ventral horn. *Journal of Comparative Neurology* **411**, 578-590, doi:https://doi.org/10.1002/(SICI)1096-9861(19990906)411:4<578::AID-CNE4>3.0.CO;2-L (1999).

2068 111 Morris, J. L., Lindberg, C. E. Y. & Gibbins, I. L. Different levels of immunoreactivity for
2069 synaptosomal-associated protein of 25 kDa in vasoconstrictor and vasodilator axons of guinea-
2070 pigs. *Neuroscience Letters* **294**, 167-170, doi:https://doi.org/10.1016/S0304-3940(00)01568-8
2071 (2000).
2072 112 Greenlee, M. H., Roosevelt, C. B. & Sakaguchi, D. S. Differential localization of SNARE complex
2073 proteins SNAP-25, syntaxin, and VAMP during development of the mammalian retina. *J Comp*
2074 *Neurol* **430**, 306-320, doi:10.1002/1096-9861(20010212)430:3<306::aid-cne1032>3.0.co;2-b
2075 (2001).
2076 113 Gibbins, I. L., Jobling, P., Teo, E. H., Matthew, S. E. & Morris, J. L. Heterogeneous expression of
2077 SNAP-25 and synaptic vesicle proteins by central and peripheral inputs to sympathetic neurons. *J*
2078 *Comp Neurol* **459**, 25-43, doi:10.1002/cne.10527 (2003).
2079 114 Xue, R. *et al.* Expression of Cystic Fibrosis Transmembrane Conductance Regulator in Ganglia of
2080 Human Gastrointestinal Tract. *Sci Rep* **6**, 30926, doi:10.1038/srep30926 (2016).
2081 115 Wang, W. *et al.* Selective Expression of a SNARE-Cleaving Protease in Peripheral Sensory Neurons
2082 Attenuates Pain-Related Gene Transcription and Neuropeptide Release. *Int J Mol Sci* **22**,
2083 doi:10.3390/ijms22168826 (2021).
2084 116 Tender, G. C., Kaye, A. D., Li, Y. Y. & Cui, J. G. Neurotrophin-3 and tyrosine kinase C have
2085 modulatory effects on neuropathic pain in the rat dorsal root ganglia. *Neurosurgery* **68**, 1048-
2086 1055; discussion 1055, doi:10.1227/NEU.0b013e318208f9c4 (2011).
2087 117 de Jonge, H. R., Ardelean, M. C., Bijvelds, M. J. C. & Vergani, P. Strategies for cystic fibrosis
2088 transmembrane conductance regulator inhibition: from molecular mechanisms to treatment for
2089 secretory diarrhoeas. *FEBS Lett* **594**, 4085-4108, doi:10.1002/1873-3468.13971 (2020).
2090 118 de Lima, J. B. M. *et al.* ARC(GHR) Neurons Regulate Muscle Glucose Uptake. *Cells* **10**,
2091 doi:10.3390/cells10051093 (2021).
2092 119 Chaudhury, A., Dendi, V. S. & Mirza, W. Colligative Property of ATP: Implications for Enteric
2093 Purinergic Neuromuscular Neurotransmission. *Front Physiol* **7**, 500,
2094 doi:10.3389/fphys.2016.00500 (2016).
2095 120 Daugherty, M., Luo, Q. & Sokoloff, A. J. Myosin heavy chain composition of the human
2096 genioglossus muscle. *J Speech Lang Hear Res* **55**, 609-625, doi:10.1044/1092-4388(2011/10-0287)
2097 (2012).
2098 121 Parathan, P., Wang, Y., Leembruggen, A. J., Bornstein, J. C. & Foong, J. P. The enteric nervous
2099 system undergoes significant chemical and synaptic maturation during adolescence in mice. *Dev*
2100 *Biol* **458**, 75-87, doi:10.1016/j.ydbio.2019.10.011 (2020).
2101 122 Zhu, H., Hasman, R. A., Barron, V. A., Luo, G. & Lou, H. A nuclear function of Hu proteins as neuron-
2102 specific alternative RNA processing regulators. *Mol Biol Cell* **17**, 5105-5114, doi:10.1091/mbc.e06-
2103 02-0099 (2006).
2104 123 Epstein, M. L., Saffrey, M. J. & Poulsen, K. T. Development and birthdates of vasoactive intestinal
2105 peptide immunoreactive neurons in the chick proventriculus. *Journal of Comparative Neurology*
2106 **321**, 83-92, doi:https://doi.org/10.1002/cne.903210108 (1992).
2107 124 Zanini, F. *et al.* Northstar enables automatic classification of known and novel cell types from
2108 tumor samples. *Scientific Reports* **10**, 15251, doi:10.1038/s41598-020-71805-1 (2020).
2109 125 Wang, Z. *et al.* Single-cell RNA sequencing reveals a novel cell type and immunotherapeutic
2110 targets in papillary thyroid cancer. *medRxiv*, 2021.2002.2024.21251881,
2111 doi:10.1101/2021.02.24.21251881 (2021).
2112 126 Zhang, Y., Aevermann, B., Gala, R. & Scheuermann, R. H. Cell type matching in single-cell RNA-
2113 sequencing data using FR-Match. *Scientific Reports* **12**, 9996, doi:10.1038/s41598-022-14192-z
2114 (2022).

127 Zheng, G. X. Y. *et al.* Massively parallel digital transcriptional profiling of single cells. *Nature Communications* **8**, 14049, doi:10.1038/ncomms14049 (2017).
128 Genomics, X. *What fraction of mRNA transcripts are captured per cell?*, <https://kb.10xgenomics.com/hc/en-us/articles/360001539051-What-fraction-of-mRNA-transcripts-are-captured-per-cell-> (
129 Song, Y., Su, M., Panchatsharam, P., Rood, D. & Lai, L. c-Met signalling is required for efficient postnatal thymic regeneration and repair. *Immunology* **144**, 245-253, doi:https://doi.org/10.1111/imm.12365 (2015).
130 Dai, C., Huh, C. G., Thorgeirsson, S. S. & Liu, Y. Beta-cell-specific ablation of the hepatocyte growth factor receptor results in reduced islet size, impaired insulin secretion, and glucose intolerance. *Am J Pathol* **167**, 429-436, doi:10.1016/s0002-9440(10)62987-2 (2005).
131 Ishibe, S. *et al.* Met and the epidermal growth factor receptor act cooperatively to regulate final nephron number and maintain collecting duct morphology. *Development* **136**, 337-345, doi:10.1242/dev.024463 (2009).
132 Arechederra, M. *et al.* Met signaling in cardiomyocytes is required for normal cardiac function in adult mice. *Biochimica et Biophysica Acta (BBA) - Molecular Basis of Disease* **1832**, 2204-2215, doi:https://doi.org/10.1016/j.bbadis.2013.08.008 (2013).
133 Golden, J. P., DeMaro, J. A., Osborne, P. A., Milbrandt, J. & Johnson, E. M., Jr. Expression of neurturin, GDNF, and GDNF family-receptor mRNA in the developing and mature mouse. *Exp Neurol* **158**, 504-528, doi:10.1006/exnr.1999.7127 (1999).
134 Papaconstantinou, J. *et al.* Attenuation of p38alpha MAPK stress response signaling delays the in vivo aging of skeletal muscle myofibers and progenitor cells. *Aging (Albany NY)* **7**, 718-733, doi:10.18632/aging.100802 (2015).
135 Soret, R. *et al.* Glial Cell-Derived Neurotrophic Factor Induces Enteric Neurogenesis and Improves Colon Structure and Function in Mouse Models of Hirschsprung Disease. *Gastroenterology* **159**, 1824-1838 e1817, doi:10.1053/j.gastro.2020.07.018 (2020).
136 Grider, J. R., Heuckeroth, R. O., Kuemmerle, J. F. & Murthy, K. S. Augmentation of the ascending component of the peristaltic reflex and substance P release by glial cell line-derived neurotrophic factor. *Neurogastroenterol Motil* **22**, 779-786, doi:10.1111/j.1365-2982.2010.01489.x (2010).
137 Melo, C. G. S. *et al.* Identification of intrinsic primary afferent neurons in mouse jejunum. *Neurogastroenterology and motility : the official journal of the European Gastrointestinal Motility Society* **32**, e13989, doi:10.1111/nmo.13989 (2020).
138 Saffrey, M. J. Aging of the mammalian gastrointestinal tract: a complex organ system. *Age (Dordr)* **36**, 9603, doi:10.1007/s11357-013-9603-2 (2014).
139 Cossais, F. *et al.* Altered enteric expression of the homeobox transcription factor Phox2b in patients with diverticular disease. *United European Gastroenterology Journal* **7**, 349-357, doi:10.1177/2050640618824913 (2019).
140 Schafmayer, C. *et al.* Genome-wide association analysis of diverticular disease points towards neuromuscular, connective tissue and epithelial pathomechanisms. *Gut* **68**, 854, doi:10.1136/gutjnl-2018-317619 (2019).
141 Muller, P. A. *et al.* Microbiota-modulated CART(+) enteric neurons autonomously regulate blood glucose. *Science* **370**, 314-321, doi:10.1126/science.abd6176 (2020).
142 Becker, L., Kulkarni, S., Tiwari, G., Micci, M.-A. & Pasricha, P. J. Divergent fate and origin of neurosphere-like bodies from different layers of the gut. *American Journal of Physiology-Gastrointestinal and Liver Physiology* **302**, G958-G965, doi:10.1152/ajpgi.00511.2011 (2012).
143 Becker, L., Peterson, J., Kulkarni, S. & Pasricha, P. J. Ex vivo neurogenesis within enteric ganglia occurs in a PTEN dependent manner. *PLoS One* **8**, e59452 (2013).

144 Becker, L., Peterson, J., Kulkarni, S. & Pasricha, P. J. Ex vivo neurogenesis within enteric ganglia occurs in a PTEN dependent manner. *PLoS One* **8**, e59452, doi:10.1371/journal.pone.0059452 (2013).
145 Shenje, L. T. *et al.* Precardiac deletion of Numb and Numblike reveals renewal of cardiac progenitors. *Elife* **3**, e02164, doi:10.7554/eLife.02164 (2014).
146 Susaki, E. A. *et al.* Whole-brain imaging with single-cell resolution using chemical cocktails and computational analysis. *Cell* **157**, 726-739, doi:10.1016/j.cell.2014.03.042 (2014).
147 Young, H. M., Furness, J. B., Sewell, P., Burcher, E. F. & Kandiah, C. J. Total numbers of neurons in myenteric ganglia of the guinea-pig small intestine. *Cell Tissue Res* **272**, 197-200, doi:10.1007/BF00323587 (1993).
148 Zhou, Y. *et al.* Enteric nervous system abnormalities are present in human necrotizing enterocolitis: potential neurotransplantation therapy. *Stem Cell Res Ther* **4**, 157, doi:10.1186/scrt387 (2013).
149 Hosie, S. *et al.* Gastrointestinal dysfunction in patients and mice expressing the autism-associated R451C mutation in neuroligin-3. *Autism Res* **12**, 1043-1056, doi:10.1002/aur.2127 (2019).
150 Lefevre, C. *et al.* Enteric Nervous System Remodeling in a Rat Model of Spinal Cord Injury: A Pilot Study. *Neurotrauma Rep* **1**, 125-136, doi:10.1089/neur.2020.0041 (2020).
151 Qiu, X. *et al.* NEDL2 regulates enteric nervous system and kidney development in its Nedd8 ligase activity-dependent manner. *Oncotarget* **7**, 31440-31453, doi:10.18632/oncotarget.8951 (2016).
152 Bray, N. L., Pimentel, H., Melsted, P. & Pachter, L. Near-optimal probabilistic RNA-seq quantification. *Nat Biotechnol* **34**, 525-527, doi:10.1038/nbt.3519 (2016).
153 Haghverdi, L., Lun, A. T. L., Morgan, M. D. & Marioni, J. C. Batch effects in single-cell RNA-sequencing data are corrected by matching mutual nearest neighbors. *Nat Biotechnol* **36**, 421-427, doi:10.1038/nbt.4091 (2018).
154 Gu, Z., Eils, R. & Schlesner, M. Complex heatmaps reveal patterns and correlations in multidimensional genomic data. *Bioinformatics* **32**, 2847-2849, doi:10.1093/bioinformatics/btw313 (2016).
155 Lun, A. T. L. *et al.* EmptyDrops: distinguishing cells from empty droplets in droplet-based single-cell RNA sequencing data. *Genome Biol* **20**, 63, doi:10.1186/s13059-019-1662-y (2019).
156 Griffiths, J. A., Richard, A. C., Bach, K., Lun, A. T. L. & Marioni, J. C. Detection and removal of barcode swapping in single-cell RNA-seq data. *Nat Commun* **9**, 2667, doi:10.1038/s41467-018-05083-x (2018).
157 Lun, A. T., McCarthy, D. J. & Marioni, J. C. A step-by-step workflow for low-level analysis of single-cell RNA-seq data with Bioconductor. *F1000Res* **5**, 2122, doi:10.12688/f1000research.9501.2 (2016).
158 McCarthy, D. J., Campbell, K. R., Lun, A. T. & Wills, Q. F. Scater: pre-processing, quality control, normalization and visualization of single-cell RNA-seq data in R. *Bioinformatics* **33**, 1179-1186, doi:10.1093/bioinformatics/btw777 (2017).
159 Csárdi, G. & Nepusz, T.

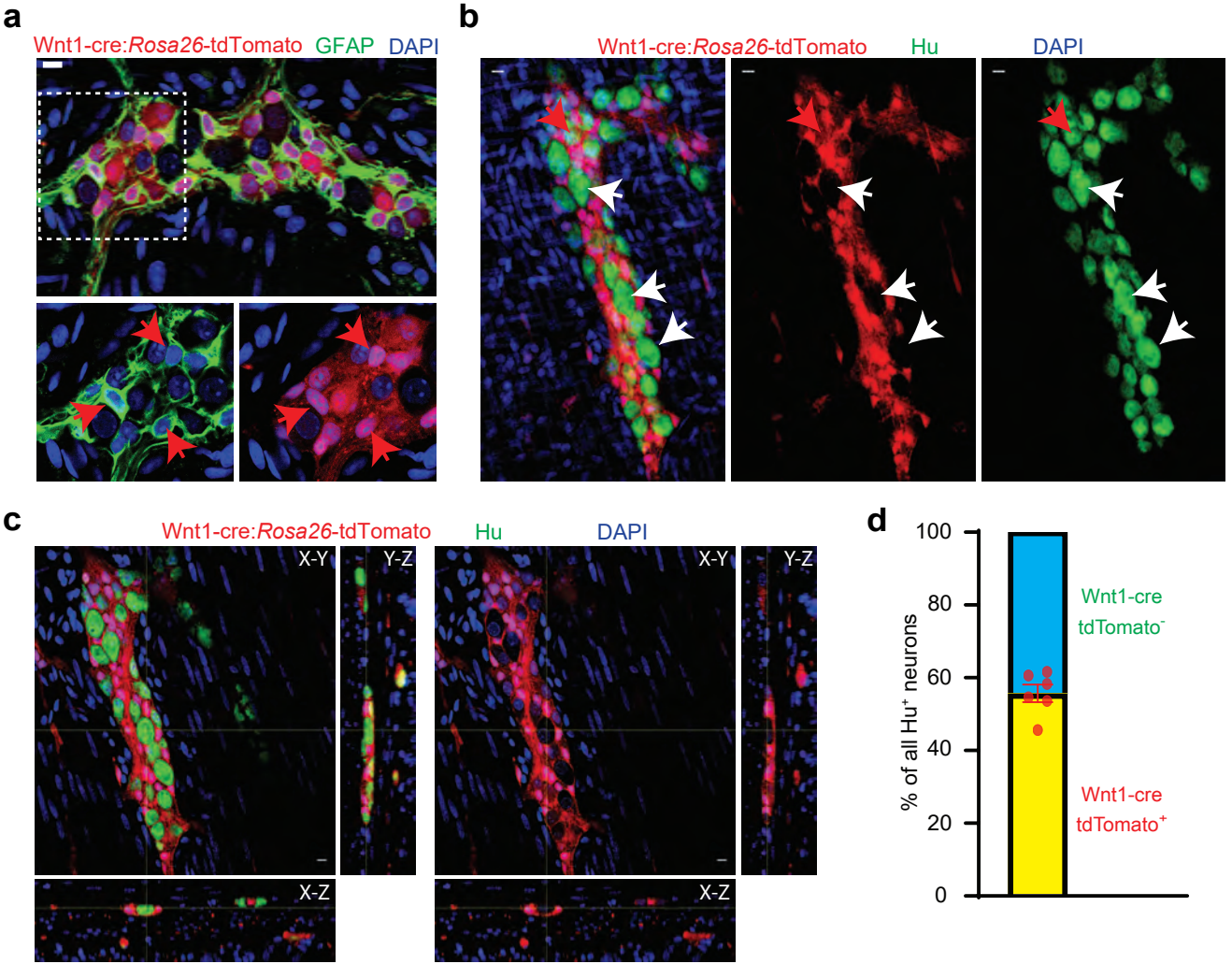
a
Wnt1-cre:Rosa26-tdTomato
GFAP
DAPI
b
Wnt1-cre:Rosa26-tdTomato
Hu
DAPI
c
Wnt1-cre:Rosa26-tdTomato
Hu
DAPI
X-Y
Y-Z
X-Z
d
% of all Hu+ neurons
100
80
60
40
20
0
Wnt1-cre
tdTomato-
Wnt1-cre
tdTomato+

Figure 1

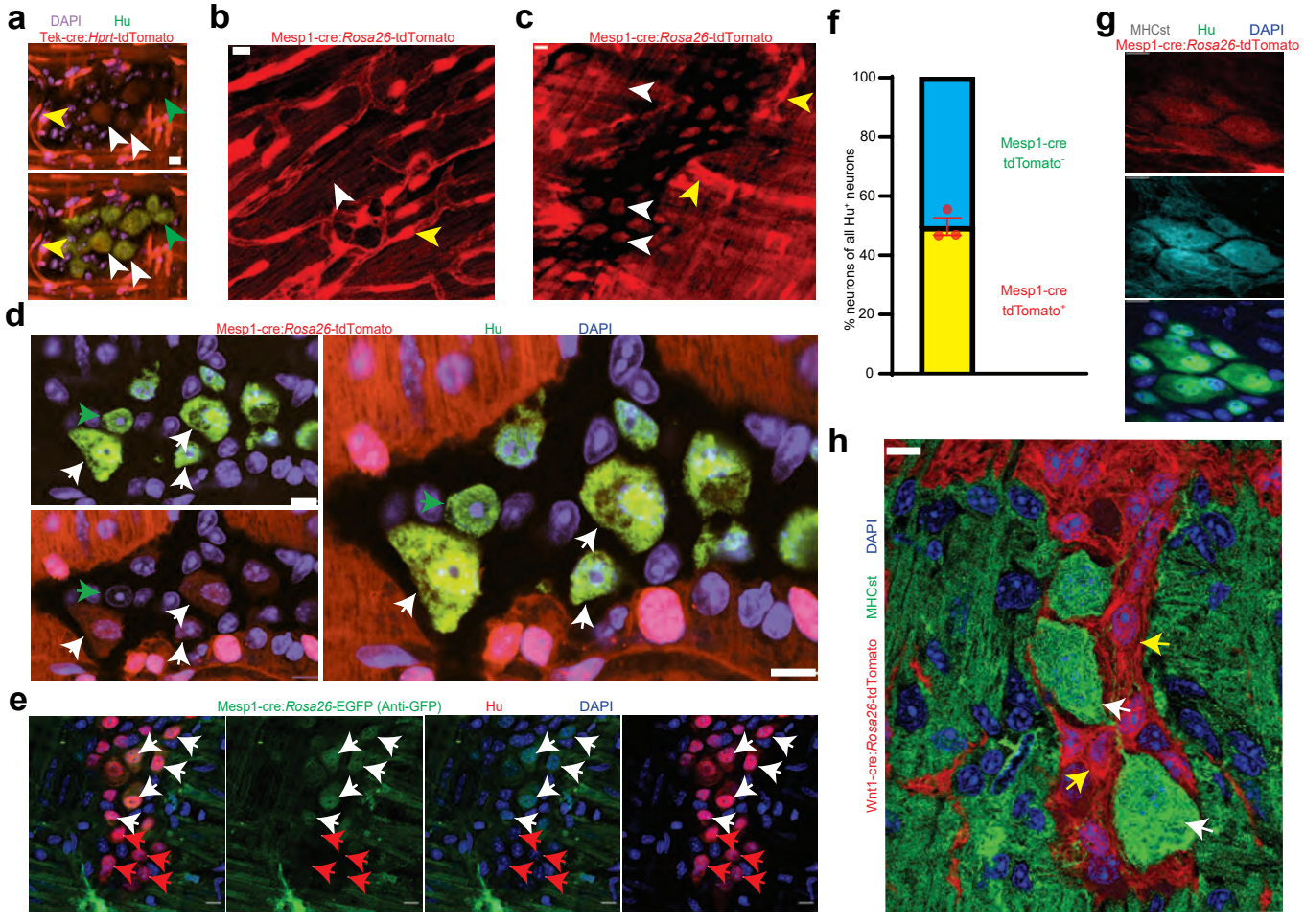
a
DAPI
Hu
Tek-cre:Hprt-tdTomato
b
Mesp1-cre:Rosa26-tdTomato
c
Mesp1-cre:Rosa26-tdTomato
f
100
80
60
40
20
0
% neurons of all Hu+ neurons
Mesp1-cre
tdTomato-
Mesp1-cre
tdTomato+
g
MHCst
Hu
DAPI
Mesp1-cre:Rosa26-tdTomato
d
Mesp1-cre:Rosa26-tdTomato
Hu
DAPI
e
Mesp1-cre:Rosa26-EGFP (Anti-GFP)
Hu
DAPI
h
DAPI
MHCst
Wnt1-cre:Rosa26-tdTomato

Figure 2

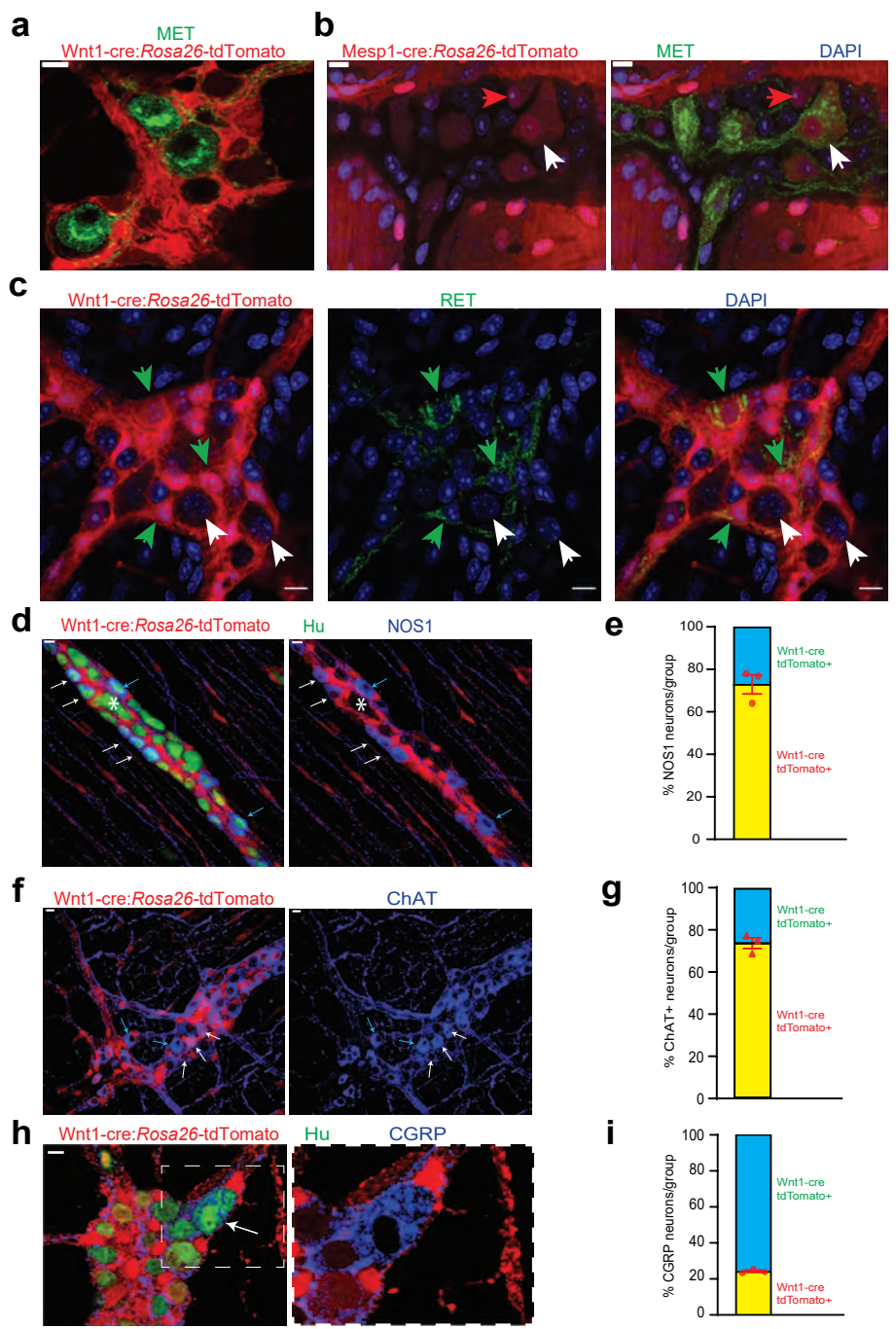
a
MET
Wnt1-cre:Rosa26-tdTomato
b
Mesp1-cre:Rosa26-tdTomato
MET
DAPI
c
Wnt1-cre:Rosa26-tdTomato
RET
DAPI
d
Wnt1-cre:Rosa26-tdTomato
Hu
NOS1
e
% NOS1 neurons/group
Wnt1-cre tdTomato+
Wnt1-cre tdTomato+
f
Wnt1-cre:Rosa26-tdTomato
ChAT
g
% ChAT+ neurons/group
Wnt1-cre tdTomato+
Wnt1-cre tdTomato+
h
Wnt1-cre:Rosa26-tdTomato
Hu
CGRP
i
% CGRP neurons/group
Wnt1-cre tdTomato+
Wnt1-cre tdTomato+

Figure 3

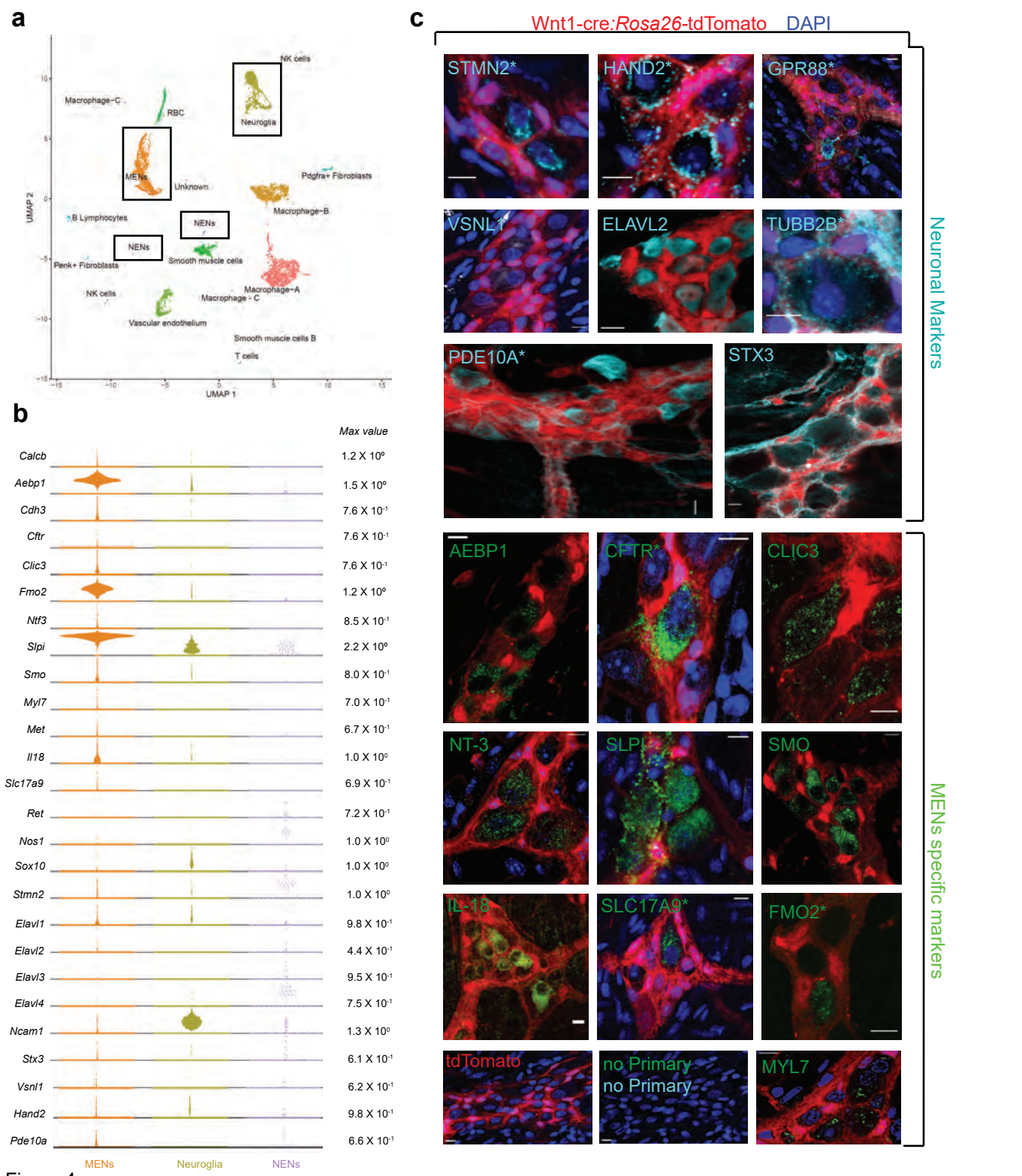
a
NK cells
Macrophage-C
RBC
Neuroglia
MENs
Unknown
Pdgfra+ Fibroblasts
Macrophage-B
B Lymphocytes
NENs
NENs
Smooth muscle cells
Penk+ Fibroblasts
Macrophage-A
NK cells
Macrophage - C
Vascular endothelium
Smooth muscle cells B
T cells
UMAP 2
UMAP 1
b
Max value
Calcb 1.2 X 10⁰
Aebp1 1.5 X 10⁰
Cdh3 7.6 X 10⁻¹
Cftr 7.6 X 10⁻¹
Clic3 7.6 X 10⁻¹
Fmo2 1.2 X 10⁰
Ntf3 8.5 X 10⁻¹
Slpi 2.2 X 10⁰
Smo 8.0 X 10⁻¹
Myl7 7.0 X 10⁻¹
Met 6.7 X 10⁻¹
Il18 1.0 X 10⁰
Slc17a9 6.9 X 10⁻¹
Ret 7.2 X 10⁻¹
Nos1 1.0 X 10⁰
Sox10 1.0 X 10⁰
Stmn2 1.0 X 10⁰
Elavl1 9.8 X 10⁻¹
Elavl2 4.4 X 10⁻¹
Elavl3 9.5 X 10⁻¹
Elavl4 7.5 X 10⁻¹
Ncam1 1.3 X 10⁰
Stx3 6.1 X 10⁻¹
Vsnl1 6.2 X 10⁻¹
Hand2 9.8 X 10⁻¹
Pde10a 6.6 X 10⁻¹
MENs
Neuroglia
NENs
c
Wnt1-cre:Rosa26-tdTomato DAPI
STMN2*
HAND2*
GPR88*
VSNL1
ELAVL2
TUBB2B*
PDE10A*
STX3
Neuronal Markers
AEBP1
CFTR*
CLIC3
NT-3
SLPI
SMO
IL-18
SLC17A9*
FMO2*
tdTomato
no Primary
no Primary
MYL7
MENs specific markers

Figure 4

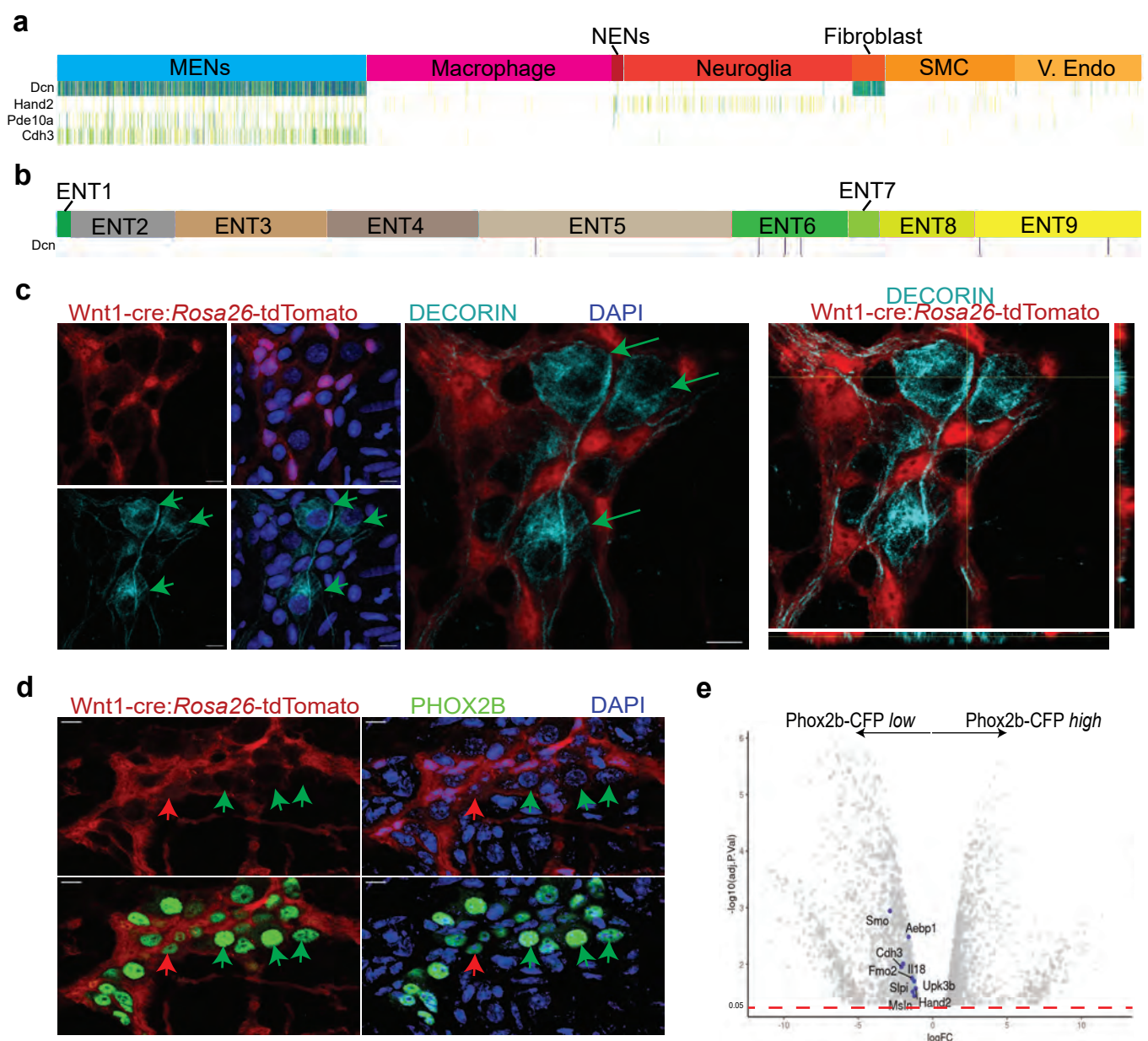
a
NENs
Fibroblast
MENs
Macrophage
Neuroglia
SMC
V. Endo
Dcn
Hand2
Pde10a
Cdh3
b
ENT1
ENT7
ENT2
ENT3
ENT4
ENT5
ENT6
ENT8
ENT9
Dcn
c
Wnt1-cre:Rosa26-tdTomato
DECORIN
DAPI
DECORIN
Wnt1-cre:Rosa26-tdTomato
d
Wnt1-cre:Rosa26-tdTomato
PHOX2B
DAPI
e
Phox2b-CFP low
Phox2b-CFP high
-log10(adj.PVal)
logFC
Smo
Aebp1
Cdh3
Fmo2
Il18
Slpi
Upk3b
Msln
Hand2
0.05

Figure 5

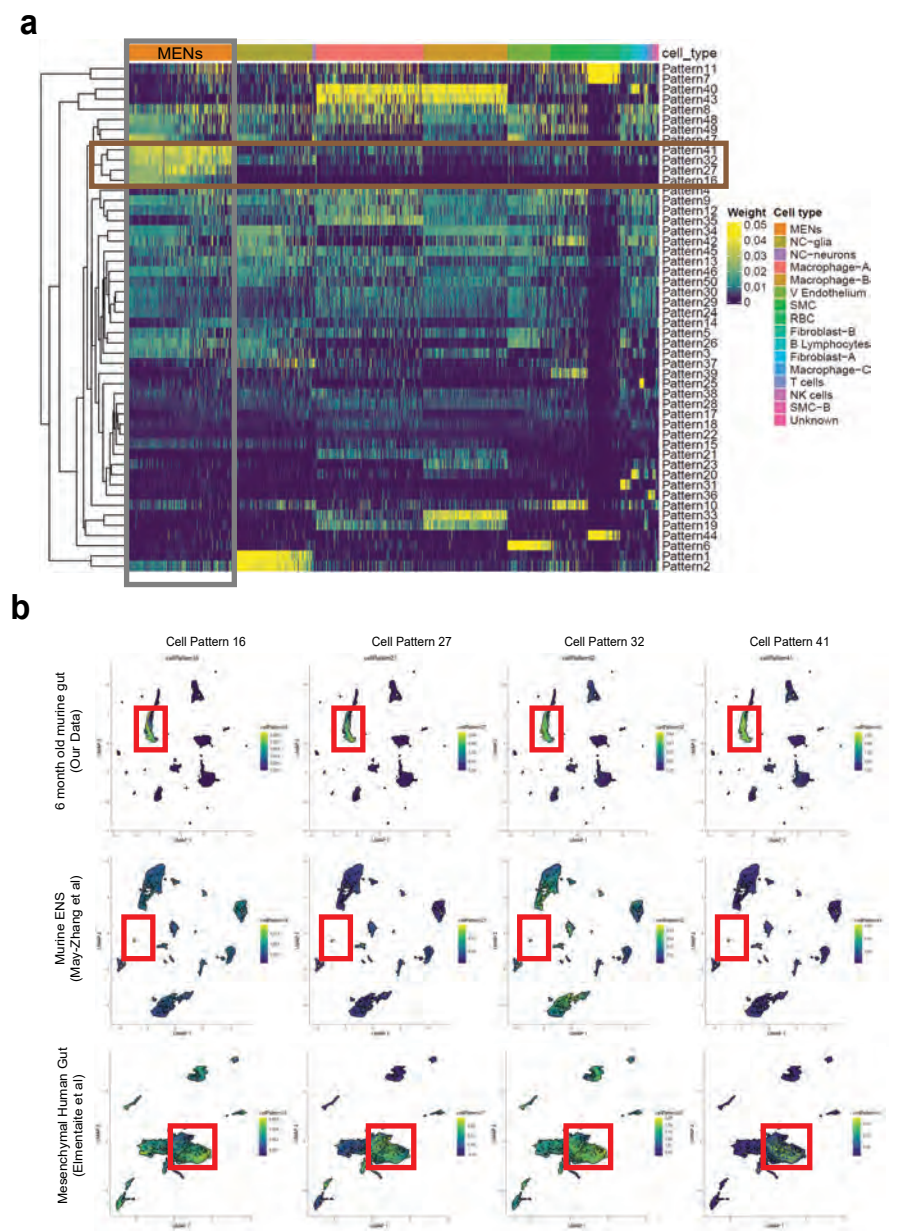
a
MENs
cell_type
Pattern11
Pattern7
Pattern40
Pattern43
Pattern8
Pattern48
Pattern49
Pattern41
Pattern32
Pattern27
Pattern16
Pattern4
Pattern9
Pattern12
Pattern35
Pattern34
Pattern42
Pattern45
Pattern13
Pattern46
Pattern50
Pattern30
Pattern29
Pattern24
Pattern14
Pattern5
Pattern26
Pattern3
Pattern37
Pattern39
Pattern25
Pattern38
Pattern28
Pattern17
Pattern18
Pattern22
Pattern15
Pattern21
Pattern23
Pattern20
Pattern31
Pattern36
Pattern10
Pattern33
Pattern19
Pattern44
Pattern6
Pattern1
Pattern2
Weight
0.05
0.04
0.03
0.02
0.01
0
Cell type
MENs
NC-glia
NC-neurons
Macrophage-A
Macrophage-B
V Endothelium
SMC
RBC
Fibroblast-B
B Lymphocytes
Fibroblast-A
Macrophage-C
T cells
NK cells
SMC-B
Unknown
b
Cell Pattern 16
Cell Pattern 27
Cell Pattern 32
Cell Pattern 41
6 month old murine gut
(Our Data)
Murine ENS
(May-Zhang et al)
Mesenchymal Human Gut
(Elmentaite et al)

Figure 6

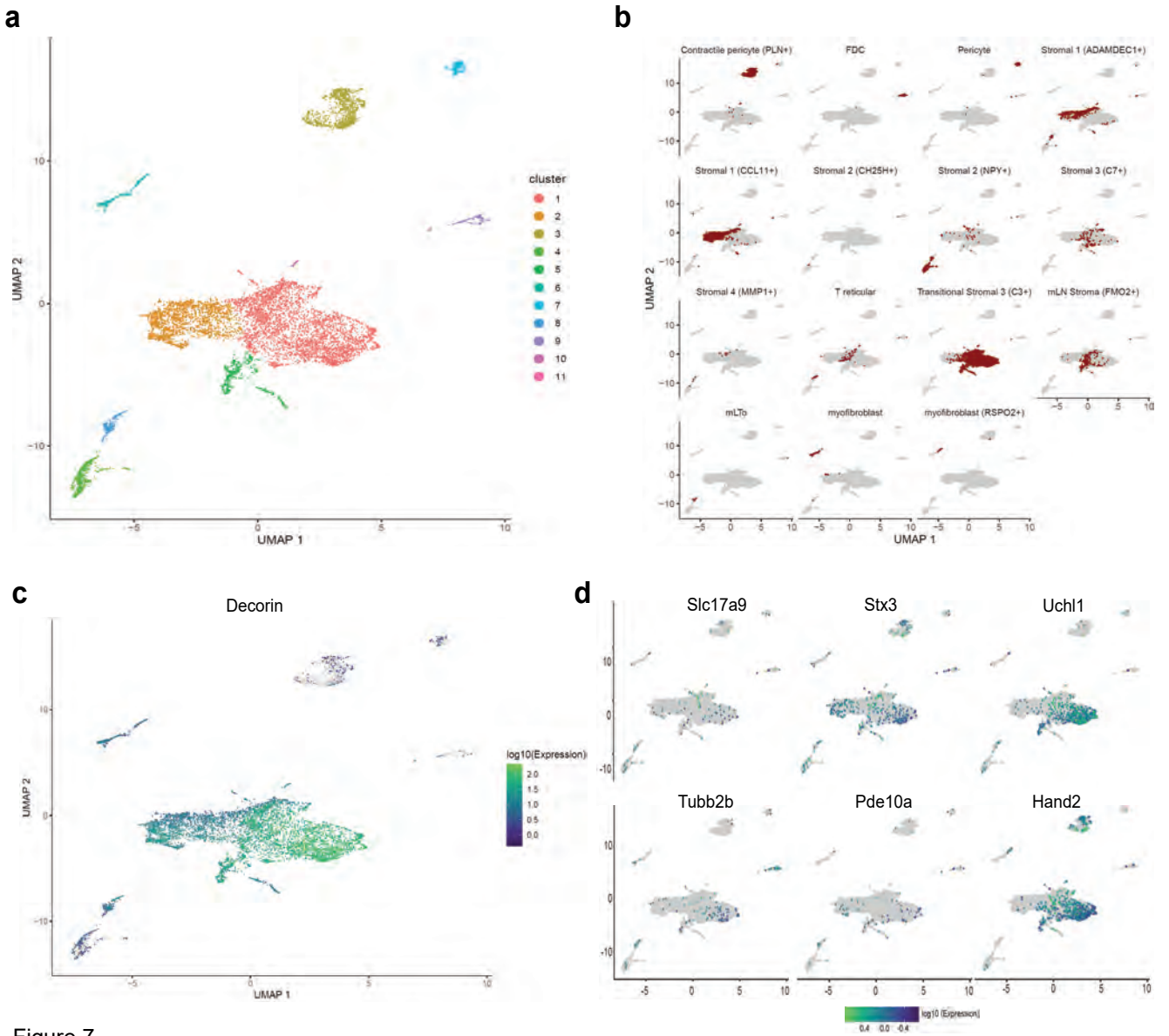
a
cluster
1
2
3
4
5
6
7
8
9
10
11
UMAP 1
UMAP 2
b
Contractile pericyte (PLN+)
FDC
Pericyte
Stromal 1 (ADAMDEC1+)
Stromal 1 (CCL11+)
Stromal 2 (CH25H+)
Stromal 2 (NPY+)
Stromal 3 (C7+)
Stromal 4 (MMP1+)
T reticular
Transitional Stromal 3 (C3+)
mLN Stroma (FMO2+)
mLTo
myofibroblast
myofibroblast (RSPO2+)
UMAP 1
UMAP 2
c
Decorin
log10(Expression)
UMAP 1
UMAP 2
d
Slc17a9
Stx3
Uchl1
Tubb2b
Pde10a
Hand2
log10 (Expression)

Figure 7

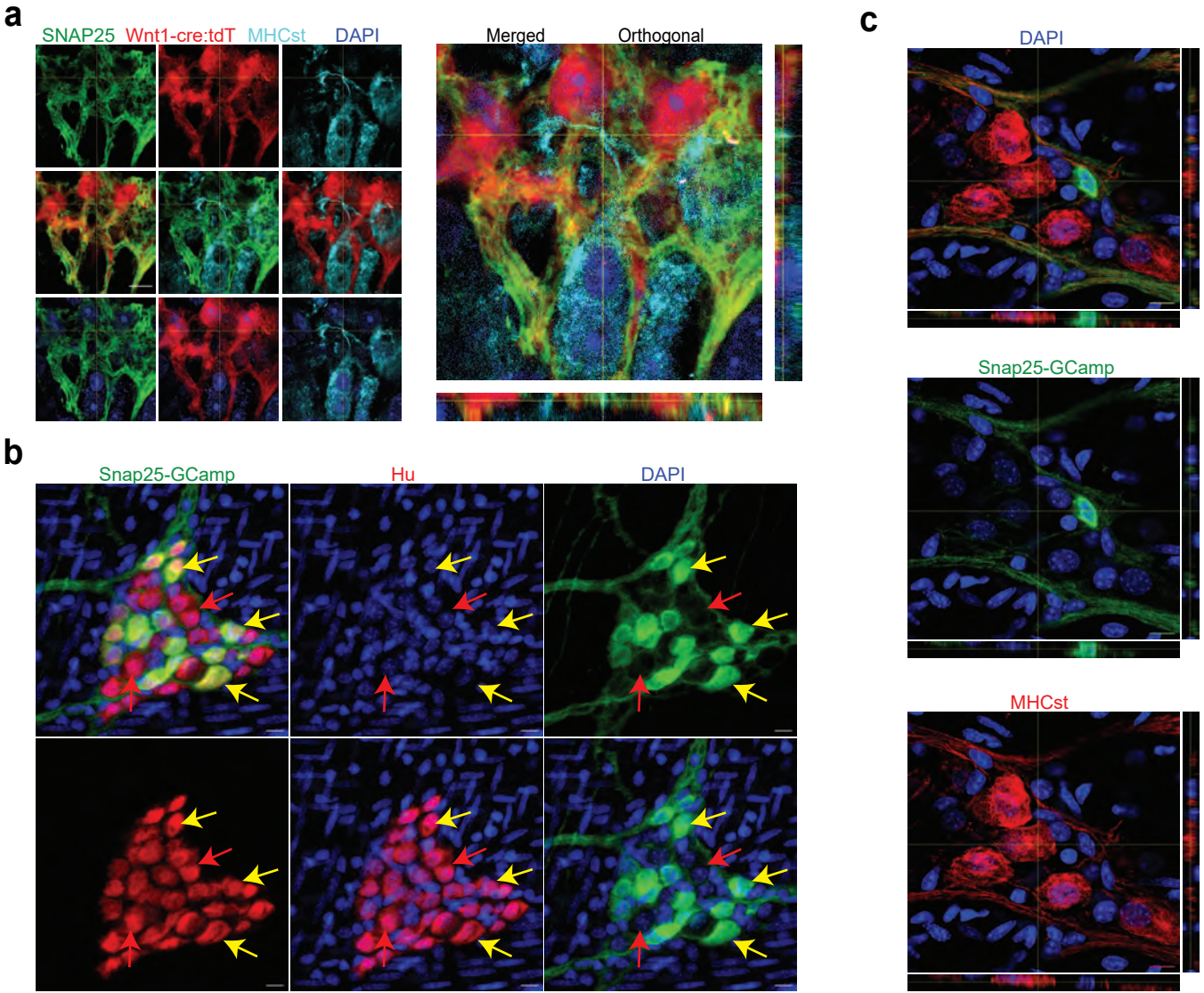
a
SNAP25
Wnt1-cre:tdT
MHCst
DAPI
Merged
Orthogonal
b
Snap25-GCamp
Hu
DAPI
c
DAPI
Snap25-GCamp
MHCst

Figure 8

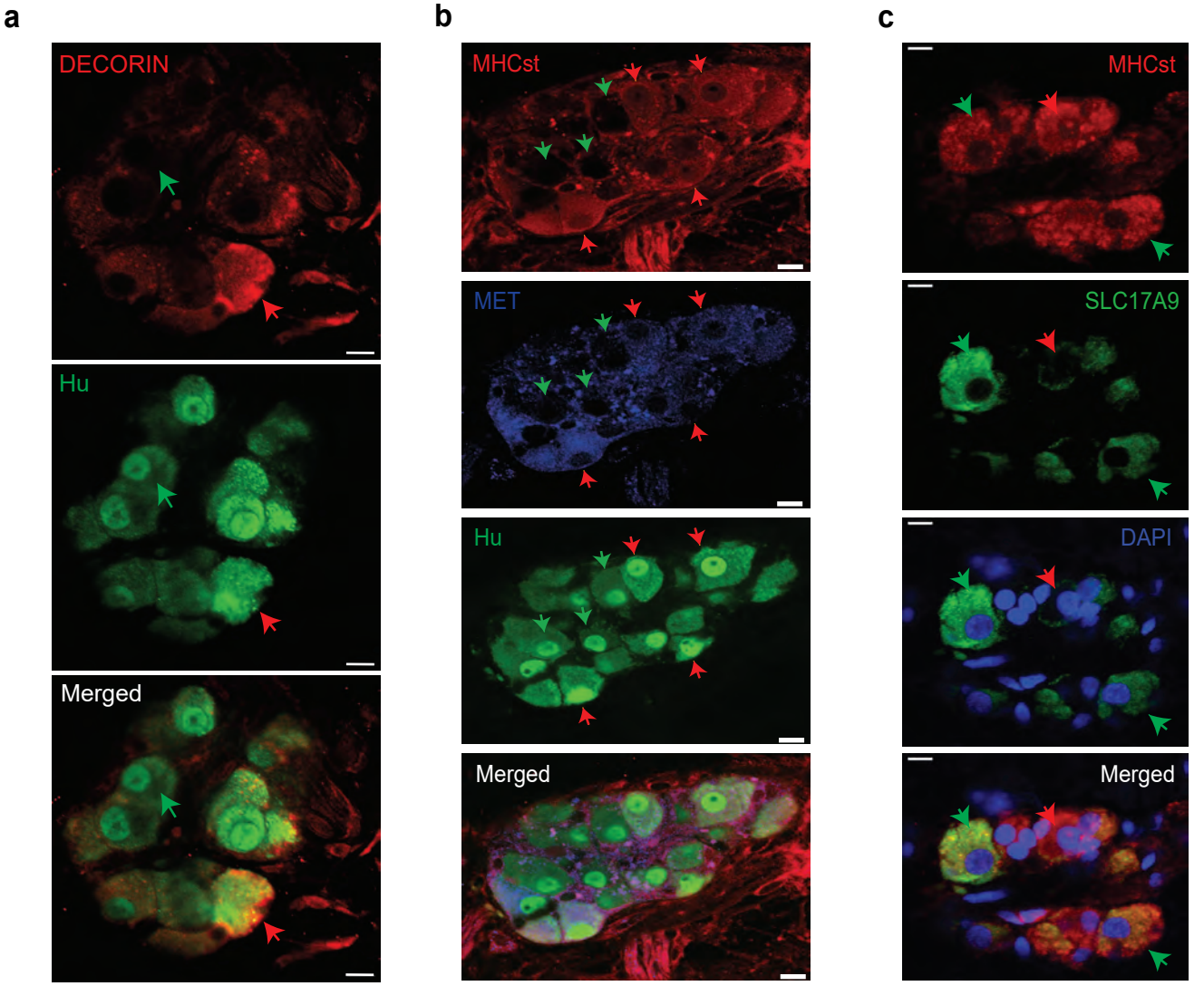
a
DECORIN
Hu
Merged
b
MHCst
MET
Hu
Merged
c
MHCst
SLC17A9
DAPI
Merged

Figure 9

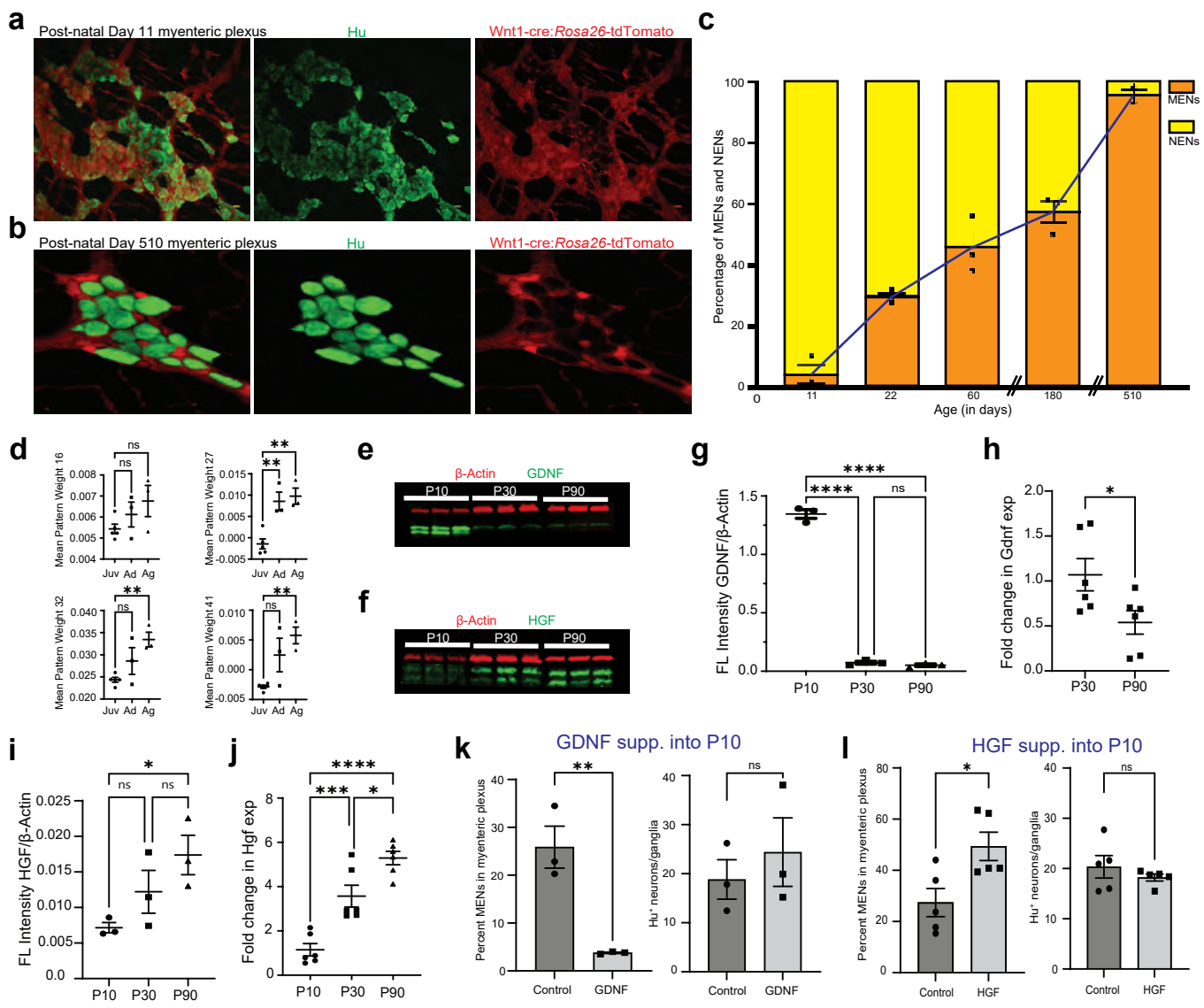
a
Post-natal Day 11 myenteric plexus
Hu
Wnt1-cre:Rosa26-tdTomato
b
Post-natal Day 510 myenteric plexus
Hu
Wnt1-cre:Rosa26-tdTomato
c
Percentage of MENs and NENs
MENs
NENs
Age (in days)
0
11
22
60
180
510
d
Mean Pattern Weight 16
Mean Pattern Weight 27
Mean Pattern Weight 32
Mean Pattern Weight 41
Juv
Ad
Ag
ns
**
e
β-Actin
GDNF
P10
P30
P90
f
β-Actin
HGF
P10
P30
P90
g
FL Intensity GDNF/β-Actin
****
ns
P10
P30
P90
h
Fold change in Gdnf exp
*
P30
P90
i
FL Intensity HGF/β-Actin
*
ns
P10
P30
P90
j
Fold change in Hgf exp
****
***
*
P10
P30
P90
k
GDNF supp. into P10
Percent MENs in myenteric plexus
Hu+ neurons/ganglia
**
ns
Control
GDNF
l
HGF supp. into P10
Percent MENs in myenteric plexus
Hu+ neurons/ganglia
*
ns
Control
HGF

Figure 10

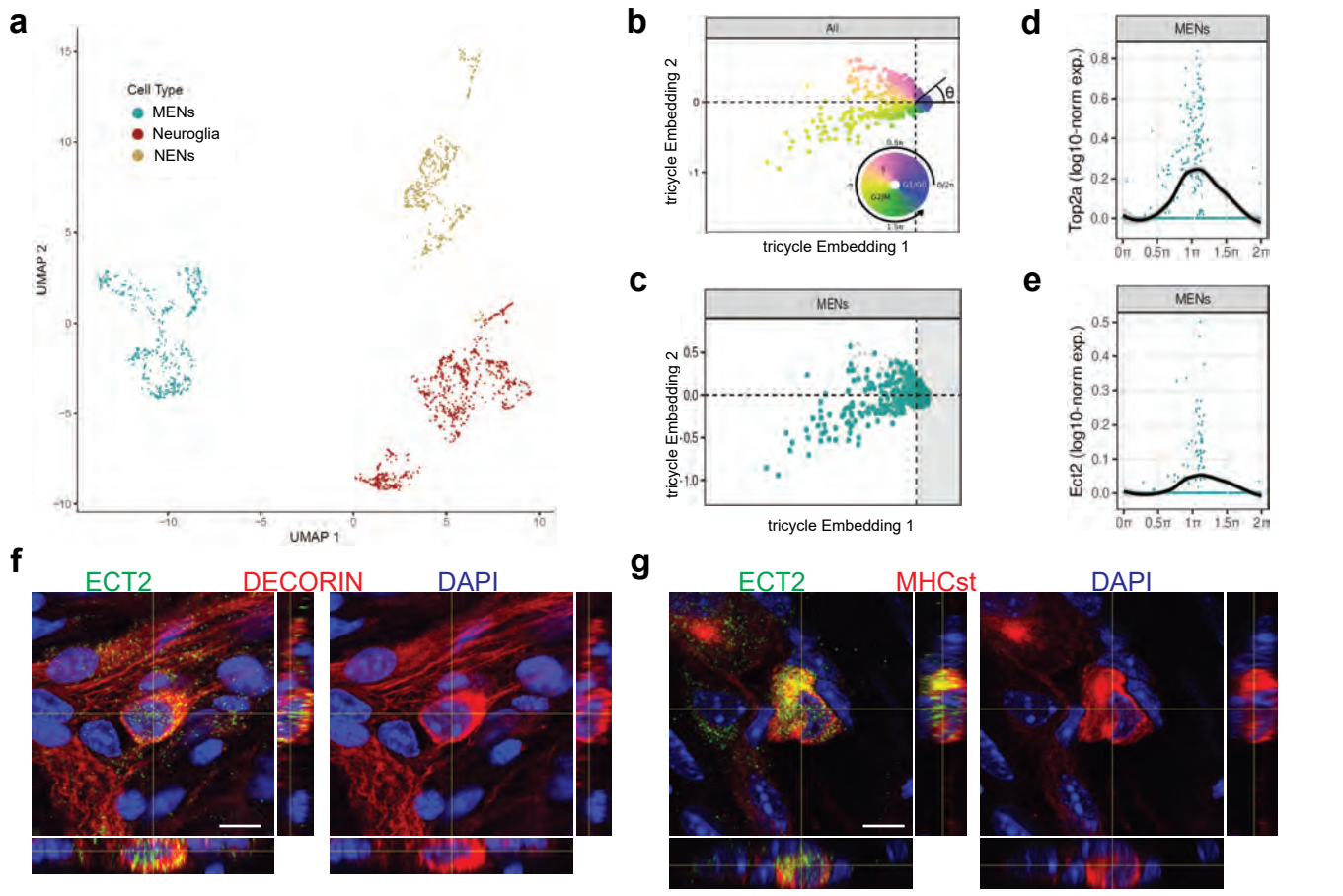
a
Cell Type
MENs
Neuroglia
NENs
UMAP 2
UMAP 1
b
All
tricycle Embedding 2
tricycle Embedding 1
θ
c
MENs
tricycle Embedding 2
tricycle Embedding 1
d
MENs
Top2a (log10-norm exp.)
e
MENs
Ect2 (log10-norm exp.)
f
ECT2
DECORIN
DAPI
g
ECT2
MHCst
DAPI

Figure 11

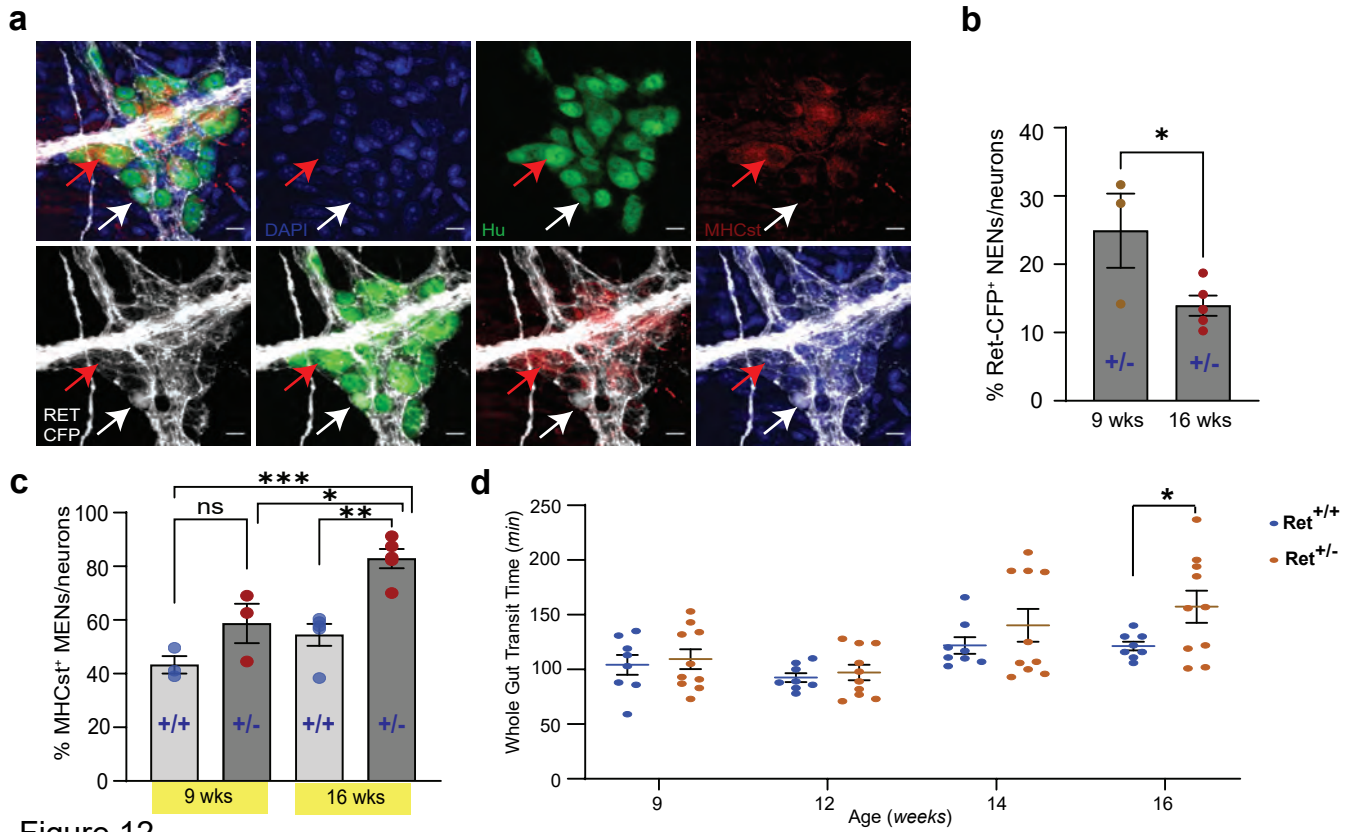
a
DAPI
Hu
MHCst
RET
CFP
b
% Ret-CFP+ NENs/neurons
40
30
20
10
0
*
+/-
+/-
9 wks
16 wks
c
% MHCst+ MENs/neurons
100
80
60
40
20
0
***
ns
*
**
+/+
+/-
+/+
+/-
9 wks
16 wks
d
Whole Gut Transit Time (min)
250
200
150
100
50
0
*
Ret+/+
Ret+/-
9
12
14
16
Age (weeks)

Figure 12

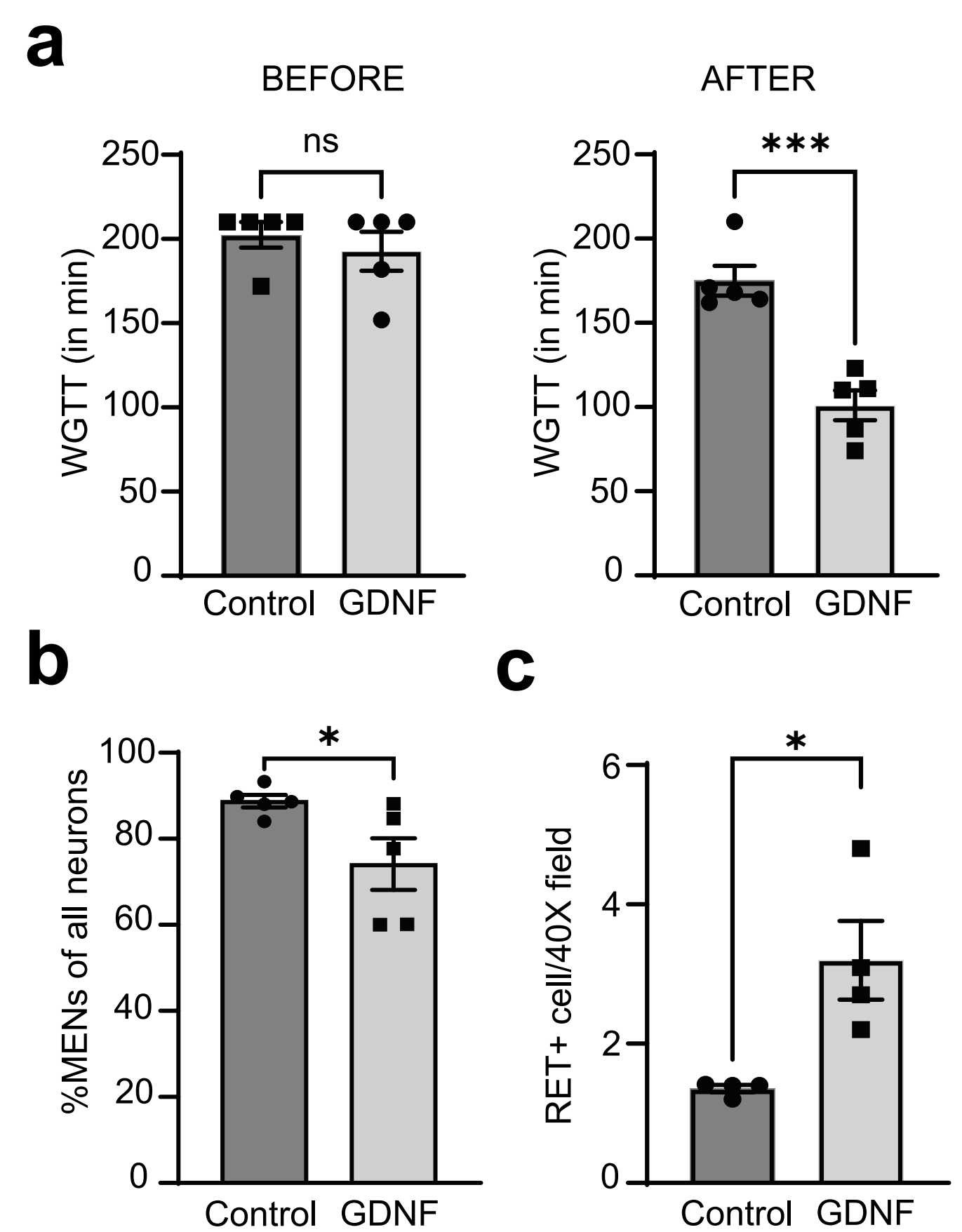
a
BEFORE
AFTER
ns
***
WGTT (in min)
250
200
150
100
50
0
Control
GDNF
b
c
%MENs of all neurons
100
80
60
40
20
*
RET+ cell/40X field
6
4
2

Figure 13

a

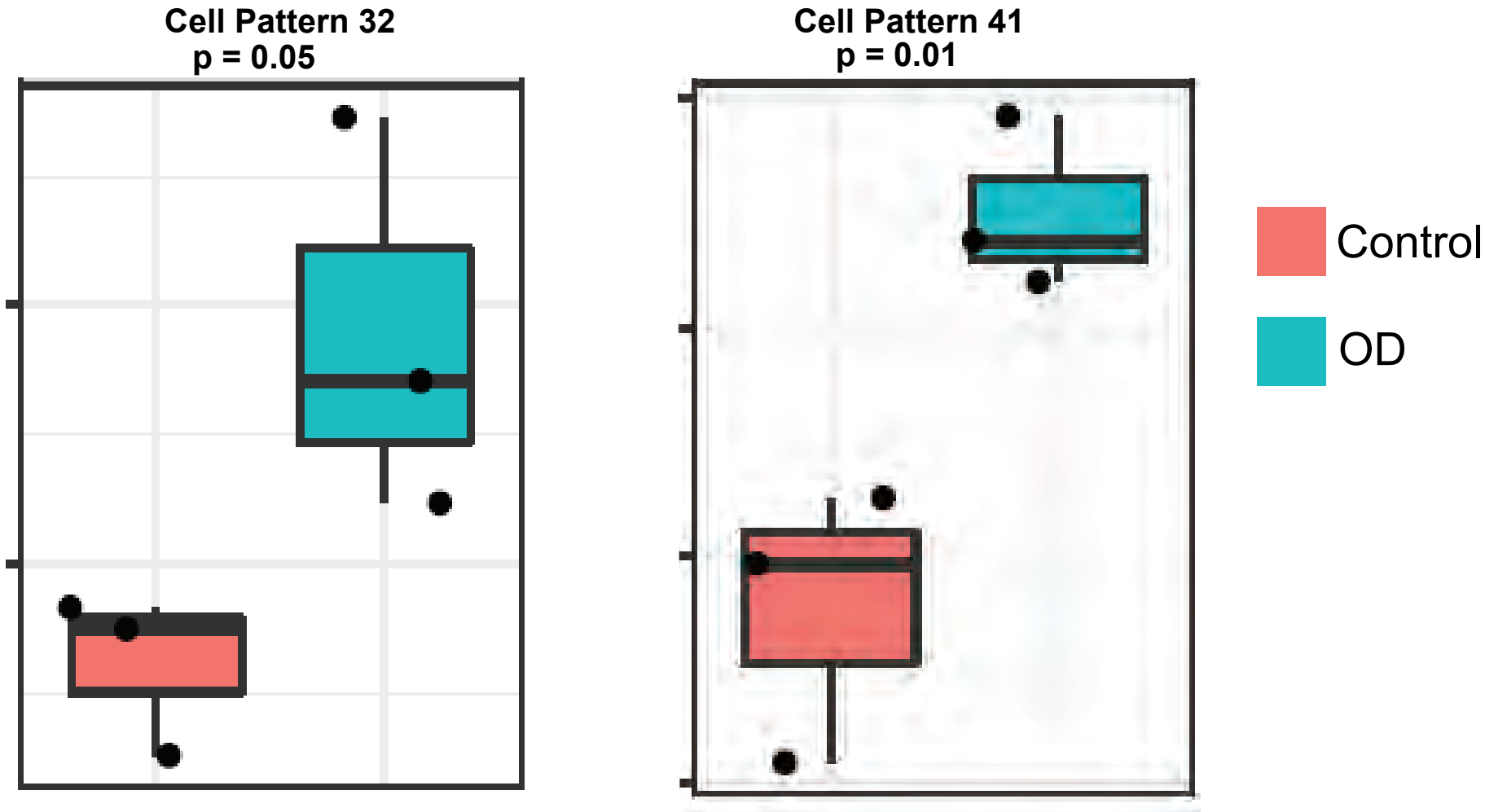

b

HGNC Symbol	Direction	Gene type	Description	Coding	Mean RC	log FC	P-value	Adj. P-value
SNAP25	Reduced in OD	protein_coding	synaptosomal-associated protein, 25kDa [Source:HGNC Symbol;Acc:11132]	yes	419	-3.56	2.68E-15	1.25E-12
KLHL1	Reduced in OD	protein_coding	kelch-like family member 1 [Source:HGNC Symbol;Acc:6352]	yes	5	-2.92	2.43E-06	7.07E-05
NOS1	Reduced in OD	protein_coding	nitric oxide synthase 1 (neuronal) [Source:HGNC Symbol;Acc:7872]	yes	775	-2.91	3.29E-06	9.06E-05
CHAT	Reduced in OD	protein_coding	choline O-acetyltransferase [Source:HGNC Symbol;Acc:1912]	yes	17	-2.78	2.00E-07	9.34E-06
GDNF	Reduced in OD	protein_coding	glial cell derived neurotrophic factor [Source:HGNC Symbol;Acc:4232]	yes	649	-2.75	2.27E-10	2.98E-08
RET	Reduced in OD	protein_coding	ret proto-oncogene [Source:HGNC Symbol;Acc:9967]	yes	474	-2.59	6.38E-18	5.29E-15
CLIC3	Increased in OD	protein_coding	chloride intracellular channel 3 [Source:HGNC Symbol;Acc:2064]	yes	98	2.95	1.74E-12	4.54E-10
UPK3A	Increased in OD	protein_coding	uroplakin 3A [Source:HGNC Symbol;Acc:12580]	yes	49	2.93	1.47E-06	4.68E-05
CDH3	Increased in OD	protein_coding	cadherin 3, type 1, P-cadherin (placental) [Source:HGNC Symbol;Acc:1762]	yes	252	2.66	9.87E-06	2.20E-04
SLPI	Increased in OD	protein_coding	secretory leukocyte peptidase inhibitor [Source:HGNC Symbol;Acc:11092]	yes	1,924	2.56	9.84E-06	2.20E-04
SLC17A9	Increased in OD	protein_coding	solute carrier family 17 (Vesicular nucleotide transporter). [Source: HGNC]	yes	1,997	2.15	9.67E-06	2.17E-07

Figure 14